(2)

US Army Night Vision and Electro-Optics Laboratory
Final Scientific and Technical Report

Contractor:	Department of Electrical and Computer Engineering University of Illinois 1406 West Green Street Urbana, Illinois 61801
Contract Number:	DAAK 20-84-K-0225
Effective Date:	September 1, 1984
Expiration Date:	August 31, 1987
Reporting Period:	September 1, 1984 - August 31, 1987
Principal Investigator:	Prof. James J. Coleman (217) 333-2555
Title:	Semiconductor laser diode arrays by MOCVD

September 1, 1987

Task Objectives:

The purpose of this program is to develop the metalorganic chemical vapor deposition (MOCVD) epitaxial growth process for semiconductor heterostructure laser diode arrays. These laser diode arrays are intended to be used as an optical pump for solid state yttrium aluminum garnet (YAG) lasers. In particular, linear uniform arrays having high output power, high efficiency, low laser threshold current density and precisely controlled emission wavelength are required.

Technical Problems:

There are three technical problems associated with this task. The first problem is development of individual laser diode device structures which satisfy the requirements for efficiency, threshold and wavelength control and are suitable for incorporation into laser arrays. There are a number of possible structures varying in complexity from conventional five-layer double heterostructures having alloy AlGaAs active regions to very sophisticated quantum well heterostructures (QWH). The second problem is an analytical study of the waveguide properties of multi-element laser arrays. Simple arrays of conventional double heterostructure laser diodes have been studied but extension of this work to other laser diode geometries is non-trivial. Preliminary and optimum geometries for the individual structures and the photomasks used for device processing require some modeling of the optical properties of these arrays. The third problem, and the major point of this entire program, is experimental development of suitably designed individual laser diode structures in a well modeled multi-element array. An additional and pervasive problem is the continued development of the MOCVD growth process and AlGaAs-GaAs heterostructure materials science as it applies to these specific structures.

General Methodology:

Three approximately parallel efforts, having a great deal of overlap, comprise the general methodology of this program. These are, as described above, development of individual laser diode

structures, development of a waveguide model for array structures and experimental development of laser array structures.

• Individual laser devices

We are concerned with two aspects of the development of individual laser device structures. The first is design of a suitable structure in terms of control over emission wavelength. The requirement for emission centered near λ = 8080Å has resulted in previous work focusing on conventional double heterostructure lasers having AlGaAs active layer composition. The direct energy gap of $Al_xGa_{1-x}As$ is given by

$$E_g = 1.427 + 1.247x \text{ (eV)}.$$

The energy of emisssion corresponding to 8080Å is 1.534 eV which corresponds to x = 0.086. Conventional double heterostructure lasers having 8-9% Al active layer composition and 35% Al confining layer composition are considered here to be the standard from which development should proceed. Broad area conventional structures are grown and processed throughout the program for the sake of comparison with more sophisticated structures and to serve as a test structure when source or system changes are implemented in the MOCVD epitaxial growth reactor system. Another way of obtaining control over the emission wavelength of a semiconductor laser diode is by reducing the size of a GaAs active layer below 200Å (an electron wavelength) so that quantum effects become important. These structures, called quantum well heterostructures (QWH), have the effect that electrons and holes behave like particles confined in a potential well. This results in discrete energy levels for optical transitions at energies higher than the band gap energy. For example, the wavelength of the n=1 transition of a 45Å GaAs quantum well corresponds to about λ = 8080Å. Such thin layer structures, while difficult to grow by such conventional growth methods as liquid phase epitaxy (LPE), are easily grown by the MOCVD process. The structure of most interest for this program is the graded barrier quantum well heterostructure which has a number of improvements relative to the conventional DH laser. The

confining layer composition is raised to 60-85% Al in order to increase the carrier confinement by raising the energy gap of the confining layers. This also affects optical mode properties by lowering the index of refraction in the confining layers. The active layer consists of a 45Å quantum well flanked on either side by a parabolically graded (composition) region that is typically 0.4-0.5 μm wide and graded from x = 0.2 up to the confining layer composition. The carrier collection eficiency of a single 45Å well is low. The graded region acts like a funnel, however, to collect energetic carriers and allow them to thermalize into the lowest order quantum state where they are available for a recombination event. The graded region also affects the waveguide properties of the laser by providing a region of intermediate average index of refraction between confining layers.

The second aspect of individual laser device development in this program is a study of current confinement stripe geometries suitable for laser arrays. The most common form of stripe definition is the oxide defined stripe which consists of a layer of silicon dioxide deposited on the surface of the laser wafer with stripe openings defined by photolithographic techniques. This stripe is easy to define but has two disadvantages relative to incorporation into laser arrays. The first disadvantage is that, since the stripe is on the surface of the laser structure, losses due to current spreading will be a maximum resulting in minimum efficiency. The second disadvantage is that since the oxide layer is some distance away from the active region, it has little impact on the optical properties of the laser. The only contributions to the transverse mode structure come from changes in index of refraction resulting from regions of gain or loss (gain guiding). Several structures are of interest in this program as improvements on this elementary stripe geometry. The first and most important is the self-aligned stripe laser in which an absorbing GaAs layer is located physically near the active layer in all but the stripe region. This layer, when close enough to the active layer, strongly impacts the optical mode and results in changes in the complex effective refractive index. If the layer is made n-type, it also serves as a current blocking layer, confining the drive current to the stripe region by means of a reverse biased pn junction. Other structures of

interest are the buried stripe laser and the narrow diffused stripe laser. The former is of less interest owing to more difficult processing requirements and the latter is is of less interest since there is no real index guiding mechanism and gain guiding predominates. For array structures where mode interaction is unnecessary (below), the narrow diffused stripe structure may be of interest for ease of processing. All of these stripe structures can be made with both conventional alloy active regions or with graded barrier quantum well heterostructure active regions.

• Device and array modeling

Any linear array must consist of a number of individual diode laser elements driven in parallel. As these elements are moved physically close to each other there will be interaction of the optical modes of each of the elements. The extent of this interaction will depend on the nature of the optical properties of the individual diodes as well as the number of, and spacing between, elements. In order to determine preliminary requirements, at least, for the process mask sets of any of the diode structures above and for the array structures to be described below, some effort must be made to model the optical properties of the individual diode structures. Subsequently these models must be extended to multiple elements. Although this program is intended to be mainly experimental, some attention is given to modeling as described here.

• Array structures

Four array structures are of interest in this program. As for individual device structures, a common array structure is identified as a basis structure to which comparison of more complicated structures may be made. This basis structure is the oxide defined stripe laser array. As described above, this structure is simple to fabricate from conventional photolithographic techniques but has the limitations that current spreading is a maximum and the only optical guiding results from variations in index resulting from either gain or loss. A second array structure of interest is the shallow mesa laser array. In this structure, stripes are etched into a finished laser wafer through the GaAs:p+ cap layer, into the AlGaAs:p confining layer to a point near the active layer. The relatively

poor (high resistance) contact to the AlGaAs results in current confinement to the stripe region. If the stripes are etched deep enough, the presence of a semiconductor-metal interface near the active region results in real index changes and subsequent mode control. A third array structure is a multiple element self-aligned stripe laser array. The fourth array structure of interest is a multiple element array of narrow diffused stripe lasers.

Technical Results - Year 1:

• Conventional alloy active region lasers

Alloy active region conventional DH lasers having 8 and 10% Al active regions and 35% Al confining layers were grown and processed into broad area lasers. These laser structures had average broad area laser threshold current densities lower (1200 A/cm2 for 300 μm length) than previously reported for structures grown by other epitaxial growth methods. These structures were optimized with respect to doping and growth temperature (and other MOCVD process parameters). These devices serve as a basis for comparison with other, more complicated, structures.

• Graded barrier quantum well heterostructure lasers

Two graded barrier quantum well heterostructure laser structures were studied. In both cases, the active region consisted of a single quantum well 45-50Å thick centered in a parabolically graded region 0.44 μm thick. The graded region varied in composition from x = 0.22 to the confining layer composition. The two different structures had confining layer compositions of x = 0.40 and x = 0.60. Average broad area laser threshold current densities for the 40% structures were 650 A/cm2 (l = 8250Å and length 300 μm). When the confining layer composition was raised to 60%, the average broad area threshold current density dropped to 445 A/cm2. This is 2.7 times lower than for comparable alloy active region DH lasers grown by MOCVD and somewhat lower yet than for DH lasers grown by LPE.

• Conventional self-aligned stripe laser

This structure is formed by growing (on an n-type GaAs substrate) a GaAs:n buffer layer, a AlGaAs:n confining layer, the active layer structure (conventional DH or graded barrier QWH), part of the AlGaAs:p confining layer and a GaAs:n current confinement/mode control layer. In a photolithographic processing step, stripes are etched through the GaAs:n layer. The sample is

returned to the reactor and the rest of the AlGaAs:p confining layer and a GaAs:p+ cap layer are grown. DH lasers having GaAs active layers and 60% confining layers were fabricated in this manner. Two problems exist. The etch rates of GaAs and 60% AlGaAs are very different (GaAs being much slower) making control of the processing difficult when the GaAs:n layer is close to the active layer. Also, the regrowth interface in 60% AlGaAs can be of poor quality from residual oxidation. This results in high turn on voltages in some devices. In order to avoid these problems, various thin (< 50Å) etch-stop and regrowth layers have been incorporated into the structure with limited results. Devices having 5 μm stripe widths showed 2.5 V turn on and threshold currents of 75 mA.

• Complementary self-aligned laser

A new process was developed to fabricate self-aligned lasers without encountering the problems associated with the conventional self-aligned structure. This complementary process consists of two growth steps also, with the first being an entire laser structure. After growth, a stripe pattern is protected by a layer of silicon dioxide on the surface of the laser wafer and the region on either side of the stripe is etched in a manner similar to the shallow mesa laser structure. The processed wafer is returned to the reactor and a layer of GaAs:n is grown over the surface. This layer is the current confinement/mode control layer. No GaAs grows on the oxide mask which is removed by etching. The advantages of this structure are that all etching takes place in AlGaAs and is more easily controlled and that there is no overgrowth interface within the laser stripe region. The regrowth interface lies outside the stripe region where it is removed from high current densities and large optical fields. Conventional DH laser structures made this way and having GaAs active layers and 4 μm stripe width operated at threshold currents of 33-45 mA (lengths 305-380 μm). The broad area threshold current density of the starting wafer was 1075 A/cm2. No kinks were observed in the L-I characteristics and near- and far-field measurements indicate fundamental mode operation to currents in excess of $2xI_{th}$.

• Narrow diffused stripe lasers

The equipment necessary for diffusing zinc into MOCVD grown AlGaAs-GaAs heterostructures has been assembled as a part of this program. Preliminary experiments to characterize the process of diffusion into heterostructures were begun.

• Device modelling

Preliminary modelling of the optical field properties in the self aligned laser structure has been done. Calculations of the changes in effective loss and refractive index as a function of the distance between the active region and the current confinement/mode control layer have been made. The devices become predominately real-index guided for separations less than 0.25 μm and are otherwise essentially gain guided. This has been confirmed on experimental structures.

• Oxide-defined stripe arrays

A 60% graded barrier QWH structure was processed into 2 and 4-element oxide-defined stripe arrays. L-I measurements show kinking and optical spectra indicate multiple filament operation. Current spreading is expected to be large in oxide-defined stripe structures and 4-element devices may not be sufficiently phase-locked for kinkless operation. Near field measurements on arrays having more elements show that all elements are not being driven uniformly. This is probably a processing problem.

• Shallow mesa arrays

Shallow mesa arrays have been fabricated from a 60% graded barrier QWH laser wafer. The array consists of 1, 2, 4, 6 and 10 elements (4 μm width and 4 μm spacing). The mesas were etched to within 1 μm of the active region. The single stripe laser operates in the fundamental lateral mode, weak phase locking is apparent in the 2- and 4-element arrays and stronger phase locking is present in the 6- and 10-element devices. The extent of phase locking is estimated by

considering the shape of measured far-field patterns. The threshold current per stripe for the 10-element array is low - less than 15 mA/stripe.

Technical Results - Year 2:

• Thermal conductivity and optimum confining layer composition

Thermal conductivity is related to alloy scattering and is a minimum at 50%. The indirect-direct crossover in AlGaAs occurs at 44% and at this point donor energies are large, making doping a practical problem. Therefore doped confining layers should be either much higher or lower in composition. For optimum carrier confinement, the heterostructure discontinuity should be as large as possible. For all of these reasons, the conclusion is that the optimum confining layer composition is as high as practically possible. This means approximately 85-90% Al for MOCVD grown structures.

• Zinc diffusion process for the NDS laser

Zinc diffusion in $Al_{0.6}Ga_{0.4}As$ has been calibrated for a closed tube diffusion process. Controlled diffusion has been obtained at T = 670°C with a diffusion rate of 3.15 μm-$hr^{1/2}$. Two drive diffusion processes have been investigated for zinc in AlGaAs, both using a predep diffusion with $ZnAs_2$ as the first step. These are1) sealed tube drive diffusion with elemental As and 2) sealed tube diffusion with a protective cap layer of Si_3N_4. The substrate background doping concentration was found not to be a critical factor in junction depth. Open tube zinc diffusion was attempted in the MOCVD reactor, by flowing the vapors of diethylzinc (DEZn) and arsine. No diffusion was observed, presumably because the partial pressure of DEZn was much smaller than the solid solubility.

• Die and wire bonding of laser diodes for continuous operation

Cw bonding of laser diodes has been accomplished by bonding the laser diodes with indium onto gold plated copper slabs. The graded barrier quantum well structure was used for these arrays. The confining layers were 2.0 μm $Al_xGa_{1-x}As$ (x=0.60), each graded layer was parabolically graded from x=0.20-0.60 over 2200 Å, and the active layer was a single GaAs quantum well 45 Å

thick. The GaAs cap layer was 0.2 μm thick. The wire bond is made from an insulator covered with Cr:Au. Single stripe, 4-stripe, and 6-stripe shallow mesa lasers and laser arrays have been operated cw using this procedure without any sign of heating. Broad area lasers have been operated cw up to 250 mW per uncoated facet. The broad area devices had stripe widths of 150 μm, with cavity lengths ranging from 300 μm to 500 μm. The characteristics were not strongly dependent on cavity length.

• Shallow mesa stripe lasers and laser arrays

L-I characteristics of a single 4-μm stripe shallow mesa graded barrier quantum well laser have shown very low thresholds currents (15mA) as well as high differential quantum efficiencies (70%) and output powers up to 25 mW cw per facet. We tested many diodes of various lengths ranging from 300 μm to 500 μm. These devices usually operate in a single longitudinal mode above threshold. The transverse modes are not stable, however, and higher order modes appear just above threshold. Shallow mesa graded barrier quantum well 6-element laser arrays operating cw have a threshold current of 90mA and have been operated up to 60 mW without any signs of heating. The threshold for 4-stripe lasers are about 80mA and the diodes are phase locked, showing a double lobed far field pattern, up to 120 mA. (4-stripe array: I_{th} = 80 mA, η = 16 % per facet, 6-stripe array: I_{th} = 90 mA, η = 21 % per facet, broad area: I_{th} = 160-180 mA, η = 20 % per facet) The near field patterns indicate that below 120 mA most of the optical intensity is under the two inner stripes. Above 120 mA higher order modes are observable under some of the stripes. Single longitudinal mode operation is observed up to 120 mA, where two modes appear.

• Complementary self-aligned lasers and laser arays

Single stripe complementary self-aligned dh lasers with 4, 6, 8, 10, and 12 μm stripe widths have been fabricated with the intent of finding an optimum width which gives the highest power with a stabilized mode pattern. These devices were etched to within 0.3 μm of the 500Å GaAs active layer before regrowth. Stripe widths of 4 μm yield 23 mW output power with a completely

stabilized transverse mode. Larger stripe widths show kinks in the L-I curves at lower power levels. Near field observations indicate that the laser operates in the fundamental transverse mode until the kink point, at which the optical intensity either shifts toward the edge of the stripe or breaks into a higher order mode. These devices definitely show higher order mode discrimination which is characteristic of self-aligned lasers. By comparison, shallow mesa lasers operate in higher order modes at threshold, for stripe widths greater than 4μm. Several 6-stripe self-aligned dh laser arrays have been processed. Most devices show all 6 stripes lasing close to the array threshold. Far field patterns indicate that the devices are not operating with the elements phase locked due to large center-to-center spacing. Smaller stripe separations or LOC active layers should increase the coupling between the stripes and result in phase locked operation. The individual elements of the array operate in a single transverse mode up to 50 mW where a kink in the L-I curve occurs. The differential quantum efficiency ranges from 20% to 37%, depending on confining layer composition, cavity length, stripe width, t (thickness between guide layer and active layer), and the quality of the starting material. For arrays the range was 20 % to 28 %.

The self-aligned laser array has been fabricated using graded barrier quantum well active regions, with the intent of improving device performance and facilitating coupling between array elements. Five-stripe arrays have been fabricated using a graded barrier quantum well active region containing a 30 Å quantum well. A 10 μm center-center spacing was used with stripe widths between 7-7.5 μm. Devices which were etched to within 0.2 μm (t=0.2) of the graded layer have threshold currents of 80 mA (L=14 mil) and show stable mode operation up to about 100 mW (pulsed) without phase locked operation. Samples etched to within 0.4 μm (t=0.4) of the graded region in order to improve optical coupling between the array elements operate phase locked in a small region above threshold, up to about 15 mW (pulsed).

• Narrow diffused stripe lasers and laser arrays

Six-stripe double heterostructure narrow zinc diffused stripe (DH-NDS) laser arrays have been fabricated and tested. The stripe width of the 6-stripe DH-NDS arrays was 6 μm, with a 12 μm center to center spacing between array elements. The fabrication process is a single step sealed tube zinc diffusion at 670°C. The pulsed laser threshold currents for these six-stripe DH-NDS arrays range from 150 mA (L = 250 μm) to 200 mA (L = 356 μm). The threshold current of a single stripe device was about 40-50 mA for the same stripe widths and lengths. Pulsed L-I curves show no kinks up to the limit of our pulse generator, at a power of 160 mW per facet for the six-stripe DH-NDS laser array. The maximum cw power from the array was 30 mW per facet, with a cw threshold current of about 250 mA for a length of 350 μm. Near field measurements indicate that the laser is gain guided since small peaks are observed between the stripes just above threshold. The far field patterns of these devices have 3 or 4 very narrow peaks just above threshold, with many more peaks appearing as the current is increased. The near and far field patterns at threshold are very similar to the calculated field patterns of a gain guided phase locked array and are also similar to the patterns observed for proton bombarded stripe laser arrays. This indicates that these lasers are phase locked.

We have fabricated single element narrow diffused stripe lasers with a graded barrier quantum well active region, using a 50 Å GaAs active layer, and 2200 Å $Al_xGa_{1-x}As$ layers graded from x=0.2 to x=0.6. The threshold current of these single element devices was 20-25 mA when w=7-15 μm, for cavity lengths ranging from 290 μm to 400 μm. The threshold current of these quantum well lasers is a factor of 2x lower than the single element narrow diffused stripe laser with a double heterostructure active layer. The wavelength of these lasers was 8260 Å, and up to 67 mW per facet (pulsed) was observed from a narrow diffused stripe laser with L=405 μm and w=6 μm. The near and far field patterns remained stable up to 4 times I_{th}.

• Reflection and antireflection coatings

Experiments were begun using reflection and antireflection coatings on the facets of the lasers in an attempt to increase the power output. The reflection coating is a four-layer quarter wavelength reflector consisting of alternating layers of Al_2O_3 and Si. Each layer has an optical thickness of a quarter wavelength. The antireflection coating is a single layer of Al_2O_3. The effect of the antireflection coating (R_1) on the threshold current density and the external quantum efficiency with $R_2 = 0.95$ has been calculated. The power output ratio of mirror 1 to that of mirror 2 as a function of R_1 when R_2 is held constant at 0.95 has also been calculated. These curves can be used as guidelines for choosing the desired value of R_1. Initial work on reflection and antireflection coatings were on laser diodes with a graded barrier quantum well active (GBQW) layer. The total external differential quantum efficiency of these lasers without coatings was measured to be about 15% per facet, and the threshold current of a laser with a 50 μm wide stripe and a 445 μm long cavity was 160 mA. The output from the facet with the reflection coating is significantly reduced, indicating a high reflectivity at that facet. The differential quantum efficiency of the laser is 42% for the facet with the antireflection coating. The threshold current of the coated laser increased to 210 mA, as expected when an antireflection coating is used.

We have mounted some coated and uncoated graded barrier quantum well lasers on heat sinks for high power pulsed operation. The diodes tested were broad area lasers with 150 μm wide stripes. The maximum power achieved from lasers with uncoated facets was 420 mW per facet at a current of 2 A, and a pulse width of 6 μs. The laser diodes are a graded barrier quantum well structure with a 50 Å well and a 380 μm long cavity. The coated diodes with 30 Å wells and 150 μm wide stripes were mounted and pulsed for high power operation. The maximum power from the output facet was 668 mW at a drive current of 2 A and a pulse width of 7 μs, an improvement of 59%. The cavity length of this laser was 483 μm. All the lasers suffered catastrophic damage at higher pumping levels. Some lasers first had lower output and later shorted out completely, while others immediately shorted out when the laser was pumped too hard.

• Buffer layer and growth temperature effects

We have studied the effect of buffer layers on the quality of graded barrier quantum (GBQW) well lasers with 85% AlGaAs confining layers grown by MOCVD. Four wafers, identical except for the buffer layers, were grown and tested. One wafer was grown with only the normal GaAs buffer layer, while the other wafers had, in addition to the GaAs buffer layer, either a compositionally graded buffer (CGB) layer, a superlattice buffer layer (SLB), or both CGB and SLB layers. Lasers fabricated from the wafer with a GaAs buffer layer only showed somewhat more scatter in the broad area threshold current density data compared with data from lasers having additional buffer layers. In all other respects, particularly the average broad area threshold current density, all showed excellent laser characteristics. These data illustrate that CGB or SLB layers may be useful for slightly improving the uniformity of MOCVD-grown lasers, but otherwise serve little purpose. We have also investigated the effect of growth temperature on the quality of the GBQW lasers with $Al_{0.85}Ga_{0.15}As$ confining layers, and found that lasers grown at 800°C have slightly lower thresholds than lasers grown at 820°C or 760°C.

Technical Results - Year 3:

• Buried heterostructures by ion implantation

We have studied the development of real-index guided buried heterostructure layers by ion implantation impurity induced disordering. The structure we studied for ion implantation disordering is a graded barrier quantum well heterostructure with two GaAs wells and three AlAs barriers. The confining layers are 1.0 μm $Al_{0.85}Ga_{0.15}As$, and the graded layers are parabolically graded in aluminum composition from x=0.85 to x=0.40 over a thickness of 1200 Å. Each of the 30 Å GaAs wells is surrounded on both sides by 10 Å AlAs barriers. We implanted this wafer with doubly-ionized Si at 300 kV, so the energy is 600 keV. The implanted sample was then annealed at T=845°C for t = 1 hr in an evacuated quartz ampule. The surface of the wafer was capped with a layer of Si_3N_4 to prevent the As from evaporating. The room temperature photoluminescence (PL) peak from this implanted and annealed wafer was 6800 Å, a substantial shift from the original value of 7250 Å, indicating that the active region was compositionally disordered. Three 10 Å AlAs barriers and two 30 Å GaAs wells would disorder into $Al_{0.33}Ga_{0.67}As$ and would have a PL peak of 6775 Å, which is close to the measured 6800 Å. An as-grown sample from the same wafer was annealed at 845°C for t = 1hr, without Si implantation. The room temperature PL peak from this wafer was 7300 Å, indicating that disordering does not occur for these times and temperatures, without the Si ion implant.

These ion implantation disordered buried heterostructure lasers were processed using a 1000 Å Si_3N_4 mask. This mask thickness was later found to be inadequate since the implant could be seen both inside and outside the stripe region in SEM images of the device. Subsequently, a Si_3N_4 layer and a photoresist mask were used protect the stripe region from a 300 keV Si+ implant. The entire wafer is then annealed at 850°C for 1-2 hr to anneal and disorder the quantum well outside the stripe region. We found that a shallow zinc diffusion in the stripe region is necessary after the annealing step in order to form a good ohmic contact. The Si+ implant does not reach the active layer, but the quantum well is apparently disordered to an extent by the

implant, since the emission from the well shifted, after the Si+ implant and anneal, from 8250 Å to 7950 Å. The presence of the Si in the top contact layer outside the stripe region forms a very effective barrier to current flow outside the stripe region, resulting in low thresholds of 20-25 mA for single element lasers with stripe widths of 4-8 μm. These lasers are not stable with kinks in the L-I curve at powers as low as 4 mW.

• Narrow zinc diffused stripe arrays

During this reporting period we fabricated and tested 10 element arrays of narrow zinc diffused stripe (NDS) lasers having graded barrier quantum well active layers and $Al_{0.85}Ga_{0.15}As$ confining layers. The as-grown structure has 1200 Å parabolically graded $Al_xGa_{1-x}As$ layers (x=0.85-0.20) and a 50 Å GaAs quantum well layer. The GaAs cap layer and the upper 1.25 μm of the top confining layer are grown n-type, and a zinc diffusion through a Si_3N_4 mask (T=625°C, t=30 min, $ZnAs_2$ source) is used to form the laser elements. Ten element arrays, having either 4 μm stripes and 8 μm center to center spacings or 8 μm stripes and 12 μm center to center spacings, were fabricated. Pulsed (1.5 μsec, 2 kHz) L-I measurements indicate the threshold current of the lasers with 8 μm stripes ranges from 90 mA for diodes with a cavity length of 250 μm to 120 mA for a length of 530 μm. The measured emission wavelength from these diodes is 8300 Å, and the total external differential quantum efficiency was 38%-46% at a power of 10-20 mW. Pulsed power of 195 mW/facet is observed at a current of 1 A. The threshold current of the lasers with 4 μm wide stripes ranged from 105 mA to 120 mA for lengths ranging from 356 μm to 457 μm. This is slightly higher than observed for the 8 μm wide stripe lasers. The total external differential quantum efficiencies ranged from 39% to 41% at a power of approximately 10-20 mW. A pulsed power of 215 mW/facet was observed at a current of 950 mA. Near and far field pattern measurements indicate the arrays with 4 μm wide elements have more stable field patterns than the lasers with 8 μm wide elements. The measured T_o of the lasers with 4 μm wide stripes was 180°C at T=20-40°C, and 100°C at T=40-80°C. The cw power output of these lasers was limited to about 40 mW due to inadequate heat sinking.

• Wavelength tuning and uniformity of quantum well heterostructure lasers

We have studied tuning the graded barrier quantum well laser to a wavelength of 8080 Å using two approaches. We independently varied the well width and the barrier composition (the Al composition of the graded layers adjacent to the well). The confining layer Al composition and the graded layer thickness were kept constant at 0.85 and 1200 Å, respectively. The structure we studyied previously has a 50 Å well and a barrier with Al composition x=0.20. This combination yields an emission wavelength of 8250 Å, in close agreement with the wavelength calculated by assuming the transition occurs between the n=1 states of the conduction band and the valence band in a single square potential well. We calculated that the width of the GaAs quantum well should be 38 Å, with an x=0.20 barrier, to achieve a wavelegth of 8080 Å, or that the barrier should be x=0.35 with a 50 Å GaAs well to obtain 8080 Å. We fabricated and tested broad area laser diodes operating at a wavelength of 8060 Å using two different graded barrier quantum well active layer structures, one with a 35 Å GaAs well and 1200 Å graded $Al_xGa_{1-x}As$ (x=0.85-0.20) layers, and another with a 50 Å GaAs well with 1200 Å graded $Al_xGa_{1-x}As$ (x=0.85-0.35) layers. We also tested for uniformity of wavelength several diodes from another wafer (50 Å GaAs well and 1200 Å graded $Al_xGa_{1-x}As$, x=0.85-0.20) which lases at 8285 ± 5 Å, for L > 400 μm. The wavelength shifts for shorter cavity lengths to 8240 ± 5 Å at L = 254 μm. The wavelength remains nearly constant (± 5 Å), however, for several diodes with the same cavity length.

• Wavelength shifts with heating

During this reporting period we have studied the dependence of emission wavelength of 150 μm broad area oxide defined stripe lasers on output power for various pulse widths or for cw operation. The graded barrier quantum well structure was used. The confining layers were 1.5 μm $Al_xGa_{1-x}As$ (x=0.85), with 1200 Å graded regions of $Al_xGa_{1-x}As$ (x=0.85-0.20) surrounding a 50 Å GaAs quantum well. The cw threshold current of the 150 μm wide broad area laser was typically 200 mA, with a single ended slope efficiency of 27 % per uncoated facet. We have studied

diodes using a 30%-70% lead-indium alloy solder with flux, which melts at 174 °C and a pure indium solder without flux. Diodes mounted p-side down with 350 Å Cr, 2000 Å Au p-type contacts with the pure indium solder are always ruined by the soldering process, but are not ruined if a Ti/Pt/Au contact is used. The layer thicknesses were 300 Å Ti, 450 Å Pt, and 2000 Å Au. A 2000 Å layer of nickel, and a 1000 Å layer of indium was evaporated onto the copper heat sink block, and then the copper block was indium plated to a thickness of 2-3 μm. No gold was plated or evaporated onto the copper heat sink. The diode was then placed on the mount in an H_2 atmosphere and slowly heated to 250 °C for 15 seconds. No flux was used in this process. Several diodes were mounted using this process, with better results than from diodes mounted using the alloy solder. For example, a 310 μm long diode with a 150 μm wide stripe mounted with the pure In solder operated at a cw power of 234 mW per facet, at 950 mA of current, wheras the diodes mounted with the alloy solder tend to overheat before reaching that power level.

We deduced the operating temperature of the diode junction under cw operation by two independent methods. First, we tested the wavelength variation of diodes under cw operation as a function of output power, and observed the wavelength shift, which is attributed to the temperature dependence of the energy gap of GaAs. The wavelength shift was not observed for low duty cycle pulsed operation, in agreement with the above assumption. The temperature was deduced by comparing the measured data with the calculated temperature dependence of emission wavelength based on the n=1 electron to heavy hole transition in the quantum well. Second, the cw L-I curve was compared with T_o data taken under low duty cycle pulsed operation. From these data, we believe the diodes heat up to 40-50 °C. The diodes mounted with the pure In solder did not heat up as much as the diodes mounted with the alloy solder, and they also exhibited higher cw output power.

The wavelength shift associated with heating is significant. A 310 μm long diode mounted with pure In operated at 8206 Å under low duty cycle pulsed operation at any power level, but the wavelength shifted to 8260 Å when operated cw at a current of 300 mA, and the wavelength

shifted to 8326 Å when operated cw at a current of 700 mA, corresponding to an output power of 180 mW per facet. This wavelength variation must be taken into account when designing a high power laser diode for 8080 Å.

• Lasers grown on round LEC substrates

In order to determine the viability of growing laser structures on LEC substrates, which are commercially desirable because of automated processing and wafer size considerations, we examined the effect of various buffer layer structures on the material quality of bulk high composition epilayers and on the device characteristics of GBQW laser structures grown simultaneously on HB and LEC substrates. Structures were grown with either no underlying buffer layer, a compositionally graded buffer layer, a superlattice buffer layer, or a combination of a compositionally graded layer plus a superlattice. Bulk 1.5 μm layers of 85% AlGaAs were grown with each type of buffer on both types of substrate, surface morphologies were compared, and etch pit densities (EPD) were measured. The incorporation of the more sophisticated buffer layers resulted in improvements in surface morphology and EPD for both types of substrates, with the effects being dramatically more pronounced for the LEC case. As such, the material quality of epilayers grown on LEC could be made equivalent to that of epilayers grown on HB with the appropriate choice of buffer layer. GBQW laser structures with 50 Å quantum wells were also grown with all buffer layers on both substrate types and were processed into 150 μm wide broad area oxide defined stripe laser diodes with a variety of cavity lengths. Broad area threshold current densities, obtained from pulsed (1.5 μs pulse width, 2 kHz repetition rate) L-I curves, were measured and compared for the various buffer layer/substrate combinations. All diodes exhibited extremely low thresholds, with J_{th} ≈ 250 A/cm2 for 500 μm cavity lengths. More importantly, no variation in J_{th} was observed for lasers grown on the same type of substrate with any of the buffer layer structures or for lasers grown on both HB and LEC substrates with the same underlying structure. These data indicate that the device characteristics of GBQW lasers grown by MOCVD are relatively insensitive to the type of buffer layer structure or the type of substrate utilized and

that high quality laser structures can be grown on LEC substrates with no increase in J_{th} over that of identical structures grown on HB substrates.

• Wide stripe laser development

We began development of a process to fabricate very wide stripe bar lasers (1mm wide or more), in order to increase the optical power of the lasers, which is limited to roughly 300 mW per facet for 150 μm wide broad area lasers. The upper limit for the width of a laser without some form of spoiler region along the width is approximately equal to the length of the cavity, since lateral lasing and amplified spontaneous emission due to the lateral cavity will compete with the desired longitudinal modes. In order to increase the width to 1 mm or more, it is necessary to spoil the lateral cavity along the bar. We have obtained a mask which has spoiler region widths of 10, 25, 50, or 100 μm, which separate 400 μm wide laser regions. The spoiler regions may be a regrown unpumped region of GaAs, or more simply, an etched region similar to the unpumped region of the shallow mesa laser outside the stripe. We tried etching the laser structure through the active region in the spoiler regions, and then regrowing GaAs in the etched spoiler regions. We did not expect the GaAs to deposit on the SiO_2 etch mask, since it does not deposit on the narrow SiO_2 mask in a complementary self-aligned laser. This regrowth did, in fact, deposit on the oxide since the much larger surface area allowed formation of nucleation sites making it difficult to complete the processing for these lasers. To simplify the process, we tried simply etching away most of the top confining layer in the spoiler regions, as in a shallow mesa laser. The etched region should provide enough index guiding to isolate each 400 μm wide laser region. These lasers were processed into lasers, but the metalization in the etched regions shorted the junction.

We have mounted broad area oxide stripe graded barrier quantum well heterostructure lasers p-side down using evaporated Ni (1700 Å), evaporated Au (300 Å), and evaporated In (500 Å) on a copper heatsink. This heatsink was then plated with In so the total thickness of the In is several microns. The diode is then placed on the heatsink in a hydrogen atmosphere and slowly heated

to 200 °C for 2 min to solder the diode. The diodes lased cw at a power of 114 mW per facet (800 mA), and had a lasing wavelength was 8090 Å at a cw power of 27 mW per facet. The laser wavelength is 8020 Å when operated under low duty cycle pulsed conditions. This indicates that diode heating causes the wavelength to shift beyond the desired 8080 Å.

Important Findings and Conclusions:

• The graded barrier QWH structure is greatly superior to conventional DH lasers with alloy active regions in terms of threshold current.

• The complementary self-aligned stripe geometry laser is a stable, low threshold, high efficiency stripe structure which should be fully compatible with array applications.

• The shallow mesa array is an excellent candidate for efficient high power laser arrays.

• The optimum confining layer composition is as high as practically possible. This means approximately 85-90% Al for MOCVD grown structures.

• Shallow mesa graded barrier quantum well 4-element laser arrays operating cw have a threshold current of about 80mA and the diodes are phase locked, showing a double lobed far field pattern, up to 120 mA.

• Five-stripe self-aligned laser arrays using graded barrier quantum well active regions have threshold currents of 80 mA and show stable mode operation up to about 100 mW (pulsed) without phase locked operation.

• Six-stripe double heterostructure narrow zinc diffused stripe (DH-NDS) laser arrays have pulsed laser threshold currents from 150 mA to 200 mA. The threshold current of a single stripe device was about 40-50 mA for the same stripe width and length. Pulsed L-I curves show no kinks up to a power of 150 mW per facet.

• Si^+ implantation that does not reach the active layer is effective in disordering graded barrier quantum well heterostructure lasers and forms a very effective barrier to current flow outside the stripe region, resulting in low thresholds of 20-25 mA for single element lasers with stripe widths of 4-8 μm.

• Ten element arrays of narrow zinc diffused stripe (NDS) lasers having graded barrier quantum well active layers and $Al_{0.85}Ga_{0.15}As$ confining layers were measured to have a total external differential quantum efficiency of 38%-46% at a power of 10-20 mW and maximum pulsed power of 215 mW/facet (uncoated) at a current of 950 mA.

• Laser diodes operating at a wavelength of 8060 Å are obtained using two different graded barrier quantum well active layer structures, one a 35 Å GaAs well and a graded region composition minimum of x=0.20, and the other a 50 Å GaAs well with a graded region composition minimum of x=0.35. The wavelength remains nearly constant (± 5 Å) for diodes with the same cavity length.

• Laser diodes mounted to heat sinks with pure In solder without flux are more effective at dissipating heat, and also exhibited higher cw output power, than diodes mounted with a fluxed lead-indium (30:70) alloy solder.

• No variation in J_{th} was observed for lasers grown on the same type of substrate with any of the buffer layer structures or for lasers grown on both HB and LEC substrates with the same underlying structure indicating that the device characteristics of GBQW lasers grown by MOCVD are relatively insensitive to the type of buffer layer structure or the type of substrate utilized.

• Broad area oxide stripe graded barrier quantum well heterostructure lasers operate cw at a power of 114 mW per facet (800 mA) with a lasing wavelength of 8090 Å at a cw power of 27 mW per facet.

Publications supported under this Grant

Complementary self-aligned laser by metalorganic chemical vapor deposition, L J Mawst, G Costrini, C A Zmudzinski, M E Givens, M A Emanuel and J J Coleman, *Electronics Lett.* **21**, 903 (1985)

III-V heterostructure interfaces by metalorganic chemical vapor deposition, J J Coleman, G Costrini, S J Jeng and C M Wayman, *J. Appl. Phys.* **59**, 428 (1986)

Growth mechanisms of GaAsP/GaAs heterostructures by metalorganic chemical vapor deposition, S J Jeng, C M Wayman, G Costrini, M E Givens, M A Emanuel and J J Coleman, *J. Crystal Growth* **73**, 425 (1985)

Phase locked shallow mesa graded barrier quantum well laser arrays, L J Mawst, M E Givens, M A Emanuel, C A Zmudzinski and J J Coleman, *Appl. Phys. Lett.*, **48**, 1337 (1986)

Phase locked narrow zinc diffused stripe laser arrays, C A Zmudzinski, L J Mawst, M E Givens, M A Emanuel and J J Coleman, *Appl. Phys. Lett.*, **48**, 1424 (1986)

Near- and far-field observations of transient behavior in pulsed graded barrier quantum well lasers, L J Mawst, M E Givens, C A Zmudzinski, M A Emanuel and J J Coleman, *J. Appl. Phys.* **60**, 2613 (1986)

Complementary self aligned laser arrays by metalorganic chemical vapor deposition, L J Mawst, M E Givens, M A Emanuel, C A Zmudzinski and J J Coleman, *J. Appl. Phys.* **60**, 2633 (1986)

Metalorganic chemical vapor deposition of III-V compound semiconductor epitaxial layers, L J Mawst, G Costrini, M A Emanuel, M E Givens, C A Zmudzinski and J J Coleman, *Semiconductor International*, **9**, 61 (November 1986)

Effect of compositionally graded and superlattice buffer layers on the device performance of graded barrier quantum well heterostructure laser diodes, M E Givens, L J Mawst, C A Zmudzinski, M A Emanuel and J J Coleman, *Appl. Phys. Lett.* **50**, 301 (1987)

Optimization and characterization of index-guided visible AlGaAs/GaAs graded barrier quantum well laser diodes, L J Mawst, M E Givens, C A Zmudzinski, M A Emanuel and J J Coleman, *J. Quantum Electron.* **QE-23**, 696 (1987)

Index guided AlGaAs/GaAs visible graded barrier quantum well laser diodes, C A Zmudzinski, L J Mawst, M E Givens, M A Emanuel and J J Coleman Topical Meeting on Semiconductor Lasers, Technical Digest, 1987, Volume 6, p. 116 (Optical Society of America, Washington, D. C., 1987)

$$J_{th} = \left(\frac{d(mm)}{\eta_i}\right)\left[\frac{g_{th}}{\Gamma\beta} + J_1\right]$$

$$g_{th} = \frac{\alpha_{end}}{\Gamma} + \left(\frac{1-\Gamma}{\Gamma}\right)\alpha_{out} + \alpha_{Active}$$

$$J_{th} = \left(\frac{.05}{.8}\right)\left[\frac{\frac{1}{(.18)2(500\times10^{-4})}\ln\left(\frac{1}{R_1R_2}\right) + \left(\frac{.82}{.18}\right)(10\,cm^{-1}) + 10\,cm^{-1}}{.044} + 4100\right]$$

$$= 6.25\times10^{-2}\left[4100 + 1262.6\ln\left(\frac{1}{R_1R_2}\right) + 1035.35 + 227.27\right]$$

$$= 321.10 + 78.91\ln\left(\frac{1}{R_1R_2}\right)$$

$$\eta = \frac{\eta_i}{1 + \frac{2\alpha_T L}{\ln(1/R_1 R_2)}}$$

$\alpha_T = 55.55\ cm^{-1}$

$L = 500 \times 10^{-4}\ cm$

$$= \frac{.80}{1 + \frac{5.555}{\ln(1/R_1 R_2)}}$$

Reflectivity curves and equations

$$\eta = \frac{.80}{1 + 5.555 / \ln(1/R_1R_2)}$$

$$J_{th} = 321.10 + 78.91 \ln(1/R_1R_2)$$

$$\frac{P_{M_1}}{M_{2_0}} = \left(\frac{1-R_1}{1-R_2}\right)\sqrt{\frac{R_2}{R_1}}$$

$R_1 = R_2 = .32$
$J_{th} = 500.9$
$\eta = .2327$

$R_2 = .95$

R_1	$\ln(1/R_1R_2)$	J_{th}	η	η/η_0	P_{M1}/P_{M2}	J_{th}/J_0
.01	4.65646	688.5	.365	1.568	193	1.375
.05	3.047	561.5	.2833	1.2174	83	1.121
.10	2.354	506.8	.238	1.0227	55.5	1.012
.20	1.660	452	.184	.7907	34.87	.902
.30	1.255	420	.147	.6317	24.91	.838
.40	.9676	397.5	.1187	.510	18.5	.794

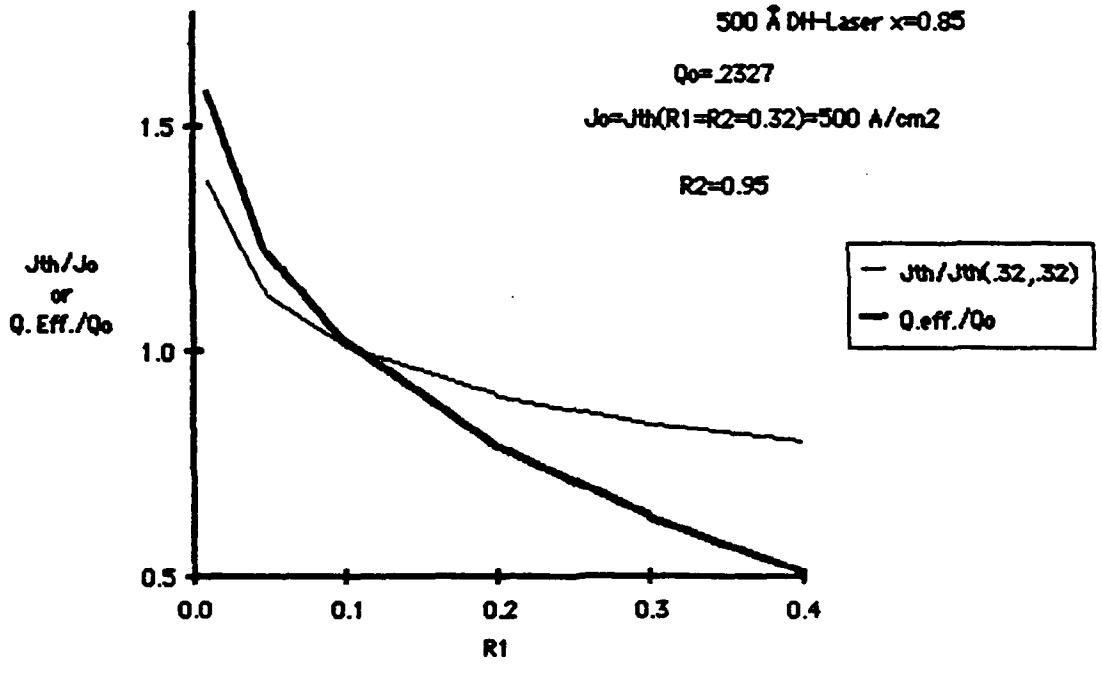
500 Å DH-Laser x=0.85
Qo=.2327
Jo=Jth(R1=R2=0.32)=500 A/cm2
R2=0.95
Jth/Jo
or
Q. Eff./Qo
1.5
1.0
0.5
0.0
0.1
0.2
0.3
0.4
R1
Jth/Jth(.32,.32)
Q.eff./Qo

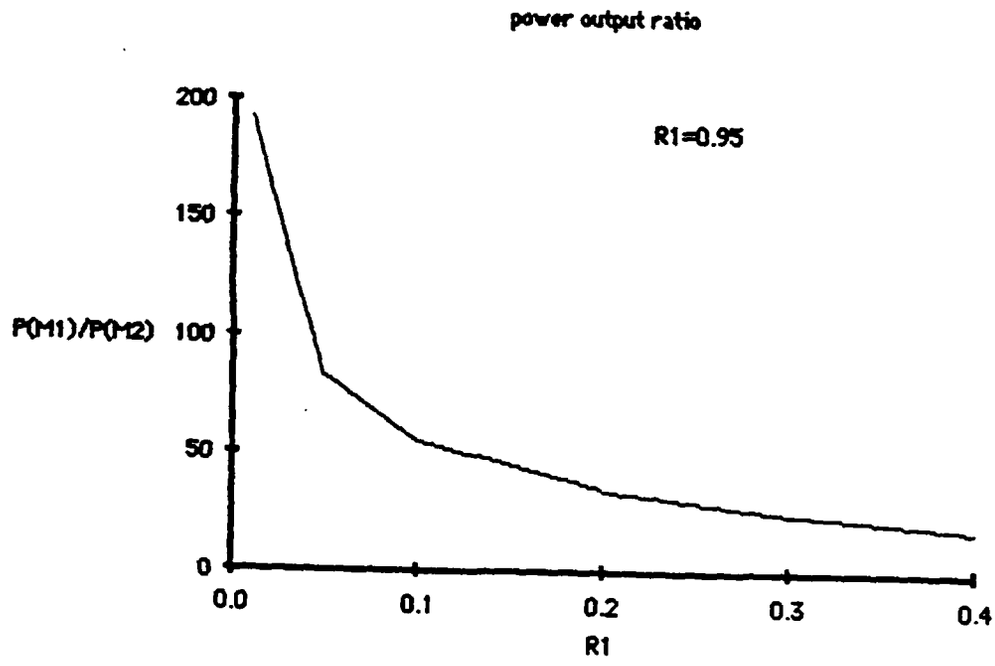
power output ratio
R1=0.95
200
150
100
50
0
P(M1)/P(M2)
0.0
0.1
0.2
0.3
0.4
R1

COMPLEMENTARY SELF-ALIGNED LASER BY METALORGANIC CHEMICAL VAPOUR DEPOSITION

Indexing terms: Lasers and laser applications, Semiconductor lasers, Vapour deposition

A complementary two-step MOCVD growth technique for the self-aligned laser is described which eliminates any possible difficulty associated with regrowth on a high composition AlGaAs layer by placing the regrowth interface outside the stripe region. Single-longitudinal-mode operation with stable near- and far-field patterns has been obtained to more than twice the laser threshold current.

Introduction: To obtain single-longitudinal-mode operation in a stripe geometry laser diode over an appreciable drive current range, the optical mode along the junction must be stabilised. This can be accomplished by introducing a built-in effective real index step across the stripe width. High-power stable-mode operation has been reported[1] for nonplanar active layer devices; however, these structures require the nonlinear growth associated with LPE, and cannot readily make use of quantum well active layers. Very low laser threshold currents have been obtained using the buried-heterostructure design;[2,3] however, the large index changes along the junction plane mean a small stripe width is needed for single-mode operation, limiting usefulness to low output power. In the case of the self-aligned laser,[4–6] a complex effective index step results from modal radiation loss into a low-bandgap high-refractive-index n-GaAs layer placed close to the active layer outside the stripe.[4] In addition to providing index guiding, the n-GaAs layer establishes current confinement by means of a reverse-biased junction outside the stripe. The self-aligned structure allows the use of any active layer, since the effective lateral index step is controlled separately by varying the distance between the n-GaAs guide layer and the active layer. In this way stripe widths of 4–5 μm can be used with all higher-order lateral modes still being cut off. Conventional self-aligned lasers have previously been fabricated using an interrupted MOCVD[5] growth process. The second growth takes place on an etched AlGaAs layer. For high aluminium concentration in the confining layers, it becomes difficult to obtain a quality electrical contact in the stripe region because of a thin native oxide layer which can form at the regrowth interface. In this letter we describe a complementary two-step MOCVD growth technique for the self-aligned laser which eliminates this difficulty by placing the growth interface outside the stripe region.

Experiment: The first step in the fabrication of the complementary self-aligned laser is the growth of any complete conventional double-heterostructure laser. In this work, a five-layer structure was grown consisting of an n-GaAs buffer layer (1·0 μm), an n-$Al_{0.6}Ga_{0.4}As$ layer (2·0 μm), a GaAs undoped active layer (500 Å), a p-$Al_{0.6}Ga_{0.4}As$ layer (2·0 μm) and a p^+-GaAs contact layer (0·2 μm). The first two layers are doped with Se (1×10^{18} cm^{-3}). The p-AlGaAs layer and the p^+-GaAs layer are doped with Zn (5×10^{17} cm^{-3} and 1×10^{19} cm^{-3}). A layer of SiO_2 (1000 Å) is deposited on the surface of the wafer and 4 μm stripes are defined along the (110) direction. The unmasked regions outside the stripe width are etched (H_2SO_4:H_2O_2:H_2O 1:8:10, 1·5°C) into the AlGaAs layer to within 0·25 μm of the active layer. With the oxide mask still in place, the mesa structures are returned to the reactor for the additional growth of 1·0 μm n-GaAs (1×10^{18} cm^{-3}). This n-GaAs layer provides enhanced mode guiding and superior current confinement relative to the shallow mesa laser.[6] The n-GaAs layer does not grow over the oxide,[7] so no additional etching step is needed to expose the stripe region, other than removing the oxide. Since the regrowth region lies outside the laser stripe width, it is immaterial whether or not an oxide forms on the exposed 60% alloy layer. An SEM cross-section is shown in Fig. 1.

Results: Typical CW threshold currents of 33–45 mA were obtained for devices 305–380 μm long, respectively. The broad-area threshold current density of the starting wafer was

Fig. 1 *SEM photograph of complementary self-aligned laser*

1075 A/cm^2 (diode length 380 μm). No kinks were observed in the L/I characteristics to more than three times the laser threshold current. Far-field data were obtained by rotating the laser diode about a silicon photodiode with a mechanical slit aperture. Near-field scans were obtained by focusing a microscope image of the facet on to an array imaging device. Near-field (Fig. 2) and far-field optical patterns (Fig. 3) show that

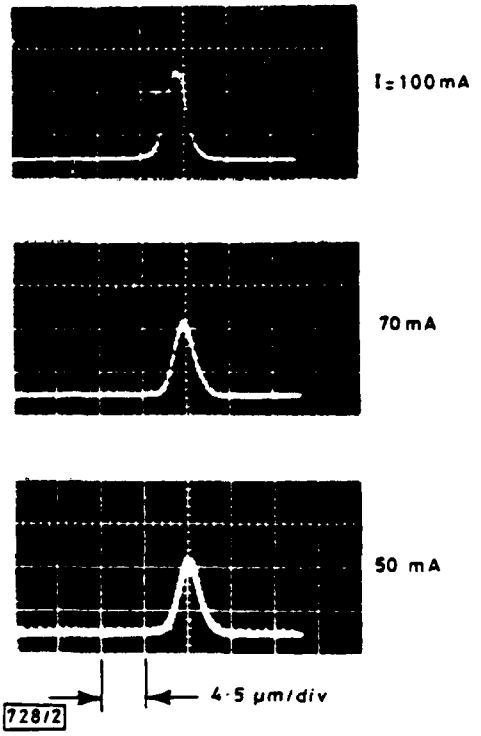

Fig. 2 *Typical CW near-field patterns above threshold*

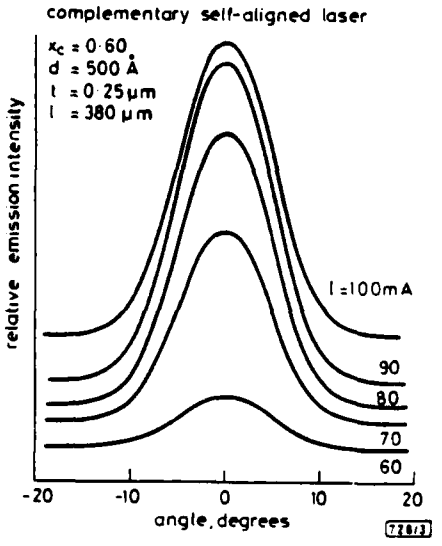

Fig. 3 *CW far-field patterns along junction plane*

the devices operate in the fundamental lateral mode to currents in excess of $2I_{th}$. Beam divergences of the far-field patterns parallel to the junction plane are 12°. Shown in Fig. 4 are CW spectra taken at two current levels above threshold (I_{th} = 46 mA). Laser operation on a single longitudinal mode occurs over a large current range, with some mode hopping, extending from slightly above threshold (50 mA) to more than twice threshold (100 mA). This stable mode behaviour indicates the presence of strong index guiding in these structures.

Conclusions: A new method for fabricating the self-aligned laser has been demonstrated which eliminates possible difficulties associated with a high composition AlGaAs interface and interrupted growth. Single-longitudinal-mode operation with stable near- and far-field patterns has been obtained to more than twice the laser threshold current. This simplified fabrication technique is now being applied to structures having other active region designs and to index-guided self-aligned laser array structures.

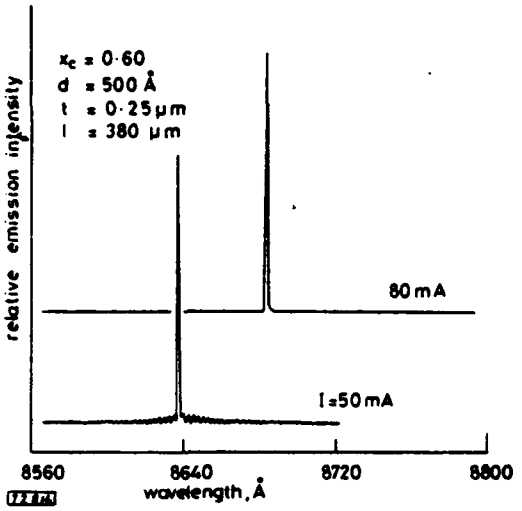

Fig. 4 *Single-longitudinal-mode CW spectra of a complementary self-aligned laser*

I_{th} = 46 mA

Acknowledgments: The authors would like to thank Y. S. Moroz and B. K. Moroz for technical assistance. This work was supported by a US Army Night Vision Laboratory contract DAAK 20-84-K-0225, and a US Navy University Research Instrumentation grant N00014-84-G-0157.

L. J. MAWST
G. COSTRINI
C. A. ZMUDZINSKI
M. E. GIVENS
M. A. EMANUEL
J. J. COLEMAN

Electrical Engineering Research Laboratory
University of Illinois
Urbana, IL 61801, USA

15th August 1985

References

1 FU, R. J., HWANG, C. J., WANG, C. S., and LALEVIC, B.: 'Single mode, high power GaAlAs/GaAs lasers', *Appl. Phys. Lett.*, 1984, **45**, pp. 716–718

2 TSANG, W. T., LOGAN, R. A., and DITZENBERGER, J. A.: 'Ultra-low threshold, graded-index waveguide, separate confinement, CW buried-heterostructure lasers', *Electron. Lett.*, 1982, **18**, pp. 845–847

3 HONG, C. S., KASEMSET, D., KIM, M. E., and MILANO, R. A.: 'GaAlAs buried-heterostructure lasers grown by a two-step MOCVD process', *ibid.*, 1983, **19**, pp. 759–760

4 YANO, M., NISHI, H., and TAKUSAGAWA, M.: 'Oscillation characteristics in InGaAsP/InP DH lasers with self-aligned structure', *IEEE J. Quantum Electron.*, 1979, **QE-15**, pp. 1388–1395

5 COLEMAN, J. J., and DAPKUS, P. D.: 'Single-longitudinal-mode metalorganic chemical-vapor-deposition self-aligned GaAlAs-GaAs double-heterostructure lasers', *Appl. Phys. Lett.*, 1980, **37**, pp. 262–263

6 TSUKADA, T., ITO, R., NAKASHIMA, H., and NAKADA, O.: 'Mesa-stripe geometry double heterostructure injection lasers', *IEEE J. Quantum Electron.*, 1973, **QE-9**, pp. 356–361

7 TAKAHASHI, Y., SAKAI, S., and UMENO, M.: 'Selective MOCVD growth of GaAlAs on partly masked substrates and its application to optoelectronic devices', *J. Cryst. Growth*, 1984, **68**, pp. 206–212

III-V heterostructure interfaces by metalorganic chemical vapor deposition

J. J. Coleman and G. Costrini
Electrical Engineering Research Laboratory and Materials Research Laboratory, University of Illinois, Urbana, Illinois 61801

S. J. Jeng and C. M. Wayman
Department of Metallurgy and Mining Engineering and Materials Research Laboratory, University of Illinois, Urbana, Illinois 61801

(Received 12 August 1985; accepted for publication 7 October 1985)

The interface characteristics of five different heterostructures grown by metalorganic chemical vapor deposition (MOCVD) have been studied using secondary ion mass spectroscopy (SIMS) and high-resolution transmission electron microscopy (TEM). Two all-binary AlAs-GaAs superlattices, ternary $Al_{0.6}Ga_{0.4}As$-GaAs and $GaAs_{0.95}P_{0.05}$-GaAs superlattices and a mismatched $GaAs_{0.8}P_{0.2}$-GaAs single interface have been examined for compositional transients and interface abruptness. When an interrupted growth process (15 s pause between layers) is used in an atmospheric pressure MOCVD reactor system, no evidence of compositional transients is observed in analysis of SIMS data interfaces of heterostructures grown in this manner and examined with high-resolution TEM and corresponding lattice imaging are found to be abrupt within a single atomic layer.

I. INTRODUCTION

The subject of interface transition width or "abruptness" is an important issue for consideration of any vapor-phase heteroepitaxial growth process. It is even more important for III-V semiconductor optical and electronic devices where the heterojunction interface is a key element in the operation of the device. Metalorganic chemical vapor deposition (MOCVD) is a rapidly developing epitaxial growth method[1] for various III-V heterostructure materials systems, which promises to be particularly amenable to large-scale commercial development. There has been, naturally, some discussion in the literature[2-8] of the quality and abruptness of heterostructure interfaces, particularly AlGaAs-GaAs interfaces. Typically, some indication of the interface quality is inferred from one or a combination of several techniques including secondary ion mass spectroscopy (SIMS), low-temperature photoluminescence (PL) and high-resolution transmission electron microscopy (TEM). The diversity of such process variables as growth temperature, growth rate, reactor pressure (atmospheric or reduced), chamber design (horizontal or vertical), and gas exchange method (interrupted or continuous) makes difficult the task of ascribing trends in measured data to specific parameters. In this paper we describe SIMS and TEM data obtained from high-quality heterostructure interfaces of superlattices in three materials systems grown by MOCVD. These systems are (1) AlGaAs-GaAs, (2) AlAs-GaAs, and (3) GaAsP-GaAs. The structures are grown in a vertical reactor operated at atmospheric pressure with an interruption between the growth of each layer. Nearly monatomic interface widths are observed without any evidence of compositional transients.

II. EXPERIMENT

Five structures have been studied using a combination of SIMS and high-resolution TEM methods. These samples are (1) an $Al_{0.6}Ga_{0.4}As$-GaAs superlattice with 500-Å layer thickness, (2) and (3) all-binary AlAs-GaAs superlattices, one with 45-Å and one with 17-Å layer thicknesses, (4) a $GaAs_{0.95}P_{0.05}$-GaAs superlattice with 500-Å layer thicknesses, and (5) a single $GaAs_{0.8}P_{0.2}$-GaAs interface. All structures were grown at temperatures in the range 700–750 °C, at atmospheric pressure, using substrates oriented (100) $\pm$ 0.5°. The total gas velocity in the vertical reaction chamber was 3.2 cm/s. Typical growth rates were approximately 10 Å/s with a 15 s pause (H_2 and AsH_3/PH_3 ambient) between layers. SIMS depth profiles were taken on a Cameca IMS-3f ion microscope equipped with Cs^+, O_2^+, and Ar^+ sources. The dynamic range and depth resolution of SIMS profiles are limited,[9,10] by atomic mixing, flatness of the sputtered crater, crater edge effects, neutral beam effects and contamination, and cannot be used as an indication of atomic layer resolution. They can be used as an indication of a minimum level of interface abruptness, and are well suited to show in a reasonably quantitative way the presence of longer-range (50–100 Å) systematic transients in AlGaAs composition.[6,7,10]

For high-resolution TEM work, (110) cross-sectional specimens were prepared by ion milling. The TEM photographs and corresponding lattice images were taken on a Philips EM420 microscope with a LaB_6 filament source. This method can image the interfaces at the near atomic level, but it can be difficult to obtain enough contrast between similar materials to infer interface quality. Lattice images were formed by including the transmitted beam, four (111) equivalent diffracted beams and two (002) equivalent diffracted beams. The (111) diffraction intensity from GaAs and AlAs is proportional to $16(f_{Ga}^2 + f_{Al}^2)$ and $16(f_{Al}^2 + f_{As}^2)$, respectively. In the case of a (002) diffracted beam, the diffraction intensity from GaAs and AlAs layers is[11] proportional to $16(f_{Ga} - f_{As})^2$ and $16(f_{Al} - f_{As})^2$, respectively. Since the scattering factors f_{Ga} and f_{As} are nearly identical, the overall diffraction intensity from GaAs layers is lower than from AlAs layers. For the alloy $Al_xGa_{1-x}As$, the (002) diffraction intensity is approximately proportional to $16x^2(f_{Ga} - f_{As})^2$. Thus,

 0021-8979/86/020428-04$02.40

the overall contrast difference between GaAs and $Al_xGa_{1-x}As$ becomes smaller as x is lowered. Very thin specimens (< 100 Å) are used to form the lattice images, and the objective lens defocus is set close to the Scherzer defocus.[12] The point resolution of the Philips EM420 with twin lens is 3.9 Å and therefore not optimum for high-resolution microscopy. Good instrumental stability (line resolution), however, allows us to see the 3.2- and 2.8 Å lattice fringes and interpret correctly the correlation between the lattice image and the interface structure. As shown below, this interpretation is made easier in higher contrast samples.

III. COMPOSITIONAL TRANSIENTS

In order to obtain abrupt transitions between grown layers of different heterostructure materials in an atmospheric pressure MOCVD reactor, the growth rate must be small compared to the time elapsed during change from a stable flow of one composition to a stable flow of another. There are two ways to do this when growing, for example, AlGaAs-GaAs heterostructures. In the first, growth is interrupted[13] while the flow of metal alkyl vapors equilibrates in lines directed to vent. The surface of the previous grown layer is protected by an atmosphere of H_2 and AsH_3. In the second, both AsH_3 and trimethylgallium (TMGa) sources flow continuously while the flow of trimethylaluminum (TMAl) is switched between the reactor and vent as needed. In the case of continuously flowing sources, compositional grading[4,6,7] can result (1) if the growth rate is not small compared to the transit time of TMAl from its inlet, (2) if the transit time is not short compared to diffusion of the TMAl vapor front, or (3) if there is a pressure differential or dead space between the TMAl line and the reactor. Such compositional transients are seen as a marked overshoot and decay in the Al signal of SIMS profiles of $Al_xGa_{1-x}As$-GaAs heterostructures and superlattices. This transient can be up to 100 Å in width but is often smaller[4,6] and occurs when the TMAl flow is directed into the reaction chamber.

In the case of interrupted growth, no such compositional transients should occur unless the relative diffusion of the TMGa and TMAl vapor fronts are very different and, at the same time, fast relative to transit time. Figure 1 is SIMS data taken on an $Al_xGa_{1-x}As$-GaAs ($x = 0.60$) superlattice having layer thicknesses of 500 Å. The As signal variation is due to the matrix effect. The Al signal measured in from the as-grown surface shows the periodicity of the superlattice. In contrast to previously reported SIMS data from superlattices grown without interruption, no overshoot transient is present in these samples. Figure 2 shows similar SIMS data taken on a $GaAs_{0.95}P_{0.05}$-GaAs superlattice. This composition is low enough that the mismatch can be accommodated without generation of dislocations. For the growth of this structure, the TMGa line is directed to vent while the flow rate of the AsH_3 flowing continuously to the reactor is adjusted and PH_3 is added. As expected, since growth only occurs when the metal alkyl vapors are present, there is no evidence of compositional transients in the P signal of the SIMS data.

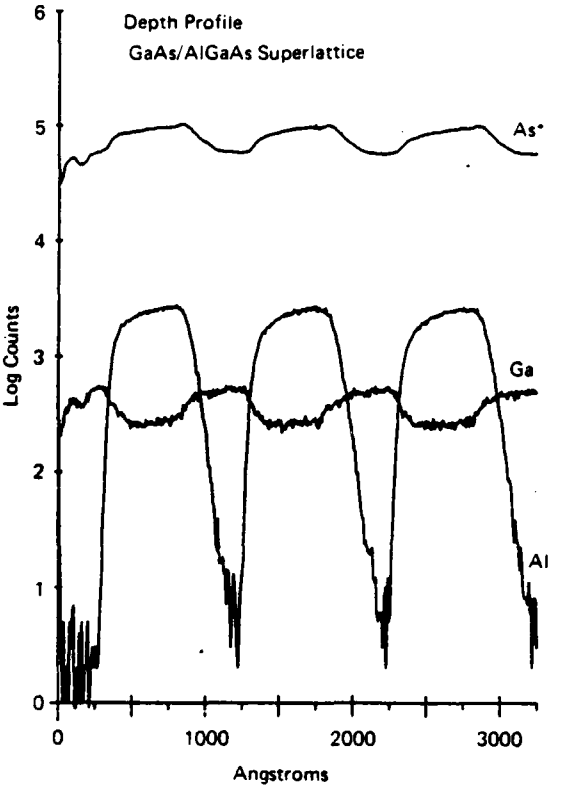

FIG. 1. SIMS profile of an $Al_xGa_{1-x}As$-GaAs ($x = 0.60$) superlattice having 500-Å layer thicknesses. No evidence of a compositional transient is observed in the Al signal.

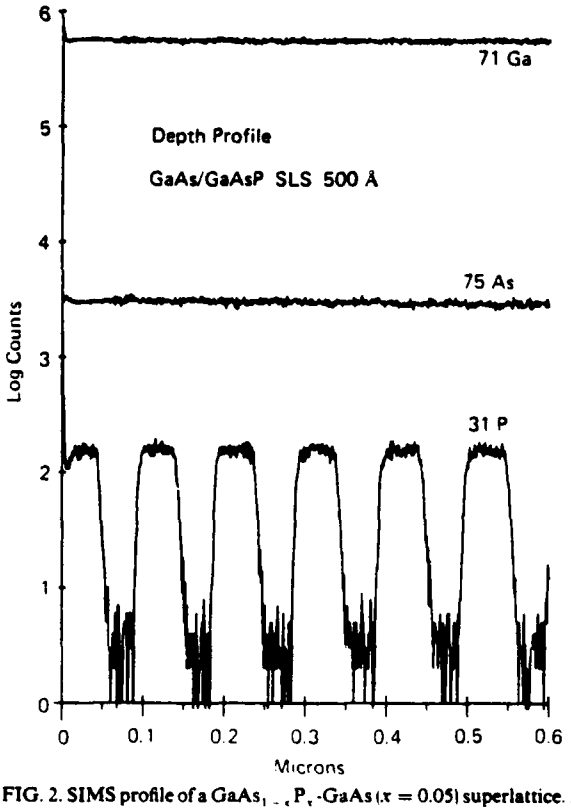

FIG. 2. SIMS profile of a $GaAs_{1-x}P_x$-GaAs ($x = 0.05$) superlattice. At this low composition, the strain introduced by mismatch is accommodated without the formation of dislocations. No compositional transient is observed in either P or As signal.

IV. HIGH-RESOLUTION TEM ANALYSIS

In analyzing high-resolution TEM data obtained from $Al_xGa_{1-x}As$-GaAs heterostructure interfaces, one must be careful to consider a number of fundamental limitations to the measurement. As the composition of the alloy layer is made smaller, contrast between layers is reduced. Also, when samples are made thin enough for effective lattice imaging, a smaller number of atomic layers in the plane of the interface are sampled. Also, as the composition is lowered, there is a stronger probability at the microscopic level of composition deviation from the macroscopic composition.[14] These facts lead to uncertainty in determining the quality and abruptness of the interface, if only lower composition alloy samples are considered. Shown in Fig. 3 is a high-resolution TEM photograph with associated lattice image of an interface (arrow) of the $Al_xGa_{1-x}As$-GaAs ($x = 0.60$) 500-Å superlattice of Fig. 1. As described above, it is difficult to clearly resolve a value for interface width.

Figures 4 and 5 show high-resolution TEM photographs with associated lattice images for parts of two AlAs-GaAs superlattices having 45-Å and 17-Å layer thicknesses, respectively. The contrast between the all-binary layers of these structures is much higher than for the alloy heterostructure of Fig. 3 and there is also no possibility of microscopic compositional variation in all-binary structures. Thus, the interfaces appear sharp and transition from one composition to another occurs in a single atomic layer. The slight difference between the GaAs-on-AlAs interfaces and the AlAs-on-GaAs interfaces in these figures may be related to the dependence of compositional grading on interruption observed by Shealy *et al.*[15] In the worst case, however, this grading occurs in no more than two atomic layers. Figure 6 is a bright-field image of a (110) cross section of an MOCVD-grown single layer (0.5 μm thick) of $GaAs_{0.8}P_{0.2}$ on GaAs. At this magnification, the interface (arrow) shows the defect structure expected for a severely mismatched materials system. The strain introduced by the mismatch between layers is accommodated by the generation of microtwins which propagate into the substrate and to the surface along (111) planes. For reference, the two longest twins are separated by 0.5 μm. Figure 7 is a high-resolution TEM photograph with lattice image of the same single layer of $GaAs_{0.8}P_{0.2}$ on GaAs. Even though this heterostructure materials system is severely mismatched at this composition and the overall diffraction intensity (and contrast) is low, it is still evident that the interface (arrow) is of high quality microscopically and that the transition between layers is abrupt. The microtwin is seen to be approximately 7 or 8 atomic layers wide.

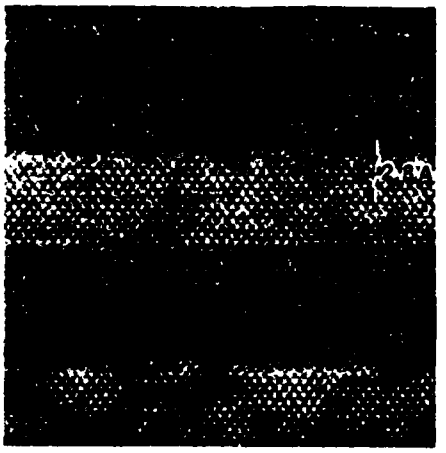

FIG. 4. High-resolution TEM photograph with corresponding lattice image of several interfaces of an AlAs-GaAs superlattice having 45-Å layer thicknesses. The interfaces are clearly distinguishable and are abrupt within a single atomic layer.

V. CONCLUSION

In terms of transients in the composition of heterostructures grown by MOCVD, SIMS data presented here suggest that growth of these structures using the interrupted flow method is preferable to continuous growth methods. It may be possible, however, especially at reduced pressure or in a

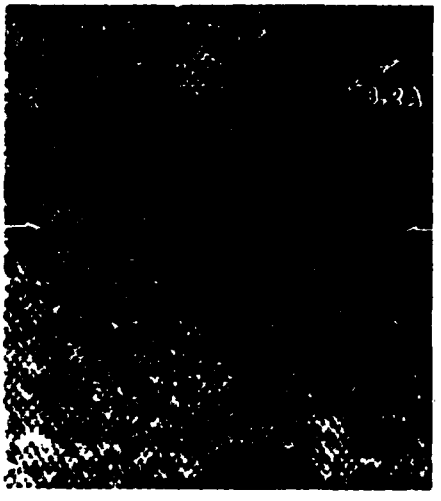

FIG. 3. High-resolution TEM photograph with corresponding lattice image of an $Al_{0.6}Ga_{0.4}As$-GaAs interface of the superlattice of Fig. 1. The interface (arrow) is difficult to distinguish because of low contrast at this composition and the thickness of the specimen.

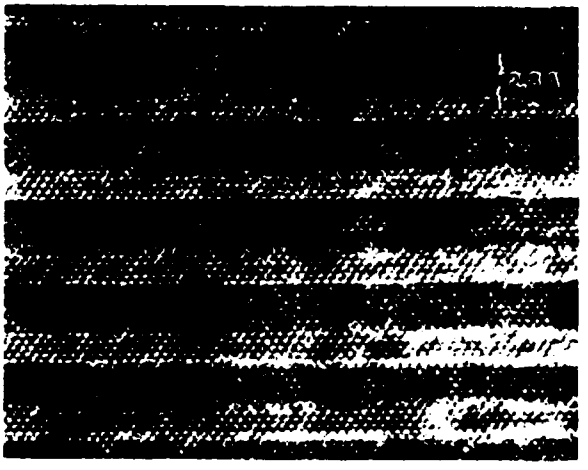

FIG. 5. High-resolution TEM photograph with corresponding lattice image of several periods of an AlAs-GaAs superlattice having 17-Å layer thicknesses. The interfaces are regular, without undulation and abrupt.

FIG. 6. Bright-field image of a (110) cross section of a single $GaAs_{0.8}P_{0.2}$-GaAs interface. The interface (arrow) at this magnification shows the defect structure expected for a mismatched system. The strain is accommodated by the generation of microtwins along (111) planes.

vacuum,[16] to design a continuous flow system which avoids these compositional transients. Since, the kinetics of growth for AlGaAs, GaAsP, GaAs, and AlAs layers is nearly identical for the structures described in this work, it is clear that any question of uniformity or abruptness in lower-composition alloy AlGaAs-GaAs heterostructures results from limitations in the measurement—not in the interrupted MOCVD growth process. It is reasonable to extrapolate from the TEM data taken on all-binary superlattices and the GaAsP-GaAs heterostructure and conclude that the interfaces of MOCVD grown AlGaAs-GaAs heterostructures is abrupt within a single atomic layer. This is, of course, only true in the sense of extension to a large number of atoms in the two-dimensional plane of the interface. As reported previously,[17] no difference between (110) and (110) cross sections is observed and no evidence for nucleation at isolated sites followed by growth along the interface is observed. No undulations[8] are observed in the interfaces of any of these structures. No attempt was made to examine the effect of varying the length of the pause between growth of consecutive layers. Variation in "squareness" or distortion in thin layer size with pause time has been reported.[5] This variation was obtained from analysis of low-temperature PL data taken on samples having confining layer compositions that were rather low ($x = 0.24$–0.36) and growth rates that are somewhat high (12–20 Å/s). There is quite large scatter in the data and no physical measurements were reported, but for shorter pause times (less than 10 s) the optical properties suggest more distortion of the layers and less abrupt interfaces.

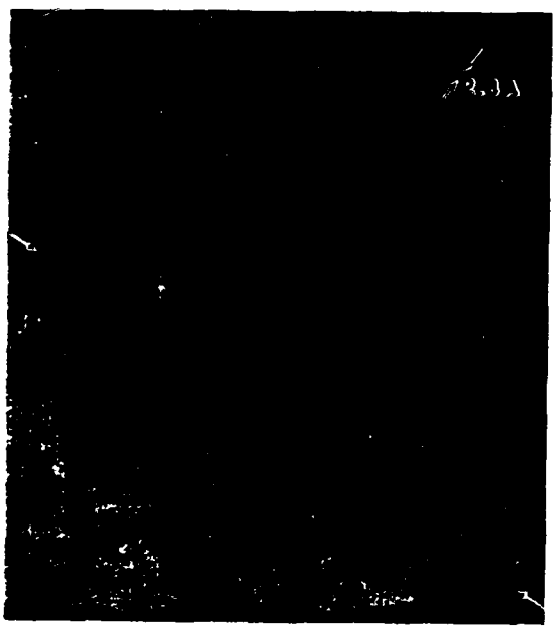

FIG. 7. High-resolution TEM photograph with corresponding lattice image of a single $GaAs_{0.8}P_{0.2}$-GaAs interface (arrow). The interface is microscopically abrupt periodic microtwins (7–8 atomic layers wide) propagating toward the surface along a (111) plane.

ACKNOWLEDGMENTS

The authors would like to thank Y. S. Moroz and P. D. Dapkus for their contributions to this work. This work was funded by the National Science Foundation Grant DMR 83-16981, Army Night Vision Laboratory Contract DAAK 20-84-k-0225 and Navy University Research Instrumentation Grant N00014-84-G-0157.

[1] P. D. Dapkus, Ann. Rev. Mater. Sci. **12**, 243 (1982).
[2] R. D. Dupuis, P. D. Dapkus, A. M. Garner, C. Y. Su, and W. E. Spicer, Appl. Phys. Lett. **34**, 335 (1979).
[3] P. M. Frijlink and J. Maluenda, Jpn. J. Appl. Phys. **21**, 574 (1982).
[4] S. D. Hersee, M. Krakowski, R. Blondeau, M. Baldy, B. de Cremoux, and J. P. Duchemin, J. Cryst. Growth **68**, 383 (1984).
[5] R. D. Dupuis, R. C. Miller, and P. M. Petroff, J. Cryst. Growth **68**, 398 (1984).
[6] E. J. Thrush, J. E. A. Whiteaway, G. Wale-Evans, D. R. Wight, and A. G. Cullis, J. Cryst. Growth **68**, 412 (1984).
[7] J. S. Roberts, N. J. Mason, and M. Robinson, J. Cryst. Growth **68**, 422 (1984).
[8] M. R. Leys, C. van Opdorp, M. P. A. Viegers, and H. J. Talen-van der Mheen, J. Cryst. Growth **68**, 431 (1984).
[9] C. W. Magee and R. E. Honig, Surf. Interf. Anal. **4**, 35 (1982).
[10] R. Holland and G. W. Blackmore, J. Cryst. Growth **68**, 271 (1984).
[11] P. M. Petroff, A. C. Gossard, W. Weigmann, and A. Savage, J. Cryst. Growth **44**, 5 (1978).
[12] J. C. H. Spence, *Experimental High Resolution Electron Microscopy* (Clarendon, Oxford, 1981).
[13] R. D. Dupuis, L. A. Moudy, and P. D. Dapkus, in *Gallium Arsenide and Related Compounds* (Inst. Phys. Conf. Ser. **45**, Bristol, England, 1978), pp. 1–9.
[14] N. Holonyak, Jr. W. D. Laidig, M. D. Camras, K. Hess, M. S. Burroughs, J. J. Coleman, and P. D. Dapkus, J. Appl. Phys. **52**, 6777 (1981).
[15] J. R. Shealy, C. F. Schaus, and G. W. Wicks, Appl. Phys. Lett. **47**, 125 (1985).
[16] L. M. Fraas, P. S. McLeod, J. A. Cape, and L. D. Partain, J. Cryst. Growth **68**, 490 (1984).
[17] S. J. Jeng, C. M. Wayman, J. J. Coleman, and G. Costrini, Mater. Lett. **3**, 89 (1985).

Journal of Crystal Growth 73 (1985) 425–430
North-Holland, Amsterdam

GROWTH MECHANISMS OF GaAsP/GaAs HETEROSTRUCTURES BY METALORGANIC CHEMICAL VAPOUR DEPOSITION

S.J. JENG and C.M. WAYMAN

Department of Metallurgy and Mining Engineering and Materials Research Laboratory, University of Illinois, Urbana, Illinois 61801, USA

and

G. COSTRINI, M.E. GIVENS, M.A. EMANUEL and J.J. COLEMAN

Compound Semiconductor Microelectronics Laboratory, University of Illinois, Urbana, Illinois 61801, USA

Received 8 September 1985

The growth mechanisms for $GaAs_{1-x}P_x/GaAs$ heterostructures grown by metalorganic chemical vapor deposition (MOCVD) have been studied by changing the P composition, which changes the extent of lattice mismatch. Two-dimensional layer growth is found to be dominant with no three-dimensional island growth in evidence, up to a lattice mismatch of 1.4%. The early stages of the epitaxial growth have been studied by conventional transmission electron microscopy and high resolution electron microscopy. Mechanisms for the generation of misfit dislocations and microtwins are described.

1. Introduction

The particular mode of growth assumed by any epitaxial deposition method has a great influence on the type of defects and the defect density in an epitaxial layer. In general, there are three modes of epitaxial growth: two-dimensional layer growth, three-dimensional island growth or a mixture of the two [1,2]. Two-dimensional layer-by-layer growth produces epitaxial layers with sharp interfaces and uniform thicknesses. Metalorganic chemical vapor deposition (MOCVD) [3] has been used to prepare semiconductor heterostructures with abrupt interfaces and large-area growth uniformity [4]. Much of the development of high performance electronic and optoelectronic devices, such as lasers and field effect transistors, is based on the MOCVD growth of sophisticated structures. The effects of growth temperature and lattice mismatch on the growth mode have previously been described for Ge_xSi_{1-x}/Si heterostructures grown by MBE [5–7]. In this paper we have studied by transmission electron microscopy the effect of lattice mismatch on the growth mode of III–V compounds grown by MOCVD. Two-dimensional layer growth is shown to be dominant, with no evidence of any three-dimensional island growth in GaAsP/GaAs heterostructures grown by MOCVD. The early stages of epitaxial growth of GaAsP on GaAs substrates have been studied by using both strong-beam diffraction techniques and high resolution electron microscopy (HREM), and generation mechanisms for misfit defects have been discerned.

2. Experimental methods

Fig. 1 is a schematic diagram of an MOCVD reactor system. Not shown is an additional hydride source line for PH_3 which is similar to the AsH_3 line. High purity trimethylgallium (TMGa) has been used as the Ga source, AsH_3 and PH_3 as the As and P sources, respectively, and H_2 is used as the carrier gas. The fundamental principles which describe the MOCVD growth process are

0022-0248/85/$03.30

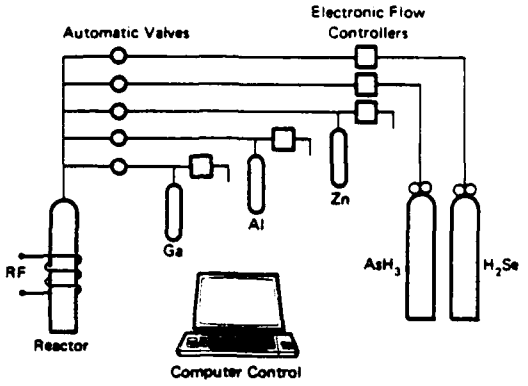

Fig. 1. Schematic diagram of an MOCVD reactor.

hydrodynamics, mass transport theory, thermodynamics and surface kinetics [3,8]. The vapors of the liquid metal alkyl are transported by the H_2 carrier gas, mixed with the gaseous hydrides, and transported to the vicinity of a heated susceptor where they diffuse through a complex boundary layer above the heated substrate. The basic reactions involved are the pyrolysis of TMGa, PH_3 and AsH_3 into Ga atoms and P_4 and As_4 molecules near the heated substrate and, subsequently, the recombination of these atoms and molecules at the substrate surface. A near-thermodynamic equilibrium condition exists at the vapor–substrate interface due to the very small chemical potential drop across the interface [9]. The growth rate is constant over a wide range of temperatures, indicating that it is controlled by the diffusion of the Ga species. For growth under conditions of excess column V reactants, the growth rate is linearly proportional to the Ga flux. Multilayers of different composition can be obtained by using automatic sequencing for switching to different sources. Prior to deposition, the substrate is cleaned with solvents and HCl to remove surface oxides and residual contamination.

$GaAs_{0.8}P_{0.2}$ and $GaAs_{0.6}P_{0.4}$ single layers with various thicknesses were grown by MOCVD on (001) GaAs substrates. (110) cross-sectional and (001) planar specimens of the GaAsP/GaAs heterostructures for TEM observations were prepared by ion-milling. Both strong-beam diffraction and HREM were performed using a Philips EM420 microscope equipped with a LaB_6 filament.

3. Growth mode

There are three modes of epitaxial growth: (1) layer-by-layer growth (Frank–Van der Merwe mode), (2) three-dimensional island growth (Volmer–Weber model), (3) and a mixed mode (Stranski–Krastanov mode) [2]. For epitaxial growth of good quality (i.e., abrupt interface and uniform layer thickness), two-dimensional layer growth is preferred. There are several parameters which will affect the growth mode. Fig. 2 contains a simplified atomistic model of epitaxial growth on a substrate with an orientation of threefold symmetry. As the fourth atom (shaded atom) joins a cluster of three atoms, it can either assume a step site and grow as form **a** (layer growth) or it can diffuse to the top of the cluster and take the form **b** (island growth). The adsorption energy of an

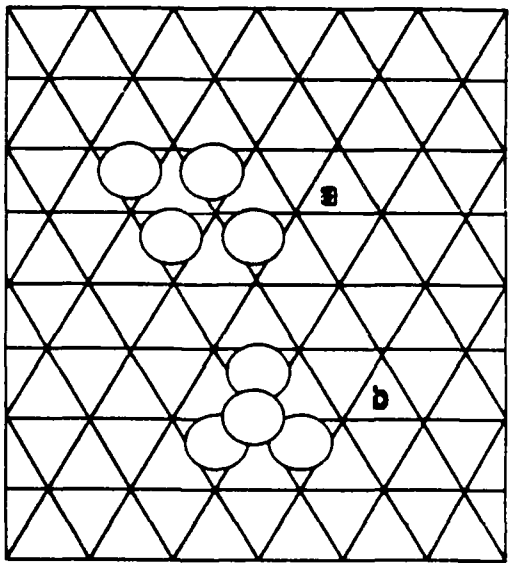

Fig. 2. Simplified atomistic model of epitaxial growth on a substrate with an orientation of three-fold symmetry. The binding energy of a nearest-neighbor bond model for a cluster of four atoms is $4E_a + 5E_b$ for form **a** (layer growth) and $3E_a + 6E_b$ for form **b** (island growth).

isolated adatom on the substrate is E_a and the binding energy between nearest neighbors in the cluster is E_b. Thus, the energy of form **a** will be $4E_a + 5E_b$ and that for form **b** is $3E_a + 6E_b$. The energy difference between the two growth modes is $E_a - E_b$. If $E_a - E_b > 0$ (or $E_a > E_b$), two-dimensional layer growth is dominant, otherwise, three-dimensional island growth dominates [10]. Two-dimensional growth tends to propagate in steps across the surface. Stringfellow has pointed out [11] that in the diamond cubic lattice the (100) and (110) faces are naturally rough, while the close-packed (111) surface is smooth. Crystallographic steps may be required for growth on a (111) substrate surface, implying that growth will occur at steps which are present due to thermal roughening or misorientation. Layer growth can also be disturbed by impurities or defects incorporated into the growing film, which may affect the nucleation kinetics or cause adsorption at kink sites at the edges of the growing layers [10,12]. In summary, then, the mode of nucleation and growth of epitaxial layers is governed by the bonding energy between deposited species and substrate E_a, the cohesive binding energy in the deposited cluster E_b, the diffusion energy of adatoms on the substrate surface, the substrate surface topography and microstructure, the presence of contaminants, the substrate temperature, and the lattice mismatch.

4. Results and discussion

Two-dimensional layer growth has been discussed by Frank and Van der Merwe [13] and Van der Merwe [14]. They proposed that when the epitaxial layer is thin, it is elastically strained to match the substrate providing the lattice mismatch, f, is less than 12%. As the film thickness is increased, part of the strain will be accommodated by misfit dislocation formation at the interface. The critical thickness, h_c, calculated by Matthews et al. [15] for the misfit dislocation formation is

$$h_c = [b/8\pi f(1+\nu)]\ \ln(h_c/b),$$

where b is the Burgers vector, ν is Poisson's ratio,

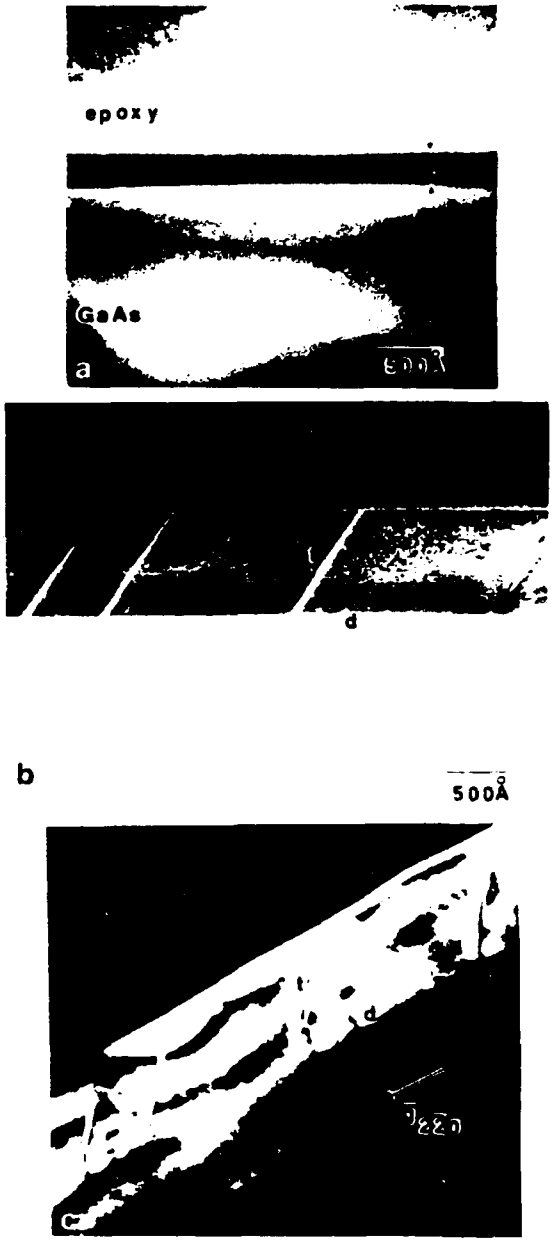

Fig. 3. (002) Dark field images of $GaAs_{0.8}P_{0.2}$/GaAs heterostructures grown by MOCVD with $GaAs_{0.8}P_{0.2}$ layer thickness of 200 Å in (a) and 800 Å in (b). For the 200 Å case, the interface is smooth and without defects indicating that layer-by-layer growth has occurred. A (2$\bar{2}$0) dark field image (c) of an 800 Å layer shows a dislocation d at the interface. The fringe contrast t is due to microtwins. (b) Marker represents 500 Å.

and f is the lattice mismatch. Fig. 3 shows (002) dark field images of $GaAs_{0.8}P_{0.2}$ single epilayers grown by MOCVD on GaAs substrates having layer thicknesses of (a) 200 Å and (b) 800 Å. For the 200 Å case, the interface is smooth and without defects indicating that the growth mode is two-dimensional layer growth. As the layer thickness is increased beyond h_c, microtwins and dislocations are formed as shown in (b). Figure 3c is a $(2\bar{2}0)$ dark field image of an 800 Å layer showing dislocations (d) at the interface. The fringe contrast (t) is due to a microtown. The mismatch between $GaAs_{0.8}P_{0.2}$ and GaAs is 0.71%, which yields a calculated h_c of 140 Å. The critical thickness, h_c, for the misfit defects formation must be greater than 200 Å (fig. 3a), which is larger than the value calculated by Matthews' model. The discrepancy may be due to (1) a large Peierls stress in zinc-blende structures, (2) an oversimplified dislocation configuration in Matthews' model, (3) interfacial nucleation [6] (only surface nucleation of dislocations is assumed in Matthews' model), or (4) dislocation-induced elastic strain.

Fig. 4 shows (002) dark field images of

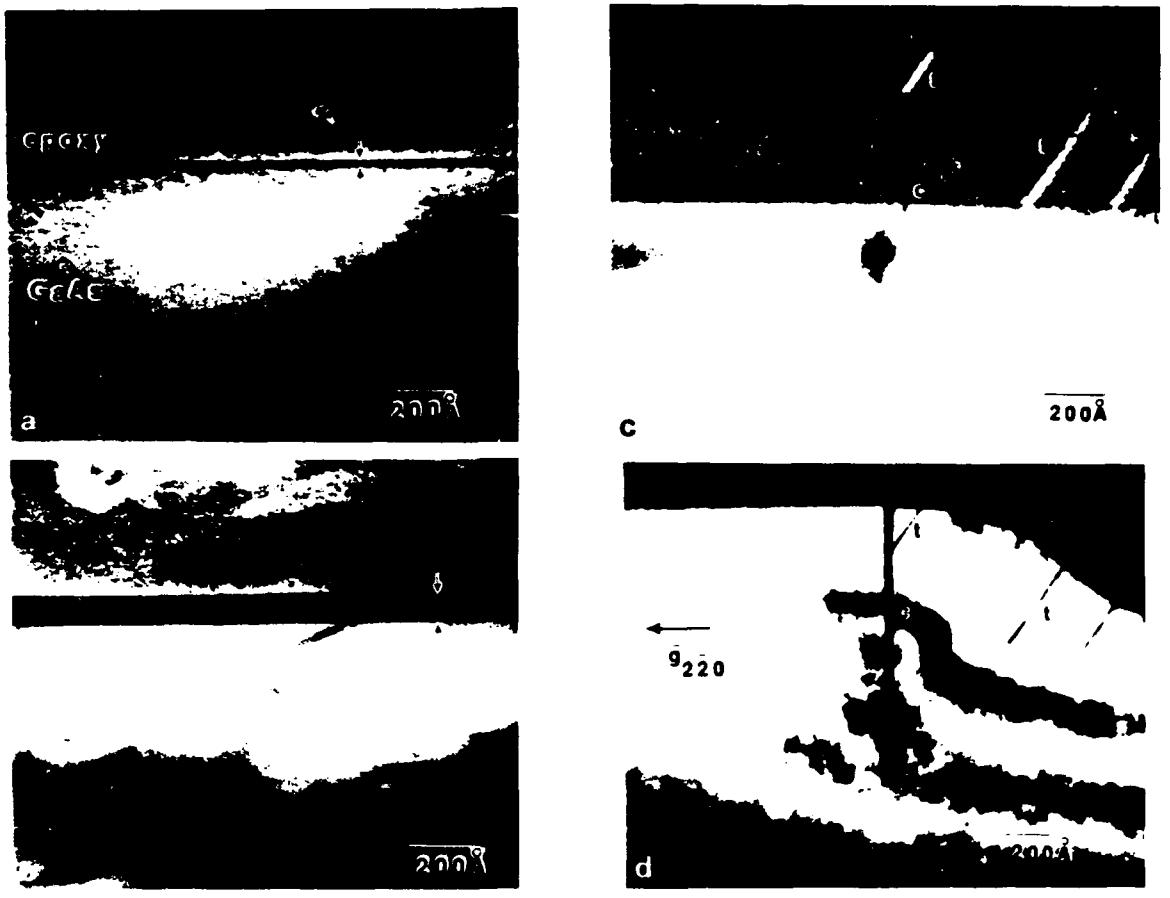

Fig. 4. (002) Dark field images of $GaAs_{0.6}P_{0.4}$/GaAs heterostructures grown by MOCVD with layer thickness of (a) 20 Å, (b) 100 Å and (c) 500 Å. Both the 20 Å and 100 Å layers show that the growth mode is layer-by-layer growth, and that the interface is smooth without defects. For the 500 Å layer, microtwins t and microcracks c are introduced. A $(2\bar{2}0)$ dark field image (d) of the 500 Å layer shows microtwins t and microcracks c.

$GaAs_{0.6}P_{0.4}$/GaAs heterostructures grown by MOCVD having layer thicknesses of (a) 20 Å, (b) 100 Å and (c) 500 Å. The interface is smooth and without defects for both 20 Å and 100 Å layers, implying that layer-by-layer growth has occurred. Fig. 4d is a $(2\bar{2}0)$ dark field image of the 500 Å layer which shows the presence of microtwins (t) and microcracks (c). Microcracks occur more read-

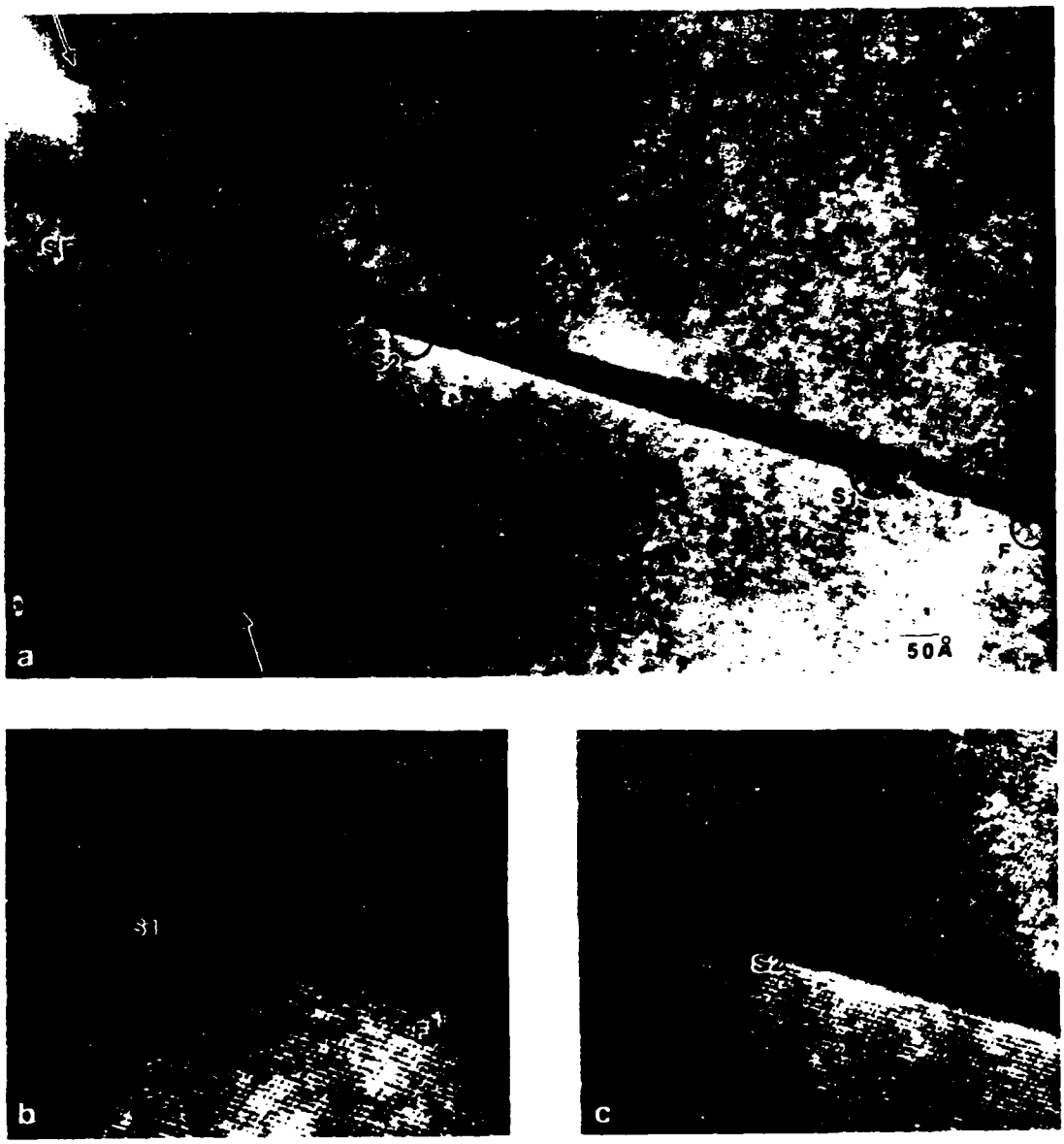

Fig. 5. Lattice image of a microtwin in a $GaAs_{0.8}P_{0.2}$/GaAs heterostructure having a $GaAs_{0.8}P_{0.2}$ layer thickness of 5000 Å. The twinning plane is {111}. Enlargement (b) of circled regions F and S1 shows a Frank partial and a Shockley partial at the twin boundary. Enlargement (c) of S2 shows another Shockley partial at the twin boundary.

ily when the epilayer is under tension rather than compression and can be eliminated by growing a compositionally graded layer prior to growth of the epilayer. The mismatch between $GaAs_{0.6}P_{0.4}$ and GaAs is 1.4% yielding a calculated h_c of 60 Å. As above, the calculated h_c is smaller than the apparent h_c (> 100 Å). There is no evidence of any island growth, and the origin of microtwins or dislocations is not likely to be due to the coalescing of misfit islands in the early stages of growth [16]. Instead, for two-dimensional layer growth, a possible nucleation mechanism for dislocations is (1) dislocation nucleation at the edge of the growing layer and slip into the interface, (2) climbing of a dislocation loop nucleus from the free surface with dissociation at the interface [17,18], or (3) interfacial nucleation occurring at a local high-stress area. The origin of the microtwins is probably nucleation of either Frank or Shockley partials at localized stress concentrators (either at the surface or interface). The motion of partial dislocations by shear stress and subsequent coalescence of the associated stacking faults will create microtwins. Fig. 5a shows a microtwin with a width of 28 Å in a $GaAs_{0.8}P_{0.2}$/GaAs heterostructure (the layer thickness of the $GaAs_{0.8}P_{0.2}$ is 5000 Å. The twinning plane is [111]. The microtwin tapers when approaching the interface (indicated by arrows). After passing the interface, the microtwin intersects a stacking fault (SF). Figs. 5b and 5c contain enlarged lattice images of the circled regions S1, F and S2 and indicate the Frank and Shockley partials located at the twin boundary.

5. Conclusion

The growth mode of $GaAs_{1-x}P_x$/GaAs heterostructures grown by MOCVD has been studied by varying the lattice mismatch between the $GaAs_{1-x}P_x$ and GaAs. Two-dimensional layer-by-layer growth dominates with no evidence of three-dimensional island growth up to lattice mismatches of 1.4%. The apparent critical thickness for misfit defect formation, h_c, is larger than that calculated from Matthews' model. The discrepancy may be due to an oversimplified dislocation configuration used in Matthews' model, the large Peierls stress in the zinc-blende structure or the possible interfacial nucleation of misfit defects. For two-dimensional layer growth, the most likely origin of misfit defect generation is the nucleation of defects at stress concentrators at either the surface or the interface.

Acknowledgements

We gratefully acknowledge the support of the Army Night Vision Laboratory (Contract DAAK 20-84-K-0225), the Office of Naval Research (Grant N00014-84-G-0157), and the National Science Foundation through the Materials Research Laboratory at the University of Illinois, Grant NSF/DMR 83-16981.

References

[1] M.J. Stowell, Defects in Epitaxial Deposits, in: Epitaxial Growth, Part B, Ed. J.W. Matthews (Academic Press, New York, 1975).
[2] R.W. Vook, Intern. Metals Rev. 27 (1982) 209.
[3] P.D. Dapkus, Ann. Rev. Mater. Sci. 12 (1982) 24.
[4] S.J. Jeng, C.M. Wayman, J.J. Coleman and G. Costrini, Mater. Letters 3 (1985) 89.
[5] J.C. Bean, L.C. Feldman, A.T. Fiory, S. Nakahara and I.K. Robinson, J. Vacuum Sci. Technol. A2 (1984) 436.
[6] R. Hull, A.T. Fiory, J.C. Bean, J.M. Gibson, L. Scott, J.L. Benton and S. Nakahara, 13th Intern. Conf. on Defects in Semiconductors, Corondo, CA, 1984.
[7] E. Kasper, H.J. Herzog and H. Kibbel, Appl. Phys. 8 (1975) 199.
[8] P.D. Dapkus, J. Crystal Growth 68 (1984) 345.
[9] G.B. Stringfellow, J. Crystal Growth 70 (1984) 133.
[10] J.A. Venables and G.L. Price, Nucleation of Thin Films, in: Epitaxial Growth, Part B, Ed. J.W. Matthews (Academic Press, New York, 1975).
[11] G.B. Stringfellow, Rept. Progr. Phys. 45 (1982) 469.
[12] B.A. Joyce, Rept. Progr. Phys. 37 (1974) 363.
[13] F.C. Frank and J.H. van der Merwe, Proc. Roy. Soc. (London) A198 (1949) 216.
[14] J.H. van der Merwe, Surface Sci. 31 (1972) 198.
[15] J.W. Matthews and A.E. Blakeslee, J. Crystal Growth 27 (1974) 118.
[16] S.J. Jeng, C.M. Wayman, G. Costrini and J.J. Coleman, Mater. Letters 3 (1985) 331.
[17] D. Cherns and M.J. Stowell, Scripta Met. 7 (1973) 489.
[18] K. Yagi, K. Takayanagi, K. Kobayashi and G. Honjo, J. Crystal Growth 9 (1971) 84.

Phase-locked shallow mesa graded barrier quantum well laser arrays

L. J. Mawst, M. E. Givens, M. A. Emanuel, C. A. Zmudzinski, and J. J. Coleman
Compound Semiconductor Microelectronics Laboratory, Department of Electrical and Computer Engineering, University of Illinois at Urbana–Champaign, Urbana, Illinois 61801

(Received 24 January 1986; accepted for publication 26 March 1986)

Graded barrier quantum well heterostructures have been grown by metalorganic chemical vapor deposition and processed into real index-guided shallow mesa laser arrays. Single-stripe devices have threshold currents as low as 14 mA (533 μm length) and ten-element arrays have threshold currents as low as 9 mA per stripe with 52% differential quantum efficiency. These arrays operate phase locked with sharp double-lobed far-field patterns up to 1.75 times threshold current.

Phase-locked semiconductor laser arrays have been shown to be capable of high output power and narrow stabilized far-field patterns.[1,2] Unless sufficient gain is introduced in the region between array elements,[3] a characteristic double-lobed far-field pattern is observed. This indicates that the laser is operating primarily in the highest order array mode with a 180° phase shift between neighboring elements.[4] In contrast to purely gain-guided devices, arrays with built-in real refractive index variations along the plane of the junction offer stable transverse modes and astigmatic output beams.[2] Several different structures have been utilized to form index-guided arrays,[2,3,5] with perhaps the simplest being the shallow mesa array. Besides relative ease of fabrication, mesa arrays have relatively small effective index changes between array elements. This allows the device to have stable near-field patterns, with sufficient coupling between elements to phase lock the output of the array.

Shallow mesa arrays, utilizing Schottky-barrier current confinement, were recently fabricated from large optical cavity active layer laser structures.[2] After masking the stripe regions, mesas are formed by wet chemical etching of the regions between the stripes up to a point near ($\sim$0.5 μm), but not through, the active layer. The entire sample is metallized with Cr/Au providing an ohmic contact in the stripe region and Schottky barriers outside the mesas. Because the device has a planar active layer, any underlying laser structure active region can be used.

In this letter we report shallow mesa arrays which have been fabricated using a graded barrier quantum well heterostructure grown by metalorganic chemical vapor deposition (MOCVD). The laser structure (shown in Fig. 1) consists of an n-GaAs buffer layer (0.5 μm), an n-AlGaAs graded layer $x = 0$–0.6 (1.0 μm), an n-$Al_{0.6}Ga_{0.4}As$ confining layer (2.0 μm), an n-AlGaAs parabolic graded region $x = 0.6$–0.2 (0.2 μm), a 50 Å undoped quantum well, a p-AlGaAs parabolic graded region $x = 0.2$–0.6 (0.2 μm), a p-$Al_{0.6}Ga_{0.4}As$ confining layer (2.0 μm), and a p^+-GaAs cap layer (0.2 μm). The n-confining layer is doped 3×10^{17} cm^{-3}, the p-confining layer at 8×10^{17} cm^{-3}, while both graded regions are doped at 2×10^{17} cm^{-3}. The graded barrier region, illustrated in Fig. 1 enhances the collection of carriers in the quantum well[6] and provides a large optical cavity which improves the laser confinement factor in comparison with a single isolated quantum well.[7] Low laser threshold currents are obtained with this structure, primarily due to the quantum size effect which shifts the peak gain towards higher energy (larger density of states for optical transitions).[8] In addition, the relatively large graded barrier active region is ideal for array structures, having increased optical coupling between array elements relative to that of a narrow conventional double heterostructure active layer.

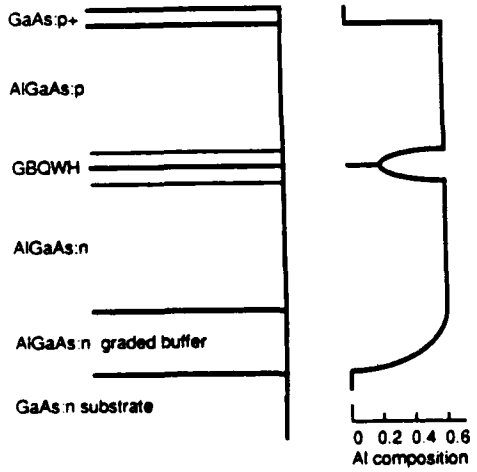

FIG. 1. Schematic diagram of graded barrier quantum well laser structure and the profile of the aluminum concentration in the structure.

FIG. 2. Scanning electron micrograph at two magnifications of ten-stripe graded barrier quantum well heterostructure shallow mesa array structure.

 0003-6951/86/201337-03$01.00

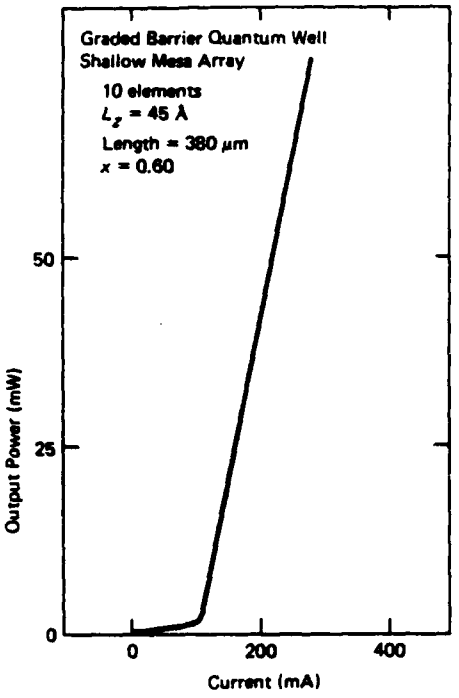

FIG. 3. Typical pulsed L-I characteristic of a ten- element graded barrier quantum well heterostructure shallow mesa laser array. Differential quantum efficiencies of 52% are obtained for this length device.

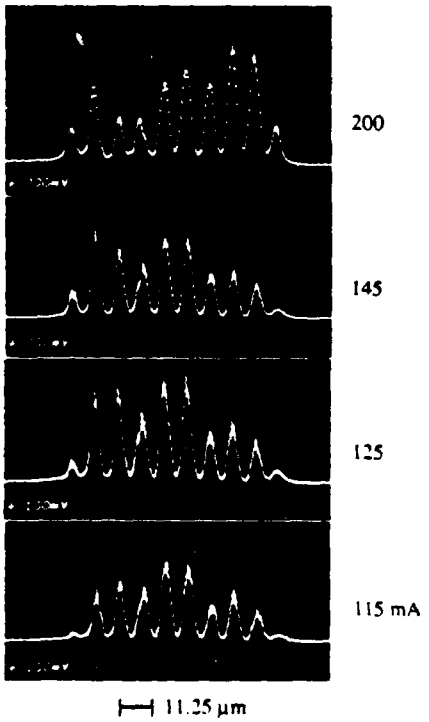

FIG. 4. Near-field radiation patterns of a ten-element graded barrier quantum well heterostructure shallow mesa laser array at several drive currents above threshold. No shift in the optical field is observed as the drive current is increased.

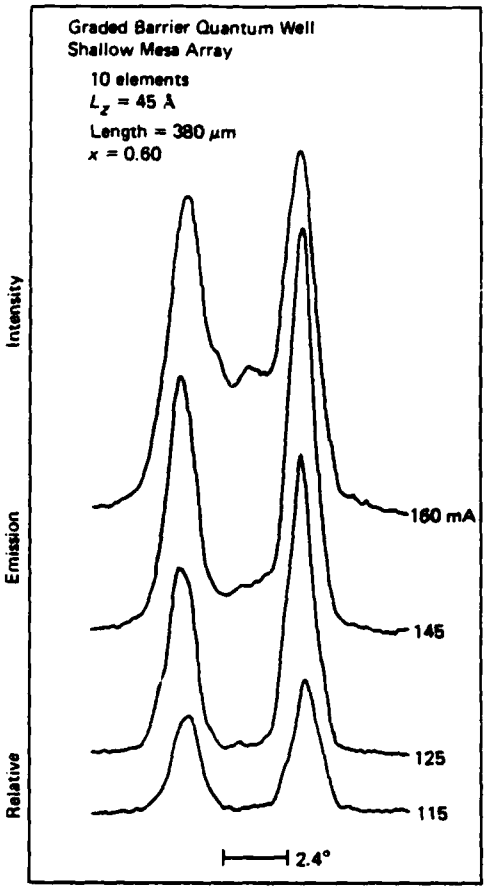

FIG. 5. Far-field radiation patterns of a ten-element graded barrier quantum well heterostructure shallow mesa laser array. Phase-locked operation is indicated by the double-lobed pattern and is observed from just above laser threshold to more than twice threshold.

Single-stripe and ten-stripe devices have been fabricated by etching (1:8:10 H_2SO_4:H_2O_2:H_2O at 0 °C) to within 0.4 μm of the edge of the graded region. All devices have 4.5-μm-wide mesas and 8-μm center-to-center spacing. A scanning electron micrograph of the ten-stripe array structure at two magnifications is shown in Fig. 2.

Single-stripe devices have threshold currents as low as 14 mA for devices 533 μm in length. These devices have been operated cw up to 25 mW per uncoated facet, with external differential quantum efficiencies of ~70%. During cw operation, a single longitudinal mode is observed at a wavelength near 8200 Å, which is close to the value expected for a 50-Å well and $x = 0.20$ Al barriers as calculated from a finite well model (8215 Å). The pulsed (1 μs, 2 kHz) light output power-current characteristics of a typical ten-stripe device are shown in Fig. 3. These devices have threshold currents between 90 and 100 mA (9–10 mA per stripe) for a 381-μm-long cavity. External differential quantum efficiencies of 52% are obtained for this length device.

The near-field pattern at several different drive currents above threshold of the ten-stripe array of Fig. 3 is shown in Fig. 4. Just above threshold all ten stripes of the array are lasing. No shift in the optical field is observed as the drive current is increased, in contrast to purely gain-guided de-

vices.[9] Far-field patterns of the same ten-element device are shown in Fig. 5. Phase-locked operation is observed from just above laser threshold to more than twice threshold. The lobe separations are 4.5° to 4.7° with the individual lobes as narrow as 1.1° at the half-power points. The expected far-field lobe separation, based on diffraction theory calculations,[9] is 5.8° for a center-to-center stripe spacing of 8 μm. At currents higher than ~ 1.75 times threshold the sharp double-lobed patterns begin to merge and additional features are observed. The optical emission spectra of these devices show single longitudinal mode operation up to the current levels at which the far-field patterns begin to show deviation from the sharply peaked double-lobed pattern ($1.75 \times I_{th}$). The onset of additional array modes at these high-current levels results in broadening of the individual lobes of the far-field pattern. Increased stabilization of the transverse modes at high drive currents, by the introduction of a stronger index variation along the junction plane, would result in a stable phase-locked far-field pattern at higher output power levels. Self-aligned lasers[10] have, in addition to strong index guiding, regions of high absorption placed outside the stripe width in order to discriminate against high-order transverse modes. The use of self-aligned lasers as array elements would force the array to operate in its highest order normal mode (180° phase shift between emitters) up to high output power levels.

In conclusion, low threshold, shallow mesa graded barrier quantum well arrays have been described. These devices operate phase locked up to $1.75 \times I_{th}$ with threshold currents as low as 9 mA per stripe. Differential quantum efficiencies of 70% and 52% have been obtained for single- and ten-stripe devices. No shifts in the near-field patterns are observed as the drive current is increased. The double-lobed far-field patterns characteristic of phase-locked operation are observed from just above laser threshold to more than twice threshold.

The authors would like to thank G. Costrini, S. J. Jeng, C. W. Trussell, D. Caffey, and Y. S. Moroz for helpful discussions and technical assistance. This work was supported by U.S. Army Night Vision Laboratory contract DAAK 20-84-K-0225 and by U.S. Army Research Office contract DAAG 29-85-G-0133.

[1] D. R. Scifres, C. Lindstrom, R. D. Burnham, W. Streifer, and T. L. Paoli, Electron. Lett. 19, 169 (1983).
[2] H. Temkin, R. A. Logan, J. P. van der Ziel, C. L. Reynolds, Jr., and S. M. Tharaldsen, Appl. Phys. Lett. 46, 465 (1985).
[3] Y. Twu, A. Dienes, S. Wang, and J. R. Whinnery, Appl. Phys. Lett. 45, 709 (1984).
[4] J. K. Butler, D. E. Ackley, and D. Botez, Appl. Phys. Lett. 44, 293 (1984).
[5] P. Gavrilovic, K. Meehan, J. E. Epler, N. Holonyak, Jr., R. D. Burnham, R. L. Thornton, and W. Streifer, Appl. Phys. Lett. 46, 857 (1985).
[6] S. D. Hersee, B. de Cremoux, and J.P. Duchemin, Appl. Phys. Lett. 44, 476 (1984).
[7] W. T. Tsang, Appl. Phys. Lett. 39, 134 (1981).
[8] D. Kasemset, C. S. Hong, N. B. Patel, and P. D. Dapkus, Appl. Phys. Lett. 41, 912 (1982).
[9] J. P. van der Ziel, R. M. Mikulyak, H. Temkin, R. A. Logan, and R. D. Dupuis, IEEE J. Quantum Electron. QE-20, 1259 (1984).
[10] L. J. Mawst, G. Costrini, C. A. Zmudzinski, M. E. Givens, M. A. Emanuel, and J. J. Coleman, Electron. Lett. 21, 903 (1985).

Phase locked narrow zinc diffused stripe laser arrays

C. A. Zmudzinski, L. J. Mawst, M. E. Givens, M. A. Emanuel, and J. J. Coleman
Compound Semiconductor Microelectronics Laboratory, Department of Electrical and Computer Engineering, University of Illinois at Urbana–Champaign, Urbana, Illinois 61801

(Received 12 March 1986; accepted for publication 31 March 1986)

Phase locked operation of an array of narrow diffused stripe conventional double heterostructure laser elements grown by metalorganic chemical vapor deposition is reported. Six-element arrays (length 356 μm) show threshold currents of 33 mA per stripe and peak power outputs of at least 160 mW per facet with total external differential quantum efficiencies of 33%. Complex near-field patterns are shown which result from two opposing mechanisms involved in guiding of the lateral modes. Three major lobes in far-field patterns, which correspond to expected patterns for the lateral modes of gain guided arrays, are described.

Phase locked semiconductor laser arrays have been studied with great interest with the goal of achieving high power operation with stable far-field patterns.[1,2] Gain guided laser arrays, such as oxide-defined stripe arrays[3] or proton-bombarded stripe arrays,[4,5] are often the simplest to fabricate since they require only current limiting stripes. This is in contrast to arrays made up of real- or complex-index guided laser elements, such as the shallow mesa stripe laser[6] or the complementary self-aligned laser,[7] which normally require more complicated processing such as chemical etching and regrowth. In this letter we report the phase locked operation of an array of narrow diffused stripe (NDS)[8] conventional double heterostructure laser elements grown by metalorganic chemical vapor deposition (MOCVD). Current confinement is provided in these structures by a reverse biased *p-n* junction outside the diffused stripe with current spreading limited to the active layer and a thin AlGaAs:*p* layer just above the GaAs active layer. The threshold characteristics and near- and far-field optical patterns of gain guided six-element phase locked NDS laser arrays having threshold currents of 33 mA per stripe are presented.

The laser structure used in this work was grown by MOCVD and is shown in Fig. 1. The as-grown structure consists of (1) a 0.5-μm GaAs:*n* buffer layer, (2) a 1.0-μm AlGaAs:*n* layer graded from $x = 0$–0.60, (3) a 2.0-μm $Al_{0.60}Ga_{0.40}As$:*n* confining layer, (4) a 500-Å undoped GaAs active layer, (5) a 0.25-μm $Al_{0.60}Ga_{0.40}As$:*p* diffusion pickup layer, (6) a 1.75-μm $Al_{0.60}Ga_{0.40}As$:*n* current blocking layer, and (7) a 0.2-μm GaAs:*n* cap layer. The *n*-type confining layer and the current blocking layer are both doped with selenium at 1×10^{18} cm^{-3}, and the *p*-type pickup layer is doped with zinc at 10^{18} cm^{-3}. A 1000-Å layer of Si_3N_4 is deposited on the wafer, and a six-stripe array (8-μm-wide stripes, 12-μm center-to-center spacing) is defined in the Si_3N_4 mask. The zinc diffusion is carried out in an evacuated quartz ampule at $T = 670$ °C for $t = 21$ min using a $ZnAs_2$ source. The time and temperature profile is adjusted so that the diffusion front traverses the AlGaAs:*n* current blocking layer and just reaches the AlGaAs:*p* diffusion pickup layer.[8] A scanning electron micrograph of a six-element narrow zinc diffused stripe array is also shown in Fig. 1. Because of the nearly isotropic nature of zinc diffusion in these structures and the resulting spreading under the mask edges, it is difficult to accurately define a stripe width. The stripe width of the devices reported here is taken to be the width at the point where the diffusion profile just reaches the diffusion pickup layer and was found to be 5.5 μm for the six-element array.

The laser diodes of this work were tested for pulsed operation with 1.5-μs pulses at a 2-kHz repetition rate. Figure 2 shows a pulsed *L-I* curve for a six-stripe array (length = 356 μm) showing a threshold current of 200 mA (33 mA per stripe) and a peak power output of at least 160 mW per facet. Higher power output per facet is possible but is beyond the current limit of our pulse generator. The threshold current of a 6.5-μm-wide single stripe device fabricated from the same starting material was approximately 50 mA. The total external differential quantum efficiency of the six-element array shown in Fig. 2 is 33%.

The near-field radiation patterns for the six-element array described above are shown in Fig. 3. Six major peaks are observed which correspond to the field intensity under each

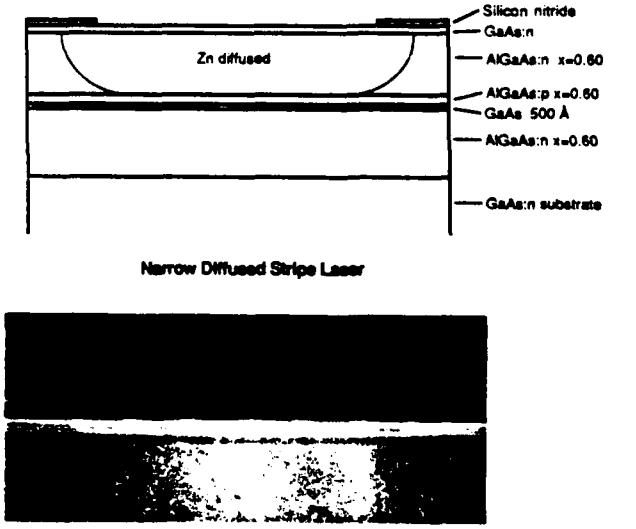

FIG. 1. Schematic diagram of the cross section of a single-element narrow diffused stripe (NDS) laser and a SEM photograph of a six-element NDS laser array. The stripe width is taken to be the width at the point where the diffusion profile intersects the top of the pickup layer.

 0003-6951/86/211424-03$01.00

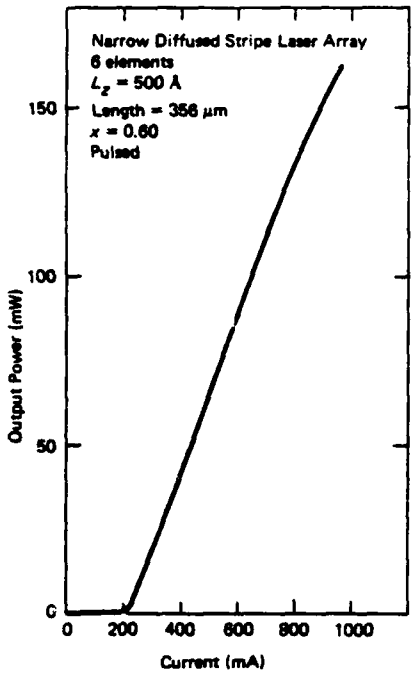

FIG. 2. Pulsed L-I curve for a typical six-element NDS laser array (length 356 μm). The threshold current is 33 mA per element, with a power output per facet of at least 160 mW and a total external differential quantum efficiency of 33%.

stripe. In addition, five smaller peaks are present, one between each stripe. These smaller intensity peaks between the stripes are characteristic of gain guided arrays and result from carrier induced antiguiding.[2,4] Two opposing mechanisms are involved with guiding of the lateral modes. Optical gain is greatest within the stripe regions, while carrier induced variations in the refractive index act to focus the light between the stripe regions. The lack of a built-in real or complex refractive index variation along the plane of the junction leads to unstable lateral modes at higher injection currents and complicates the near-field patterns. Far-field radiation patterns along the plane of the junction for a six-element array are shown in Fig. 4. Three major lobes are observed in agreement with patterns predicted by theoretical calculations of the lateral modes of uniformly pumped gain guided arrays.[2] These observed far-field patterns are also similar to the far-field patterns observed from uniformly pumped proton-bombarded laser arrays.[4] Plane-wave diffraction theory[9] correctly predicts the qualitative features of the far-field pattern even though the actual phase fronts are not planar due to the gain guiding. The three-lobed pattern with larger intensity outer lobes corresponds to an in-phase coupling array mode. Three lobes are present, instead of the single lobe usually associated with in-phase operation, as a result of broadening of the single emitter far-field pattern due to carrier induced antiguiding.[2] The center lobe is depressed because of the central minimum in the single emitter far-field pattern which results from the tilted phase fronts associated with carrier induced antiguiding.[10] The calculat-

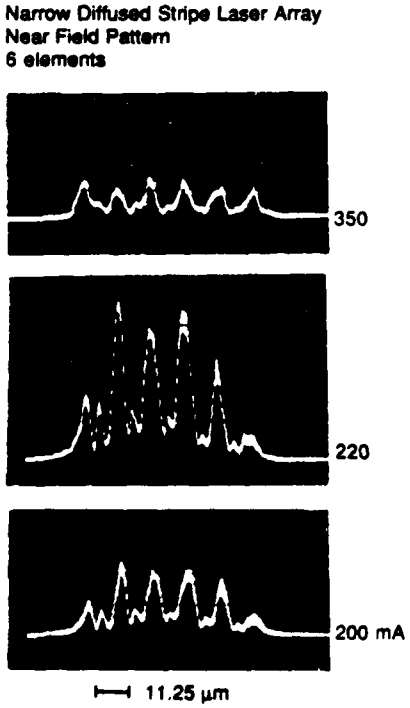

FIG. 3. Near-field radiation patterns for a six-element NDS laser array. The small peaks at threshold between elements are the result of carrier induced index variations along the junction plane which focus some of the light outside the stripe.

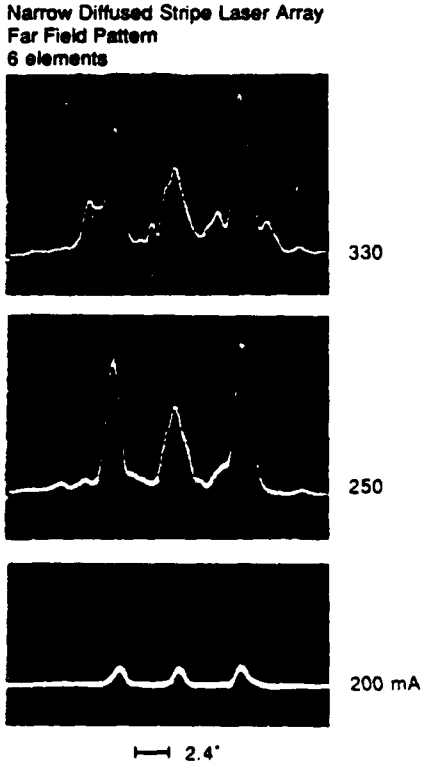

FIG. 4. Far-field radiation patterns for a six-element NDS laser array. The three-lobed far-field pattern at threshold is characteristic of uniformly pumped, phase locked, gain guided arrays.

ed outer lobe separation determined from diffraction theory for a center-to-center emitter spacing of 12 μm is 8.4°, while the experimentally measured value for these devices is 9.3°.

In this letter we have reported the phase locked operation of an array of narrow diffused stripe (NDS) conventional double heterostructure laser elements grown by metalorganic chemical vapor deposition (MOCVD). Six-stripe arrays (length = 356 μm) show threshold currents of 33 mA per stripe and peak power outputs of at least 160 mW per facet and total external differential quantum efficiencies of 33%. Complex near-field patterns have been observed which are characteristic of the two opposing mechanisms involved in guiding of the lateral modes. Three major lobes are observed in far-field patterns which correspond to expected patterns for the lateral modes of gain guided arrays. The narrow diffused stripe laser array could be improved by use of a quantum well active layer in place of the double heterostructure active layer structure reported here. In addition, the stripe widths and center-to-center spacings could be varied across the array to tailor the gain profile[1,11] in order to obtain single-lobed far-field patterns.

The authors would like to thank Y. S. Moroz, B. K. Moroz, and C. W. Trussell for their contributions to this work. This work was supported in part by ANVL contract DAAK 20-84-K-0225 and ARO contract DAAG 29-85-G-0133.

[1] C. P. Lindsey, E. Kapon, J. Katz, S. Margalit, and A. Yariv, Appl. Phys. Lett. 45, 722 (1984).
[2] G. P. Agrawal, J. Appl. Phys. 58, 2922 (1985).
[3] J. E. Ripper and T. L. Paoli, Appl. Phys. Lett. 17, 371 (1970).
[4] T. L. Paoli, W. Streifer, and R. D. Burnham, Appl. Phys. Lett. 45, 217 (1984).
[5] D. Scifres, R. D. Burnham, W. Streifer, and M. Bernstein, Appl. Phys. Lett. 41, 614 (1982).
[6] T. Tsukada, R. Ito, H. Nakashima, and O. Nakada, IEEE J. Quantum Electron. QE-9, 356 (1973).
[7] L. J. Mawst, G. Costrini, C. A. Zmudzinski, M. E. Givens, M. A. Emanuel, and J. J. Coleman, Electron. Lett. 21, 903 (1985).
[8] C. S. Hong, J. J. Coleman, P. D. Dapkus, and Y. Z. Liu, Appl. Phys. Lett. 40, 208 (1982).
[9] D. R. Scifres, W. Streifer, and R. D. Burnham, IEEE J. Quantum Electron. QE-15, 917 (1979).
[10] W. Streifer, R. D. Burnham, and D. R. Scifres, IEEE J. Quantum Electron. QE-18, 856 (1982).
[11] E. Kapon, C. P. Lindsey, J. S. Smith, S. Margalit, and A. Yariv, Appl. Phys. Lett. 45, 1257 (1984).

Near- and far-field observations of transient behavior in pulsed graded barrier quantum well lasers

L. J. Mawst, M. E. Givens, C. A. Zmudzinski, M. A. Emanuel, and J. J. Coleman
Center for Compound Semiconductor Microelectronics, Department of Electrical and Computer Engineering, University of Illinois, Urbana, Illinois 61801

(Received 2 June 1986; accepted for publication 1 July 1986)

The pulsed behavior of both gain-guided and index-guided graded barrier quantum well lasers has been studied with near- and far-field lateral mode measurements at different pulse widths. Above threshold, gain-guided devices show a transition to predominantly index-guided operation as a result of thermally induced waveguiding. Similar devices with built-in real index guiding exhibit low threshold, stable mode operation, with no observable variations with pulse width.

Extremely low threshold currents have been observed[1] in graded barrier quantum well lasers. However, several types of anomalous behavior, not observed in conventional double heterostructure devices with thick active layers, have recently been reported. These include a large increase in threshold current[2] for short cavity lengths, wavelength shifting[3] to higher energy at elevated temperature, and long lasing delay[4,5] under pulsed operation. In this communication, we describe additional experimental data on long lasing delay in oxide defined stripe graded barrier quantum well lasers, observed earlier by Prince *et al.*[4,5] and compare these data with similar data from real index-guided complementary self-aligned[6] graded barrier quantum well lasers. The phenomenon of long lasing delay was attributed[4,5] to the formation of a real-index waveguide which is thermally induced by nonradiative recombination at the interfaces of the quantum well. In this work, we have observed, in addition to the long lasing delay in gain-guided devices, a transient behavior in the pulsed output intensity response at currents well above threshold. In this transient region, measurements of near- and far-field radiation patterns clearly illustrate that a transition from gain guiding to index guiding does occur. No delay has been observed in graded barrier quantum well devices having built-in real index guiding.

In this work we report data on the pulsed response of both gain-guided and index-guided graded barrier quantum well laser devices. The $Al_xGa_{1-x}AsGaAs$ graded barrier quantum well structure was grown by metalorganic chemical vapor deposition (MOCVD) and consists of a 30-Å quantum well surrounded by a 4400-Å-thick ($x = 0.20$–0.60) graded region and $x = 0.60$ confining layers. Gain-guided oxide defined stripe lasers were fabricated with various stripe widths. Index-guided complementary self-aligned lasers[6] were fabricated with similar stripe widths for comparison. The typical pulsed photodiode response of a 10-μm-wide oxide defined stripe laser is shown in Fig. 1. The pulsed response of a larger stripe width device (50 μm) is shown in Fig. 2. These data are similar to those observed by Prince *et al.*[5] for oxide stripe graded barrier quantum well lasers with 75-Å-thick active layers. The smaller stripe width devices ($w = 10\mu$m) have lasing delay times of $\geq 1\,\mu$s, while larger stripe width devices ($w = 50\mu$m) do not exhibit any delay. As can be seen in Fig. 1, there is, in addition to the lasing delay, an additional transient period after threshold has been reached during which the output intensity stabilizes. By taking into account a thermal gradient which is produced under the stripe region by nonradiative recombination at the active layer interfaces, Prince *et al.*[4,5] have shown that modal gain and threshold measurements correspond well with theoretical calculations when the effect of a thermally induced real-index waveguide is included. Initially the device is gain guided with a correspondingly high laser threshold. The threshold lowers as the effect of the thermally induced waveguide becomes stronger until laser operation

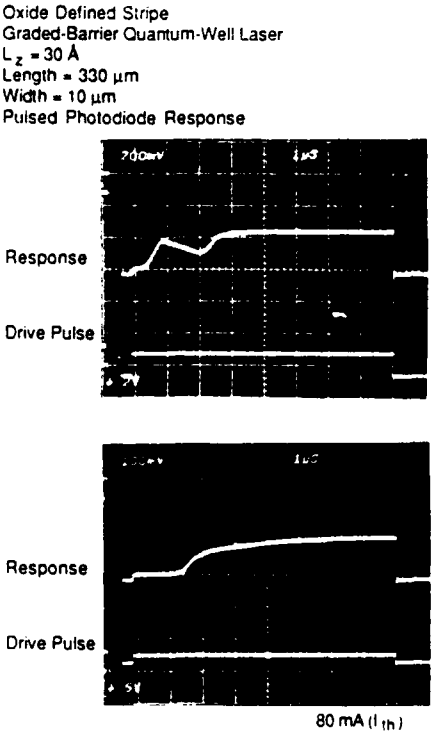

FIG. 1. Pulsed photodiode response of an oxide defined stripe graded barrier quantum well laser with a 10-μm stripe width. In addition to the lasing delay at threshold, a transient region can be seen above threshold where the device is still predominantly gain guided and beyond which index guiding begins to dominate.

 0021-8979/86/192613-03$02.40

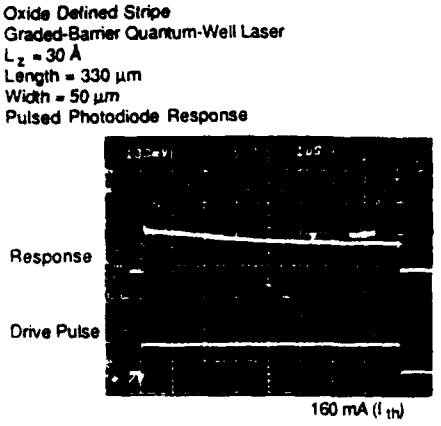

FIG. 2. Pulsed photodiode response of a large stripe width ($w = 50\ \mu m$) oxide defined stripe graded barrier quantum well laser. The lasing delay observed in small stripe width devices is not observed.

begins. At higher drive currents, the delay becomes smaller, but a finite time still passes after laser action begins before a stable complex waveguide can develop. By imaging the far-field pattern along the junction plane for different pulse widths, a gain-guided to index-guided transition can be clearly observed. Figure 3 shows the measured far-field patterns at 100 mA for two different pulse widths. For pulse widths of less than 2 μs, a double lobed far-field pattern is observed which is characteristic of gain guiding and results from tilting of the mode phase fronts.[7] As can be seen in Fig. 1, the device pulsed for 2 μs is operating in the gain-guided region and the photodiode response exhibits transient behavior. Increasing the pulse width to 5 μs places the device into the index-guided regime (Fig. 1, flat photodiode response region), resulting in the single-lobed far-field pattern of Fig. 3. Larger pulse widths have no effect on the shape of the far-field pattern. In addition, the near-field patterns for these devices show a narrowing of the lateral mode with increasing pulse width, which is indicative[7] of a transition to real index-guided operation. Similar behavior in far-field patterns has been observed[8] in single 300 Å quantum well lasers by varying the heat-sink temperature.

It was suggested[4,5] by Prince *et al.* that the introduction of a built-in index profile along the plane of the junction would eliminate the long lasing delay. In this work, low threshold devices with a built-in index guiding structure have been obtained by fabricating the graded barrier quantum well structure above into complementary self-aligned stripe geometry lasers.[6] These devices contain a lateral index step which results from the placement of a low band-gap, high refractive index GaAs layer close to the active layer outside the stripe width. The devices reported here have 9-μm stripe widths and an n:GaAs guide layer placed 0.25 μm from the edge of the graded region. The light-current characteristics, near-field patterns, and far-field patterns for these devices are shown in Fig. 4. Threshold currents were 20 mA for a 356-μm-long cavity, and the devices show stable near- and far-field patterns up to 15 mW per uncoated facet. The pulsed photodiode response for these devices is shown in Fig. 5. No lasing delay or transient behavior exists. In addition, no variations of the near- or far-field patterns are observed as the pulse width is varied.

In conclusion, we have directly observed a transition from gain guiding to thermally induced index guiding in ox-

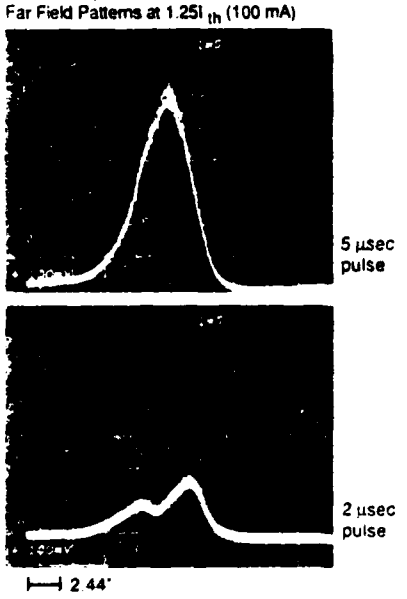

FIG. 3. Far-field pattern above threshold for an oxide defined stripe graded barrier quantum well laser for two different drive pulse widths. For pulse widths less than 2 μs a double lobed pattern, characteristic of gain guiding, is observed.

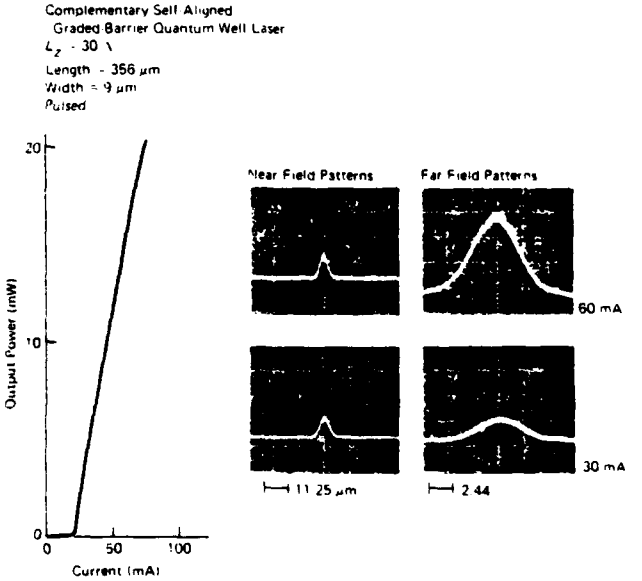

FIG. 4. L-I characteristics, near-, and far-field patterns for a real index-guided complementary self-aligned graded barrier quantum well laser. Stable mode operation is observed up to 15 mW/facet with no variation with changing pulse widths.

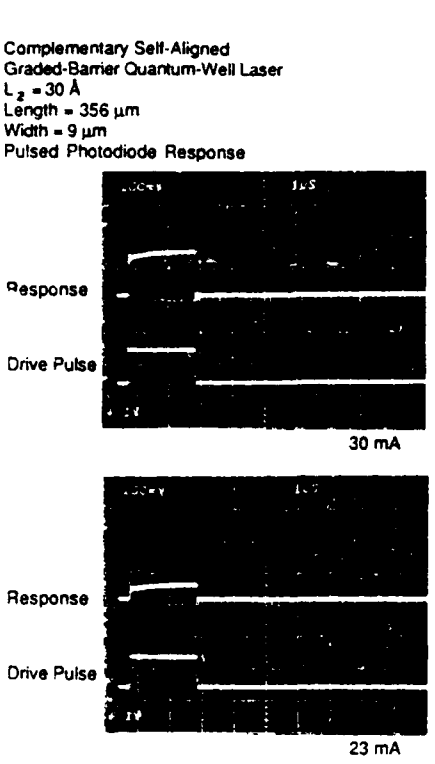

FIG. 5. Pulsed photodiode response of a real index-guided complementary self-aligned graded barrier quantum well laser. No lasing delay or transient behavior above threshold is observed in these devices.

ide defined stripe geometry graded barrier quantum well laser diodes by observing the near- and far-field patterns at different drive pulse widths. Also, low threshold devices have been fabricated with built-in index steps along the junction plane eliminating the long lasing delay and transient behavior associated with thermally induced index guiding. Stable mode behavior is observed in these devices up to 15 mW per uncoated facet.

The authors would like to thank Y. S. Moroz, B. K. Moroz, C. W. Trussel, and P. D. Dapkus for their contributions to this work. This work was supported in part by U.S. Army Night Vision Laboratory contract DAAK 20-84-K-0225 and U.S. Army Research Office contract DAAG 29-85-G-0133.

[1]W. T. Tsang, Appl. Phys. Lett. **40**, 217 (1982).
[2]P. S. Zory, A. R. Reisinger, L. J. Mawst, G. Costrini, C. A. Zmudzinski, M. A. Emanuel, M. E. Givens, and J. J. Coleman, Electron. Lett. **22**, 475 (1986).
[3]P. S. Zory, A. R. Reisinger, R. G. Waters, L. J. Mawst, C. A. Zmudzinski, M. A. Emanuel, M. E. Givens, and J. J. Coleman, Appl. Phys. Lett. **49**, 16 (1986).
[4]F. C. Prince, N. B. Patel, D. Kasemset, and C. S. Hong, Electron. Lett. **19**, 435 (1983).
[5]F. C. Prince, T. J. S. Mattos, N. B. Patel, D. Kasemset, and C. S. Hong, IEEE J. Quantum Electron. **QE-21**, 634 (1985).
[6]L. J. Mawst, G. Costrini, C. A. Zmudzinski, M. E. Givens, M. A. Emanuel, and J. J. Coleman, Electron. Lett. **21**, 903 (1985).
[7]G. P. Agrawal, IEEE J. Lightwave Tech. **LT-2**, 537 (1984).
[8]R. D. Burnham, C. Lindstrom, T. L. Paoli, D. R. Scifres, W. Streifer, and N. Holonyak, Jr., Appl. Phys. Lett. **42**, 937 (1983).

Complementary self-aligned laser arrays by metalorganic chemical vapor deposition

L. J. Mawst, M. E. Givens, M. A. Emanuel, C. A. Zmudzinski, and J. J. Coleman
Center for Compound Semiconductor Microelectronics, Department of Electrical and Computer Engineering, University of Illinois at Urbana-Champaign, Urbana, Illinois 61801

(Received 13 May 1986; accepted for publication 1 July 1986)

A two-step metalorganic chemical vapor deposition growth technique has been used to fabricate multielement arrays of complementary self-aligned lasers using graded barrier quantum well active regions. This technique eliminates any possible difficulty associated with regrowth on a high composition AlGaAs layer by placing the interface outside the stripe region. The complex index guiding and resulting mode discrimination characteristics of self-aligned lasers stabilize the near- and far-field patterns of the array. Comparison studies between shallow mesa arrays and self-aligned arrays are described.

Semiconductor laser arrays have demonstrated high output powers with stabilized far-field patterns. Such arrays, fabricated from gain-guided laser structures, are capable of high output power and are easily phase locked due to the weak refractive index variations along the plane of the junction. However, unstable lateral modes and complex far-field patterns are characteristic of these devices.[1,2] In contrast with arrays of gain-guided structures, arrays with built-in real or complex refractive index variations along the plane of the junction offer stabilized lateral modes with astigmatic output beams.[3,4] The complementary self-aligned laser structure lends itself nicely to incorporation into multielement arrays because of its simple fabrication and excellent mode control characteristics. The self-aligned laser utilizes a high refractive index, high absorption *n*-GaAs layer near the active region outside the stripe to provide current confinement and complex index guiding with resulting higher order mode discrimination.[5] The optical waveguiding characteristics of the self-aligned structure are similar to channeled substrate-planar lasers,[6] with the added advantage of automatic alignment of current confinement and lateral index steps. This communication describes the incorporation of the complementary self-aligned laser[7] element into complex, index-guided laser arrays.

The fabrication of the complementary self-aligned laser, grown by metalorganic chemical vapor deposition (MOCVD), has been described previously.[7] In this work we have used a graded barrier quantum well heterostructure as the basic underlying laser structure. The structure is similar to one previously described,[4] with confining layer composi-

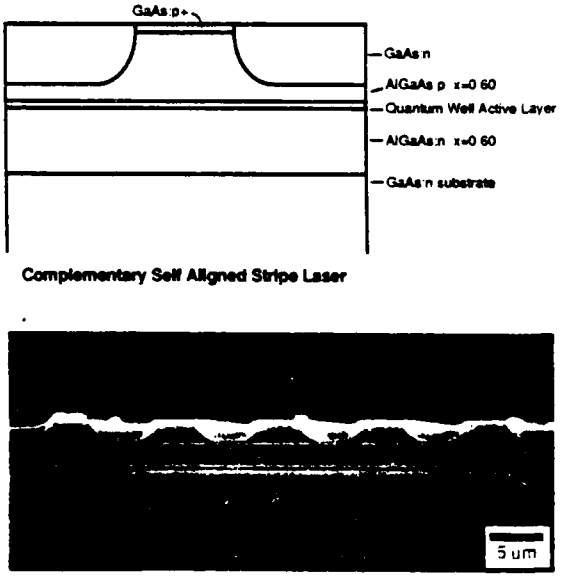

FIG. 1. SEM photograph of a 5-stripe complementary self-aligned laser array and a schematic diagram of a single element.

 0021-8979/86/192633-03$02.40

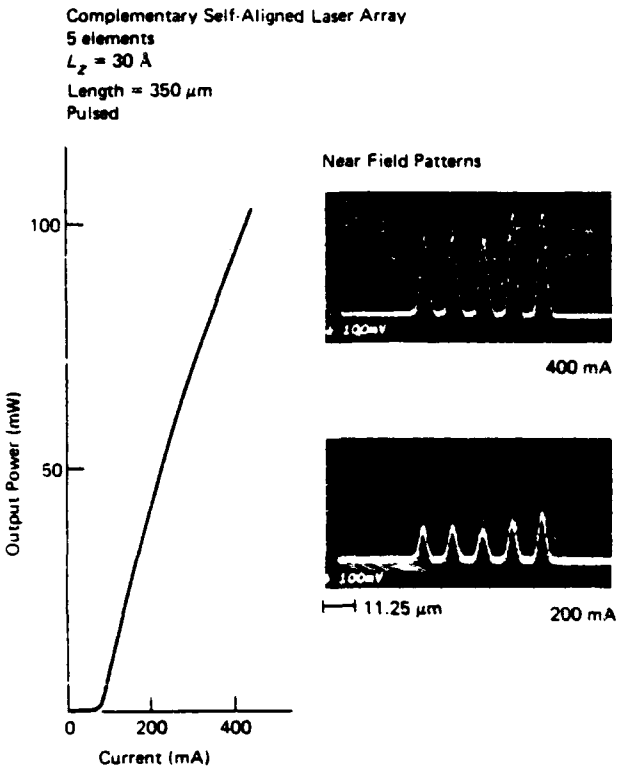

FIG. 2. Typical pulsed L-I characteristics of a 5-stripe ($t = 0.2\,\mu$m) complementary self-aligned laser array. Near-field profiles along the junction plane show stable fundamental modes up to 100 mW.

tion $x = 0.60$ and a 30-Å quantum well centered within a 4400-Å graded separate confinement region. After a layer of SiO_2 (1000 Å) is deposited on the surface of the wafer, a 5-stripe array pattern is defined along the (110) direction. The stripes have 6.5–7.0 μm widths with 10-μm center-to-center spacings. In this experiment two different samples were prepared, with the regions outside the stripe width etched to within either 0.2 or 0.4 μm of the graded region. The center-center stripe spacing is kept the same to allow observation of the extent of coupling between the array elements for different lateral index strengths. With the oxide mask still in place, the sample is returned to the MOCVD reactor for the growth of an additional 1.0 μm of n-GaAs (Se, 1×10^{18} cm^{-3}). Since the GaAs grows selectively[8] outside the stripe region, no additional processing is required other than removal of the oxide mask and contact metallization. A scanning electron microscope (SEM) cross section of the 5-stripe array is shown in Fig. 1, along with a schematic diagram of a single element. These micrographs clearly indicate that high-quality GaAs can be selectively grown between the stripe regions of the array, leaving an essentially planar laser device within the stripe.

Typical pulsed (1.5 μs at 2 kHz) L-I characteristics of a 5-stripe array which has been etched to within 0.2 μm of the graded region ($t = 0.2\,\mu$m) are shown in Fig. 2, along with the near-field radiation pattern at two different current levels. The broad area threshold current density of the starting material was 400 A/cm^2 for diodes of length 350 μm. The 30-Å quantum well active layer results in an emission wavelength at 7950–8000 Å, which corresponds well with the $n = 1$ electron to heavy-hole transition based on a finite potential well model. The near-field radiation pattern along the plane of the junction, shown in Fig. 2, indicates that the fundamental lateral mode of each array element is completely stabilized up to power levels in excess of 100 mW per uncoated facet. These devices have threshold currents of 15 mA per stripe with external differential quantum efficiencies of 43%. The far-field radiation patterns along the junction plane show a featureless single lobe (7° FWHM) indicating that the array elements are uncoupled as a result of the strong index guiding and large center-center spacings. Devices which have been etched shallower ($t = 0.4\,\mu$m) show increased coupling between array elements and operate phase locked up to about 25 mW per facet. The far-field pattern along the plane of the junction is shown in Fig. 3 for different drive current levels. A double lobed pattern is observed up to about twice threshold, above which the two lobes begin to merge together. At this point the near-field patterns show unstable lateral modes within each stripe region. The measured far-field lobe separation of 4.4° corresponds closely to the predicted spacing based on diffraction

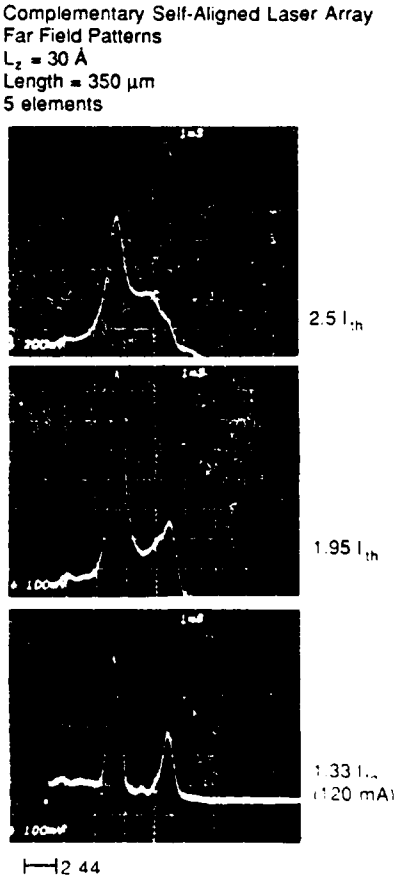

FIG. 3. Far-field radiation pattern of a 5-stripe ($t = 0.4\,\mu$m) complementary self-aligned array at different drive currents. Phase locked operation results in the double lobed pattern up to about twice threshold.

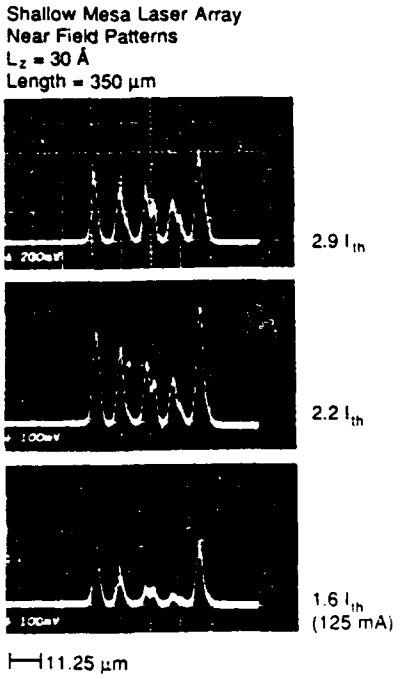

FIG. 4. Near-field pattern of a 5-stripe ($t = 0.2\,\mu m$) shallow mesa array at different drive currents. The large index changes along the junction plane result in higher order modes for this stripe width (6.5–7.0 μm).

theory (4.55°) assuming the emitters are locked 180° out of phase.

In order to obtain high output power levels with stabilized lateral modes, large stripe width devices are desirable. However, stabilization of the lateral modes requires a strong refractive index variation along the junction plane which will result in higher order modes unless the stripe width is small enough to cut off these modes. The self-aligned laser relies on a built-in loss outside the stripe region in order to discriminate against higher-order modes. In contrast with the self-aligned laser, the shallow mesa laser[9] relies primarily on a built-in real index variation along the junction plane to guide the lateral modes. Shallow mesa arrays with the same stripe width (6.5–7.0 μm) and etch depth ($t = 0.2\,\mu m$) have been fabricated for comparison with the self-aligned arrays. The near-field patterns, shown in Fig. 4, clearly show that higher order modes are present within the individual emitters. Similar comparisons between single stripe devices also show mode discrimination in self-aligned lasers for stripe widths as large as 10 μm.

In conclusion, a new method of fabricating self-aligned lasers has been implemented in the development of complex index-guided arrays. Since the device utilizes a planar active layer, graded barrier quantum well active regions have been used in order to improve output power and performance. Although these devices operate phase locked only at low-power levels, it is expected that smaller stripe spacing will produce a high-power phase-locked device with a characteristic narrow double-lobed far-field pattern. In addition, data are presented which illustrate the mode discrimination characteristics of self-aligned lasers.

The authors would like to thank Y. S. Moroz and B. K. Moroz for technical assistance. This work was supported in part by U.S. Army Night Vision Laboratory Contract DAAK 20-84-K-0225 and U.S. Army Research Office Contract DAAG 29-85-G-0133.

[1] J. P. Van der Ziel, R. M. Mikulyak, H. Temkin, R. A. Logan, and R. D. Dupuis, IEEE J. Quantum Electron. **QE-20**, 1259 (1984).
[2] G. P. Agrawal, J. Appl. Phys. **58**, 2922 (1985).
[3] H. Temkin, R. A. Logan, J. P. Van der Ziel, C. L. Reynolds, Jr., and S. M. Tharaldsen, Appl. Phys. Lett. **46**, 465 (1985).
[4] L. J. Mawst, M. E. Givens, M. A. Emanuel, C. A. Zmudzinski, and J. J. Coleman, Appl. Phys. Lett. **48**, 1337 (1986).
[5] M. Yano, N. Nishi, and M. Takusagawa, IEEE J. Qauntum Electron. **QE-15**, 138 (1979).
[6] K. Aiki, M. Nakamura, T. Kuroda, and J. Umeda, Appl. Phys. Lett. **30**, 64 (1977).
[7] L. J. Mawst, G. Costrini, C. A. Zmudzinski, M. E. Givens, M. A. Emanuel, and J. J. Coleman, Electron. Lett. **21**, 903 (1985).
[8] Y. Takahashi, S. Sakai, and M. Umeno, J. Cryst. Growth **68**, 206 (1984).
[9] T. Tsukada, R. Ito, H. Nakashima, and O. Nakada, IEEE J. Quantum Electron. **QE-9**, 356 (1973).

MOCVD of III-V Compound Epitaxial Layers

The control and uniformity of MOCVD make it useful for fabricating highly advanced structures.

L.J. Mawst, G. Costrini, M.A. Emanuel, M.E. Givens, C.A. Zmudzinski and J.J. Coleman, Center for Compound Semiconductor Microelectronics and Materials Research Laboratory, University of Illinois at Urbana-Champaign, Urbana, Ill.

Metalorganic chemical vapor deposition (MOCVD) has become an important method in recent years for the growth of high-quality epitaxial layers of various II-V semiconductor materials.[1-3] In a typical reaction, the vapors of low order metal alkyls, such as trimethylgallium (TMGa) and trimethylaluminum (TMAl), are mixed with a gaseous hydride, such as arsine. As a result of fragmentation by pyrolysis, atomic or molecular species combine at or near a heated substrate. This is most interesting when it results in deposition on a suitable single crystal substrate, such as GaAs, forming an epitaxial layer.

There are a number of attractive features associated with the MOCVD process. All constituents are in the vapor phase allowing for accurate electronic control of important system parameters, such as gas flow rates. The pyrolysis reaction is relatively insensitive to temperature, allowing for efficient and reproducible deposition of very thin layers with abrupt interfaces between layers. Complex multiple layer heterostructures can be grown utilizing computer controlled gas exchange systems. Finally, development of production scale reactor systems is fairly straightforward, analogous to the development of commercial silicon epitaxy.

The first descriptions of the MOCVD process can be traced to Manasevit and co-workers.[1] The earliest and still most commonly used reaction for the growth of compound semiconductor layers is illustrated by the practical example for the growth of epitaxial layers of the important ternary alloy AlGaAs:

$$x(CH_3)_3Al + (1\text{-}x)(CH_3)_3Ga + AsH_3 \rightarrow Al_xGa_{1-x}As + 3CH_4$$

The metal alkyls are typically liquids at or near room temperature and are kept in stainless steel bubblers in carefully-controlled refrigerated baths to maintain a stable vapor pressure of the source over its liquid. Transport is accomplished by means of a controlled rate

AlGaAs Growth Rate

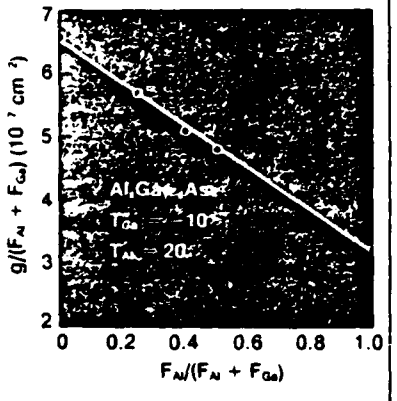

1. Growth rate normalized to total metal alkyl flow vs dimensionless flow ratio.

Growth Rate vs Radius

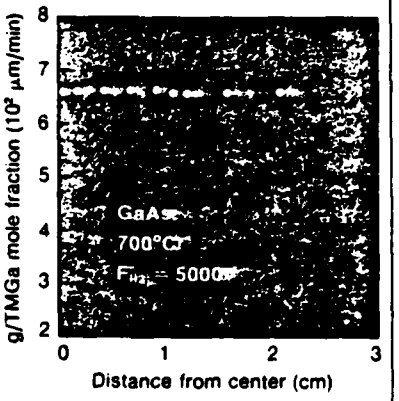

2. GaAs growth rate normalized to TMGa mole fraction vs radial position on the susceptor.

Composition vs Flow Ratio

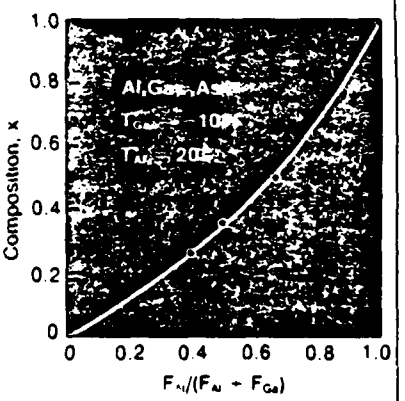

3. Composition vs metal alkyl flow ratio for AlGaAs.

of purified hydrogen passed through the liquid. The gaseous hydride sources are often contained as dilute mixtures with hydrogen. Doping is obtained by injecting small amounts of the vapors of an appropriate impurity, such as diethylzinc or hydrogen selenide, into the gas stream.

In a typical MOCVD reactor, the gas mixture system consists of a network of clean, leak-free stainless steel tubing with compression-type or welded fittings throughout. The combination and quantities of the various source and dopant vapors are determined by automatic valves and electronic mass flow controllers. For the growth of more sophisticated structures, such as thin layer quantum well heterostructures and superlattices, computer control of the system is necessary.

Cold wall reaction chambers are of either horizontal or vertical design. In either design, a deflector is often placed at the inlet to the reaction chamber to enhance mixing of the source vapors. The most common source of heat for the pyrolysis reaction is provided by rf induction heating of the graphite susceptor.

The growth of epitaxial layers of GaAs and AlGaAs normally takes place under conditions of excess column V species and dilute in a hydrogen carrier environment. A flow of the column V hydride is continued between layers to maintain the integrity of the as-grown surface against thermal decomposition. Since the pyrolysis efficiencies of the metal alkyls are essentially unity at typical growth temperatures, and since there are no competing dissolution reactions involved in the process, growth rates are linear with time and with metal alkyl mole fraction.

The growth rate of AlGaAs normalized to total metal alkyl flow as a function of a dimensionless flow ratio is given in Fig. 1. The data points are determined experimentally from measured SEM cross sections. The solid line is calculated from the gas law and from the vapor pressures of the sources. A correction factor for geometry effects is obtained by including one measured data point in the analysis. The dimensionless flow ratio term is related to the metal alkyl mole fraction by the relative vapor pressures of the sources and, thus, to the composition of the grown layer. An important feature of the MOCVD process is that growth rates

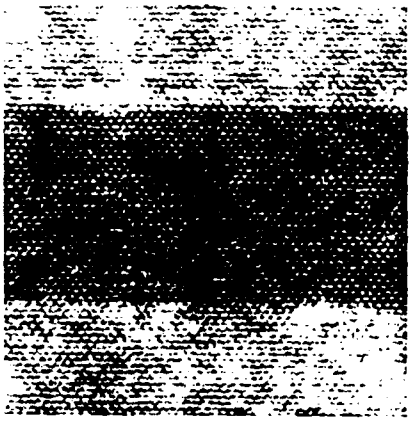

4. High resolution TEM photo with lattice image of an AlAs-GaAs superlattice having 90 Å layer size.

can be varied over a large range (from tens of Å/min to tenths of μm/min) by varying source bath temperature and flow rate. When the hydrodynamic and thermal conditions in a vertical geometry reaction chamber are optimized, exceptional thickness uniformity over large areas can be obtained.[4]

Figure 2 shows SEM-determined growth rate (normalized to TMGa mole fraction) vs radius. These combined data are from several different cleaved cross sections from the same growth run and from different runs of a multiple layer structure. The uniformity obtained is ±1.5% over greater than a 4 cm diameter.

The composition of an MOCVD-grown epitaxial layer of AlGaAs is simply determined from the mole fraction ratio of the two metal alkyls and, thus, is a function of flow rates and source bath temperatures. Shown in Fig. 3 is composition vs flow ratio for AlGaAs grown by MOCVD. The data points are experimentally determined from X-ray rocking curve measurements. The solid curve is obtained from the same simple gas law analysis involving the vapor pressures of the sources described above.

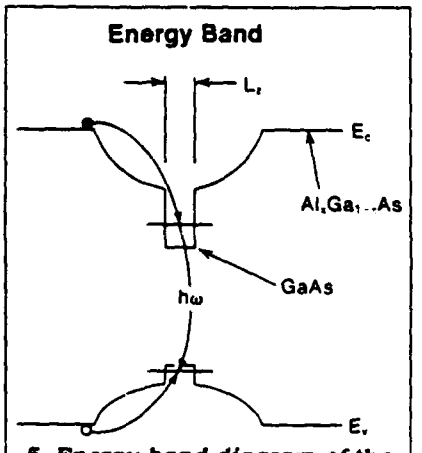

5. Energy band diagram of the graded barrier quantum well heterostructure laser.

Heterostructures and superlattices

The growth of high quality heterostructures with abrupt interfaces is necessary for development of sophisticated thin-layer quantum well heterostructure devices made from the AlGaAs-GaAs materials system. In addition, an entire area of research is developing around superlattices — structures containing a large number of thin (<200 Å) layers having electrical and optical properties determined by quantum physics, unlike the bulk properties of any of the individual layer materials.

The MOCVD process has been shown to be ideal for these structures, having the capacity for growth of very uniform layers and abrupt interfaces.[5-8] Figure 4 is a high resolution transmission electron microscope (TEM) photograph and associated lattice image[7] of part of the cross section of an AlAs-GaAs superlattice which demonstrates the excellent uniformity and defect-free structure of MOCVD-grown superlattices. The lighter layers are AlAs (90 Å) and the darker layer is GaAs (90 Å). The lattice image points formed by the intersection of the low order atomic planes indicate the position of the interfacial plane and show that the interface transition clearly occurs within a single atomic layer.

Improvement in all of the characteristics of conventional double heterostructure lasers has resulted from application of the MOCVD growth process to these structures, and the development of quantum well heterostructure lasers and superlattices has been dominated by the MOCVD growth technology.[9]

One structure that clearly illustrates many of the advantages of the MOCVD growth process for laser devices is the graded barrier quantum well heterostructure laser.[10-14] The band structure of this device is shown in Fig. 5. A single quantum well of GaAs becomes an ineffi-

Threshold current density (A/cm²)

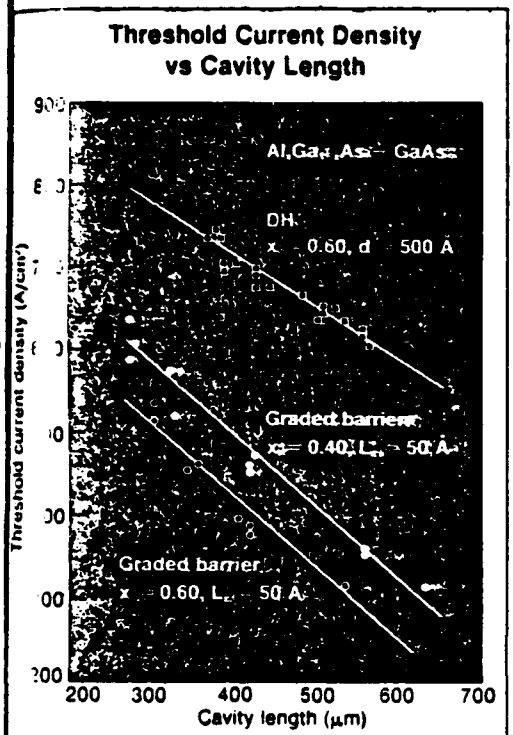

6. Broad area laser threshold current density vs cavity length for three laser structures.

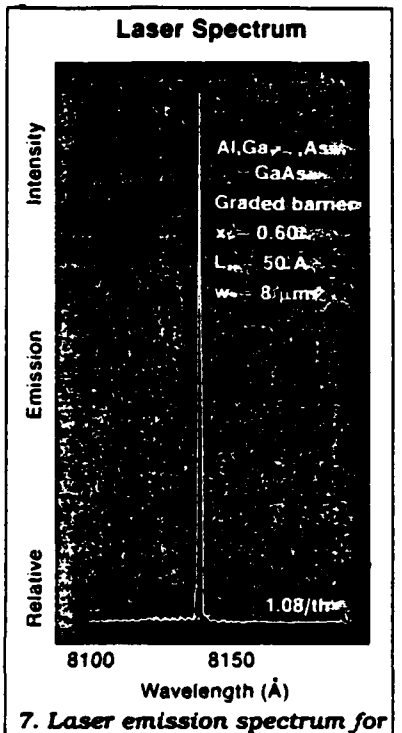

7. Laser emission spectrum for a graded barrier quantum well heterostructure having x = 0.60 and L_z = 50 Å.

cient collector of mobile electrons and holes as the size is made smaller[15] than 100 Å. An increase in laser threshold current density will result unless some structural change is made to increase the active region volume by increasing the number of wells, each separated by a thin barrier layer. Another, as shown in Fig. 5, is to create a graded region on either side of the well. Free carriers will be captured in the relatively large graded region and will thermalize quickly to the lowest quantum state in the well. Highest efficiences will be obtained from this structure when the confining layer composition is as high as possible, the graded region has a carefully controlled composition profile and the quantum well has accurately controlled thickness and abrupt interfaces.

The MOCVD growth process is well suited for the growth of graded barrier quantum well heterostructure lasers. Compositions up to x = 1.0 are possible and, for confining layers, up to x >0.85 is practical. Precise computer control of the metal alkyl flow ratio allows the growth, in principle, of any composition profile in the graded region. As described above, the process allows exceptional control over thicknesses, even for very thin layers, and the interfaces are abrupt on a monatomic scale.

Shown in Fig. 6 are broad area laser threshold current densities vs cavity length for three laser device structures. The first is a conventional double heterostructure and the others are graded barrier quantum well heterostructures having x = 0.40 and 0.60 confining layer compositions. The graded region profile of the graded barrier quantum well heterostructures is approximately parabolic.

In addition to a large improvement in laser threshold current density, operation at shorter wavelengths is possible (Fig. 7), since quantum size effects result in transitions at higher energies than in conventional double heterostructure lasers. This figure shows the laser spectrum of the x = 0.60 graded barrier lasers of Fig. 7. Extension of laser diode operation well into the visible portion of the optical spectrum is possible.[16] □

Acknowledgements

Support was provided by the Army Night Vision Laboratory (DAAK 20-84-K-0225), the Army Research Office (DAAG 29-85-K-0133) and the National Science Foundation (DMR 83-16981).

References

1. H.M. Manasevit, *J. Crystal Growth* 55, 1, 1981.
2. P.D. Dapkus, *Ann. Rev. Mater. Sci.* 12, 243, 1982.
3. J.J. Coleman and P.D. Dapkus, *Gallium Arsenide Technology*, D.K. Ferry, Ed., Howard W. Sams and Co., Indianapolis, 1985, p. 79.
4. G. Costrini and J.J. Coleman, *J. Appl. Phys.* 57, 2249, 1985.
5. R.D. Dupuis, P.D. Dapkus, A.M. Gainey, C.Y. Su and W.E. Spicer, *Appl. Phys. Lett.* 34, 335, 1979.
6. N. Holonyak Jr., W.D. Laidig, M.D. Camras, K. Hess, M.S. Burroughs, J.J. Coleman and P.D. Dapkus, *J. Appl. Phys.* 52, 6777, 1981.
7. S.J. Jeng, C.M. Wayman, J.J. Coleman and G. Costrini, *Mater. Lett.* 3, 89, 1985.
8. J.J. Coleman, G. Costrini, S.J. Jeng and C.M. Wayman, *J. Appl. Phys.* 59, 428, 1986.
9. P.D. Dapkus and J.J. Coleman, *Epitaxy of III-V Compound Semiconductors*, R.J. Malik, Ed., in press, North Holland Co., Amsterdam, 1985, and references cited.
10. W.T. Tsang, *Appl. Phys. Lett.* 39, 134, 1981.
11. D. Kasemset, C.S. Hong, N.B. Patel and P.D. Dapkus, *Appl. Phys. Lett.* 41, 912, 1982.
12. S.D. Hersee, M. Baldy, P. Assenat, B. de Cremoux and J.P. Duchemin, *Electron. Lett.* 18, 870, 1982.
13. P.S. Zory, A.R. Reisinger, L.J. Mawst, G. Costrini, C.A. Zmudzinski, M.A. Emanuel, M.E. Givens and J.J. Coleman, *Electron. Lett.* 22, 475, 1986.
14. L.J. Mawst, M.E. Givens, M.A. Emanuel, C.A. Zmudzinski, and J.J. Coleman, *Appl. Phys. Lett.* 48, 1337, 1986.
15. N. Holonyak Jr., R. M. Kolbas, R.D. Dupuis and P.D. Dapkus, *IEEE J. Quantum Elect.* QE-16, 170, 1980.
16. R.D. Burnham, W. Striefer, T.L. Paoli and N. Holonyak Jr., *J. Crystal Growth*, 68, 370, 1984.

Effect of compositionally graded and superlattice buffer layers on the device performance of graded barrier quantum well heterostructure laser diodes

M. E. Givens, L. J. Mawst, C. A. Zmudzinski, M. A. Emanuel, and J. J. Coleman
Center for Compound Semiconductor Microelectronics, Department of Electrical and Computer Engineering, University of Illinois at Urbana–Champaign, Urbana, Illinois 61801

(Received 15 September 1986; accepted for publication 8 December 1986)

The device performance of graded barrier quantum well laser diodes with various buffer layer structures grown by metalorganic chemical vapor deposition has been studied. Devices having four structures (a GaAs buffer layer only, a compositionally graded buffer layer, a superlattice buffer layer, or both a graded and a superlattice buffer layer) have been characterized. In contrast with similar studies involving laser devices grown by molecular beam epitaxy, little variation in device performance is observed. These data indicate that the quality of AlGaAs-GaAs heterostructures for optical devices may be dependent on the details of the method used for the epitaxial growth of the layers.

The need for compositionally graded and/or superlattice buffer layers has been established[1,2] for laser structures grown by molecular beam epitaxy (MBE).[3,4] In recent work[1,5] on MBE-grown laser devices, a compositionally graded buffer or superlattice buffer was shown to improve the quality of the subsequent AlGaAs/GaAs layers, and resulted in a reduction of device threshold currents and in the temperature sensitivity of threshold current. These improvements in device performance are believed to result from a variety of mechanisms, including a reduction in the propagation of defects[6] from the substrate, a relief of strain[5] at the high aluminum concentration confining layer/substrate interface, and impurity trapping[2] at the buffer layer interfaces. The importance of these prelayers, however, for laser structures grown by metalorganic chemical vapor deposition (MOCVD)[7] has not been established, and high quality, low threshold quantum well laser diodes have been grown by MOCVD without any prelayers.[8–11] In determining the design criteria for high performance MOCVD-grown devices requiring the lowest possible threshold currents, it is important to determine the usefulness of various types of buffer layers in comparable laser structures. In this letter, we describe results from a comparison study of the device characteristics of graded barrier quantum well lasers having four types of buffer layers: a GaAs buffer layer alone, a GaAs buffer layer and a compositionally graded buffer layer, a GaAs layer and a superlattice buffer layer, a GaAs buffer layer and both compositionally graded and superlattice buffer layers. These data show that the use of compositionally graded and/or superlattice buffer layers has little or no effect on the overall device performance of high quality MOCVD-grown laser structures, other than a slight improvement in uniformity. These results indicate that the need for compositionally graded or superlattice buffer layers is probably related to the material quality obtained by various epitaxial growth methods and is not a fundamental requirement for these laser structures.

The graded barrier quantum well laser structures utilized in this study were grown by atmospheric pressure MOCVD at a growth temperature of 800 °C on (100) GaAs:Si substrates. The basic structure consists of a 0.5-μm GaAs buffer ($n = 1\times10^{18}$), the intermediate buffer layer or layers, a 1.5-μm $Al_{0.85}Ga_{0.15}As$ confining layer ($n = 1\times10^{18}$), a 1200-Å parabolically graded $Al_xGa_{1-x}As$ layer ($0.85\geqslant x\geqslant0.20$, $n = 5\times10^{16}$), a 50-Å GaAs quantum well (undoped), a 1200-Å parabolically graded $Al_xGa_{1-x}As$ layer ($0.20\leqslant x\leqslant0.85$, $p = 1\times10^{17}$), a 1.5-μm $Al_{0.85}Ga_{0.15}As$ confining layer ($p = 2\times10^{18}$), and a 0.2-μm GaAs contact layer ($p = 4\times10^{19}$). The high aluminum concentration used in the confining layers ($x = 0.85$) increases the optical confinement within the active layer, allowing very low threshold current densities to be obtained. Additionally, the use of such a high composition should serve to maximize any effects that a buffer layer might have on device performance due to improvements in material quality related to the lattice mismatch between AlGaAs and GaAs layers. Structures were grown with either no additional buffer layer besides the 0.5-μm GaAs layer, or with an intermediate buffer layer(s) consisting of a 0.5-μm linearly graded compositionally graded buffer layer ($0.0\leqslant x\leqslant0.85$, $n = 1\times10^{18}$), a 20-period superlattice buffer layer of alternating 100-Å GaAs and 100-Å AlAs layers ($n = 1\times10^{18}$), or with both compositionally graded and superlattice buffer layers. All structures were grown at approximately 3.0 μm/h.

Prior to fabrication and characterization of the laser devices, the GaAs:*p* cap layer was chemically etched off part of each sample and the room-temperature photoluminescence (PL) of each laser structure was observed. No significant differences in photoluminescence intensity or structure were observed in any of the samples. Similar comparison studies of the PL intensity of single quantum well structures grown by MBE with and without superlattice buffer layers have shown[2] differences in intensity by as much as a factor of 40 at 77 K. Peak emission wavelengths were between 8275 and 8300 Å, consistent with the calculated wavelength for the $n = 1$ electron to heavy-hole transition based on a finite potential well model for a 50-Å quantum well width. Wide stripe ($w = 150\,\mu$m) oxide defined stripe lasers were fabricated in order to characterize broad area threshold current

 0003-6951/87/060301-03$01.00

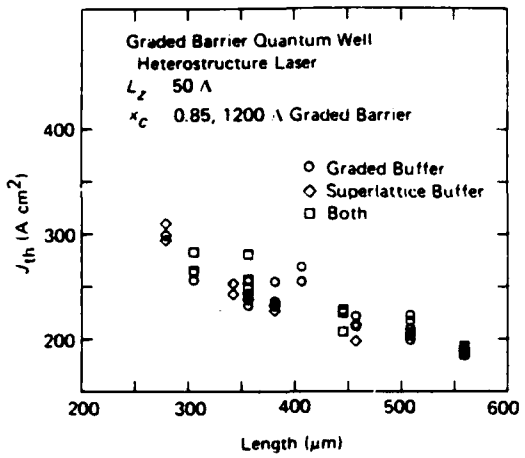

FIG. 1. Broad area threshold current densities as a function of laser cavity length for laser structures having compositionally graded buffer layers (circles), superlattice buffer layers (diamonds), or both compositionally graded and superlattice buffer layers (squares). Little variation is observed in threshold current density as a function of buffer layer structure.

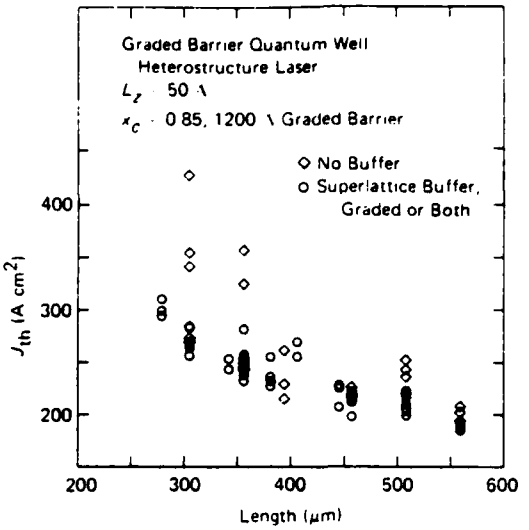

FIG. 2. Comparison of broad area threshold current densities for structures having either a GaAs buffer layer only (circles), or an additional (compositionally graded, superlattice, or both) buffer layer structure (diamonds).

densities as a function of cavity length, differential quantum efficiencies, and the temperature dependence of threshold current (T_0). Threshold currents were taken from pulsed (2 μs, 2 kHz) light-current characteristics using a current probe to monitor the drive current.

The broad area threshold current densities as a function of laser cavity length are illustrated in Fig. 1 for laser structures with a compositionally graded buffer layer (circles), a superlattice buffer layer (diamonds), and both compositionally graded and superlattice buffer layers (squares). Very low threshold current densities (for example, $J_{th} = 200$ A/cm^2, length = 450 μm) were obtained with very little scatter among devices having different buffer layers. These threshold current densities are comparable[2] to those of similar structures grown by MBE. Threshold current densities for devices with GaAs buffer layers only (circles) are shown in Fig. 2. Shown for comparison in Fig. 2 are all the data of Fig. 1 (diamonds) for devices having the additional buffer layer structures described above. The data for devices with GaAs buffer layers alone show little increase in threshold current density in comparison with devices having an additional buffer layer structure. This is in contrast to data from similar devices grown by MBE, which show[1] threshold current changes of a factor of 2 between compositionally graded buffer layers and devices with GaAs buffer layers only. However, the greater degree of scatter in the data of Fig. 2 for devices with GaAs buffer layers only indicates, perhaps, somewhat lower uniformity across the wafer. As discussed below, we believe this is due to the generation of localized defect networks originating at nonuniformly distributed imperfections along the heterointerface.

In addition to the threshold data described above, the temperature dependences of threshold current and differential quantum efficiencies were measured for all four samples. These data also show little variation among devices fabricated from the different structures. Typically, the total external differential quantum efficiencies for uncoated facets ranged from 45 to 55% for devices having 508 μm cavity length. The exponential coefficient characterizing the temperature dependence of threshold current (T_0) varied from 200 to 250 °C within a measured temperature range of from 20 to 50 °C for a 508-μm cavity length. Above approximately 50 °C the value for T_0 reduces to 140–160 °C. These values for η_{ext} and T_0 are typical of devices having any of the four buffer layer structures. In comparison, similar MBE-grown devices with either compositionally graded buffer[1] or superlattice buffer[5] prelayers exhibited an η_{ext} of 50% and T_0 of 160 K, respectively. The same structures without these buffer layers showed a reduction in device performance to a η_{ext} of 20% and T_0 of 100 K. Therefore, none of the buffer layer structures offers a significant advantage in MOCVD-grown devices, although it may be desirable to utilize additional buffer layers in order to obtain the incremental improvement in the uniformity of device characteristics described above.

Considering each type of buffer layer and comparing its effect on the device performance of MBE- and MOCVD-grown laser structures, we can make several observations concerning the two growth processes. Introduction of a compositionally graded buffer layer has been shown[1] to improve the operating characteristics of MBE-grown lasers especially for higher confining layer compositions, apparently by relaxing the strain due to lattice mismatch at the substrate/AlGaAs confining layer interface. Without a compositionally graded buffer layer, a uniform high density of defects is generated at the heterointerface during MBE growth. These defects propagate into the growing layers, yielding a lower quality AlGaAs:*n* confining layer on which the rest of the laser structure must be grown, and a quantum well active layer of poorer interfacial quality. This results in poorer device characteristics. Introduction of a superlattice buffer layer has been shown[6] to prevent the propagation of substrate defects into a growing epilayer and to relax substrate/AlGaAs confining layer interfacial strain through the

formation, and subsequent bending, of dislocations. This bending effectively interrupts vertical propagation of the defects and allows the growth of a high quality AlGaAs confining layer. Without a superlattice buffer layer, existing substrate defects are also able to propagate into the growing layers, further degrading the material quality and device performance.

In MOCVD-grown structures, the addition of a compositionally graded buffer layer or superlattice buffer layer does not significantly improve device performance. This indicates that, relative to MBE, the growth of an abrupt substrate/high composition AlGaAs confining layer heterointerface by MOCVD does not generate the same high density of interfacial defects. This may be due to fundamental differences between the growth mechanisms involved in the two epitaxial techniques and may be related, in part, to the different growth temperatures used (MBE: $T = 710\,^{\circ}\mathrm{C}$, MOCVD: $T = 800\,^{\circ}\mathrm{C}$). Defects that do form probably occur in regions of concentrated strain at the interface, localized at sites of crystalline imperfections or impurities that are present in low concentrations in all crystals. Since such imperfections are likely to be distributed in a nonuniform fashion at a relatively low density, they do not produce a uniform decrease in material quality and device performance. Rather, they lead to the somewhat greater scatter in the data taken from lasers grown by MOCVD without either type of buffer layer (Fig. 1). The ability of a compositionally graded buffer layer or superlattice buffer layer to relax interfacial strain may aid in preventing the creation and propagation of dislocation networks which would otherwise originate at these regions of localized strain. In any case, interface abruptness is not expected to be a factor as both MBE- and MOCVD-growth methods have been shown to result in monatomically abrupt interfaces.[12,13]

In conclusion, the usefulness of compositionally graded and superlattice buffer layers has been examined for MOCVD-grown laser structures. Compared to similar studies on MBE-grown structures, device performance exhibits almost no dependence on the type of buffer layer used. From a standpoint of device uniformity, the need for either a graded or superlattice buffer layer has been established. These data indicate that the growth of high quality laser structures by MBE requires a more sophisticated buffer than that required for MOCVD-grown lasers.

The authors gratefully acknowledge Y. S. Moroz, B. K. Moroz, and L. M. Miller for helpful discussions and technical assistance. This work was supported by the U.S. Army Night Vision Laboratory (contract DAAK 20-84-K-0225) and the National Science Foundation Engineering Research Center (grant CDR 85-22666).

[1] T. Hayakawa, T. Suyama, M. Kondo, K. Takahashi, S. Yamamoto, and T. Hijikata, Appl. Phys. Lett. **49**, 191 (1986).
[2] T. Fujii, S. Hiyamizu, S. Yamakoshi, and T. Ishikawa, J. Vac. Sci. Technol. B **3**, 776 (1985).
[3] A. Y. Cho and J. R. Arthur, "Molecular Beam Epitaxy," in *Progress in Solid-State Chemistry* (Pergamon, New York, 1975), Vol. 10, p. 157.
[4] W. T. Tsang, Appl. Phys. Lett. **40**, 217 (1982).
[5] O. Wada, T. Sanada, M. Kuno, and T. Fujii, Electron. Lett. **21**, 1025 (1985).
[6] M. Shinohara, T. Ito, and Y. Imamura, J. Appl. Phys. **58**, 3449 (1985).
[7] J. J. Coleman and P. D. Dapkus, "Metalorganic Chemical Vapor Deposition," in *Gallium Arsenide Technology*, edited by D. K. Ferry (H. W. Sams, Indianapolis, 1985), p. 79.
[8] R. D. Burnham, W. Streifer, T. L. Paoli, and N. Holonyak, Jr., J. Cryst. Growth **68**, 370 (1984).
[9] S. D. Hersee, M. Baldy, P. Assenat, B. de Cremoux, and J. P. Duchemin, Electron. Lett. **18**, 912 (1982).
[10] L. J. Mawst, M. E. Givens, M. A. Emanuel, C. A. Zmudzinski, and J. J. Coleman, Appl. Phys. Lett. **48**, 1337 (1986).
[11] L. J. Mawst, M. E. Givens, C. A. Zmudzinski, M. A. Emanuel, and J. J. Coleman, J. Appl. Phys. **60**, 2613 (1986).
[12] J. J. Coleman, G. Costrini, S. J. Jeng, and C. M. Wayman, J. Appl. Phys. **59**, 428 (1986).
[13] M. Tanaka, H. Sakaki, and J. Yoshino, Jpn. J. Appl. Phys. **25**, L155 (1986).

Optimization and Characterization of Index-Guided Visible AlGaAs/GaAs Graded Barrier Quantum Well Laser Diodes

L. J. Mawst
M. E. Givens
C. A. Zmudzinski
M. A. Emanuel
J. J. Coleman

Reprinted from: IEEE JOURNAL ON QUANTUM ELECTRONICS, Vol. QE-23, No. 6, JUNE 1987.

Optimization and Characterization of Index-Guided Visible AlGaAs/GaAs Graded Barrier Quantum Well Laser Diodes

LUKE J. MAWST, MICHAEL E. GIVENS, CHARLES A. ZMUDZINSKI, MARK A. EMANUEL, AND JAMES J. COLEMAN, SENIOR MEMBER, IEEE

Abstract—**Index-guided, single and multiple stripe, visible laser diodes (λ = 6950–7150 Å) have been fabricated and characterized. These structures utilize a graded barrier quantum well laser structure having high aluminum composition (x = 0.60–0.85) confining layers to obtain low threshold current. The use of thin AlAs quantum well barrier layers allows short wavelengths to be obtained from the quantum size effect in binary GaAs wells without the need for alloy $Al_xGa_{1-x}As$ wells. Index-guiding is accomplished by use of either a complementary self-aligned structure or a shallow mesa laser structure allowing stabilized single-mode laser operation.**

I. Introduction

THE use of the graded barrier quantum well laser structure has made possible very low threshold current density devices [1]–[4]. However, little work has been reported on the integration of this structure into index-guided devices, particularly in the visible region. Index-guided buried heterostructure devices with graded barrier quantum well active layers (λ = 8700 Å) which were grown by a hybrid MBE/LPE growth process have been reported [5]. In this paper, complementary self-aligned index-guided infrared and visible laser devices with graded barrier quantum well active layers which have been grown by a two-step MOCVD process [6]–[9] are reported. Through the use of high aluminum composition (x = 0.85) confining layers and optimization of the width of the graded barrier separate confinement region, we have obtained very low threshold current density laser structures. Finally, in order to obtain visible emission, the graded barrier structure has been modified by using thin AlAs barrier layers on both sides of each quantum well. These structures have been fabricated into complementary self-aligned lasers, resulting in low threshold, index-guided visible diodes.

The emission wavelengths of AlGaAs/GaAs laser structures can be shifted into the visible spectrum by either the use of an alloy active layer [10], quantum size effects [11], [12], or a combination of these two techniques [12], [13]. Alloy active layer devices, however, are sensitive to the optical quality of the AlGaAs within the active layer and do not exhibit other desirable properties, such as low threshold current, high differential quantum efficiency, and low temperature dependence of laser threshold (high T_0), which have been associated with quantum well devices [1]–[4]. Laser structures which rely exclusively on quantum size effects have been operated as laser diodes with emission wavelengths as short as 7040 Å for a 13 Å quantum well [11]. However, the growth of such small well sizes to obtain higher energy emission can be difficult. In addition, a large number of small wells must be utilized in order to obtain both sufficient carrier collection and a reasonable optical confinement factor [11]. The use of all-binary AlAs/GaAs quantum well structures [14] eliminates difficulties associated with alloy clustering and allows high energy emission to be obtained without having to rely on extremely small well sizes. In these structures, short wavelength emission can be obtained at relatively large (L_z > 20 Å) well sizes due to the large AlAs potential barrier height of either side of the quantum well.

In this paper, the optimization and characterization of the graded barrier laser structure are discussed for infrared and visible wavelength lasers. The advantages of all-binary quantum well structures have been combined with the graded barrier structure in order to obtain low threshold laser diodes operating at short wavelength. Stabilized optical modes have been obtained with the graded barrier quantum well laser by utilizing the complementary self-aligned laser structure [6]. These complex index-guided devices require a two step MOCVD growth process which results in a planar active layer device which is compatible with high aluminum concentration confining layers. In an attempt to obtain higher output power levels, index-guided shallow mesa laser arrays [15] utilizing the graded barrier quantum well active layer have been studied.

Manuscript received October 23, 1986; revised January 22, 1987. This work was supported in part by the U.S. Army Night Vision Laboratory under Contract DAAK 20-84-K-0225, the National Science Foundation Engineering Research Center under Grant CDR 85-22666, and General Motors.

L. J. Mawst was with the Department of Electrical Engineering, University of Illinois at Urbana-Champaign, Urbana, IL 61801. He is now with the TRW Electro-Optics Research Center, Redondo Beach, CA 90278.

M. E. Givens, C. A. Zmudzinski, M. A. Emanuel, and J. J. Coleman are with the NSF Engineering Research Center for Compound Semiconductor Microelectronics, University of Illinois at Urbana-Champaign, Urbana, IL 61801.

0018-9197/87/0600-0696$01.00

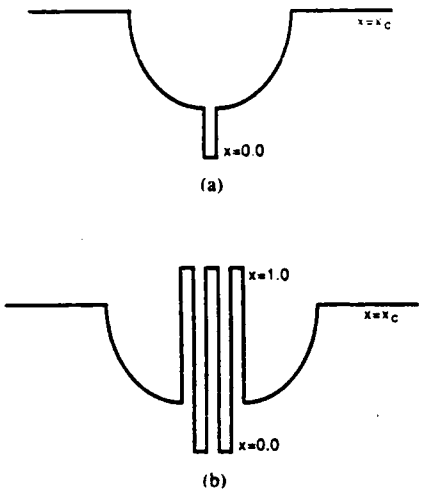

Fig. 1. Schematic diagram of aluminum composition profile in a conventional (a) and a modified (b) graded barrier quantum well laser. The modified structure contains thin AlAs quantum well barrier layers which increase the confined carrier energy levels, allowing higher energy emission to be obtained.

II. Graded Barrier Quantum Well Structure

A schematic diagram of the modified graded barrier quantum well structure containing AlAs quantum well barrier layers is shown in Fig. 1. Also shown, for comparison, is the conventional graded barrier quantum well structure. These structures consist of a GaAs:n buffer layer (1×10^{18}, 0.5 μm), a compositionally graded buffer layer $Al_xGa_{1-x}As$:n (1×10^{18}, $x = 0.00$–0.85, 1.0 μm), an $Al_xGa_{1-x}As$:n confining layer (1×10^{18}, $x = 0.85$, 1.0 μm), and $Al_xGa_{1-x}As$:n parabolic graded region (5×10^{16}, $x = 0.85$-0.20, 0.12 μm), an undoped GaAs quantum well active region with or without 10 Å AlAs barriers (based on growth rate calibrations), an $Al_xGa_{1-x}As$:p parabolic graded region (5×10^{16}, $x = 0.20$–0.85, 0.12 μm), and $Al_xGa_{1-x}As$:p confining layer (5×10^{17}, $x = 0.85$, 1.0 μm), and a GaAs:p^+ cap layer (0.20 μm). The use of high aluminum composition confining layers improves the optical confinement factor and carrier confinement of the quantum well resulting in low threshold, high efficiency, high T_o devices [4]. In addition to incorporating high aluminum composition confining layers ($x = 0.60$–0.85), the effect of the graded region width on the device performance has been studied with the intention of optimizing the structure. Broad area threshold current density as a function of laser cavity length for three different graded region widths are shown in Fig. 2. All three structures have 50 Å quantum well widths (no AlAs barriers) with $x = 0.85$ confining layers. These data indicate that the device performance of the graded barrier laser structure is relatively insensitive to the width of the graded region, which is consistent with calculations of the transverse optical confinement factor as a function of this width [16]. An essential function of the graded region is enhancement of carrier collection into the thin quantum well [17]. Recent calculations [18] have shown that the graded barrier is superior to the separate confinement structure because the graded region has a lower density of states.

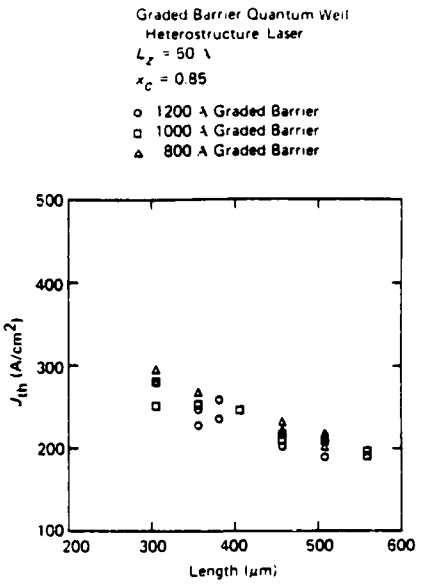

Fig. 2. Broad area threshold current density measurements as function of laser cavity length for graded barrier quantum well structures with 1200, 1000, and 800 Å graded barrier widths on each side of the quantum well active region. The small amount of threshold variation observed between the three structures indicates that the transverse optical confinement factor has a small effect on device performance.

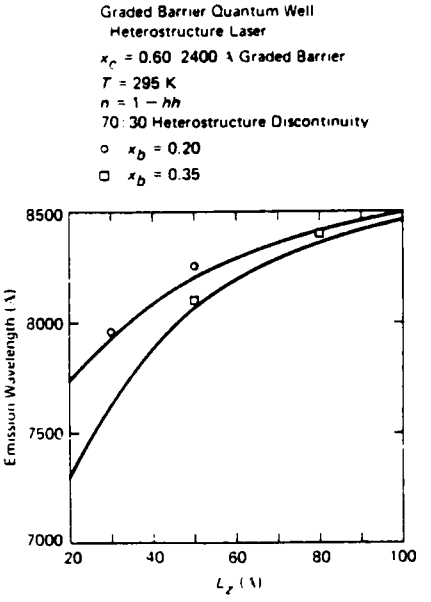

Fig. 3. Comparison between calculated and measured emission wavelength for graded barrier quantum well structures with various well sizes and aluminum compositions (x_b) at the edges of the well. Good correlation between the measured values and the calculated $n = 1$ electron to heavy hole transition, based on quantum well widths obtained from growth rate calibration, is observed.

The measured emission wavelengths of the graded barrier quantum well structure (no AlAs barriers) for different quantum well widths and aluminum mole fractions at the edges of the quantum well are shown in Fig. 3. Very good agreement is observed with the calculated values

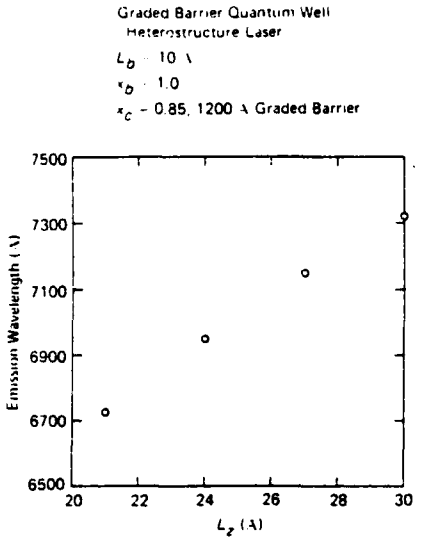

Fig. 4. Measured emission wavelength as a function of quantum well size for a double well graded barrier quantum well structure containing thin AlAs barrier layers surrounding the GaAs wells. High energies are obtained for relatively large quantum well widths.

based on a finite potential well model (solid lines) for the $n = 1$ electron to heavy hole transition, using layer thicknesses obtained from growth rate data. Thin (10 Å) AlAs barrier layers can be utilized to shorten the emission wavelength, with very little increase in threshold current. Devices with a single 50 Å quantum well and $x = 0.60$ confining layers have been characterized with and without AlAs barrier layers. For a 400 μm cavity length device, broad area threshold current densities increase from 318 A/cm^2 (without AlAs) to 365 A/cm^2 (with AlAs), while the emission wavelength shifts from $\lambda = 8200$ Å to $\lambda = 7950$ Å. Shorter wavelength graded barrier quantum well structures were grown using a double well (GaAs) structure with three 10 Å AlAs barrier layers. High aluminum concentration confining layers ($x = 0.85$) were utilized, with a 0.12 μm graded region ($x = 0.85$–0.40) on each side of the quantum well. Although the thin AlAs barrier allows significant coupling between the two GaAs wells, and this coupling will affect the step-like density of states of a single well [19], these structures have only two thin wells and the entire active region thickness is sufficiently small that a step-like density of states is retained. The measured emission wavelength of this structure for various quantum well sizes is illustrated in Fig. 4. Emission wavelengths corresponding to the $n = 1$ electron to heavy hole transition have been calculated for these structures by numerical integration of the Shrödinger equation using the Numerov technique [20]. Comparison of observed emission wavelengths and calculated values indicate that the actual quantum well thicknesses could be 5–6 Å larger than expected based on growth rate calibrations. However, a more plausible explanation is that the finite potential well model and effective mass theory do not adequately describe the structure due to the thin layer widths and high energies involved. Oxide defined stripe lasers with 6 μm stripe widths have been fabricated. Threshold currents for devices with 330–355 μm cavity lengths were 90 mA ($L_z = 30$ Å), 130 mA ($L_z = 27$ Å), and 320 mA ($L_z = 24$ Å). No laser emission was observed from the structure with $L_z = 21$ Å. Calculations indicate that, for this small well size, the confined electron energy level is probably located within the graded region surrounding the quantum well. This would inhibit carrier collection in the well, thereby increasing the laser threshold current. It may prove to be necessary to utilize a larger aluminum composition just outside the quantum wells, at the edges of the graded regions, in order to insure that the confined energy levels are located within the quantum well.

III. Index-Guided Complementary Self-Aligned Laser Structure

A schematic diagram of the self-aligned laser structure along with the transverse and lateral refractive index variations is illustrated in Fig. 5. The self-aligned laser structure incorporates two important features for achieving stable single-mode operation. The placement of a low bandgap, high refractive index GaAs:n layer outside the stripe region creates a built-in complex effective index step along the junction plane which results in the optical waveguide necessary to stabilize the lateral optical mode [21]. In addition, the GaAs:n layer forms a reverse biased p–n junction outside the stripe region, which self aligns the current injection with the lateral optical waveguide. This type of index guided structure is attractive for quantum well active layer devices since it is a planar device with the active layer grown prior to any processing steps.

The self-aligned laser structure can be difficult to fabricate, especially for high aluminum confining layer devices ($x \geq 0.40$) [22], [23]. This difficulty stems from the formation of oxides on the exposed AlGaAs surface prior to the second growth step. This structure is sensitive to the quality of the regrowth interface which is located in the region of high current density. These problems are avoided by use of a complementary self-aligned laser structure which places the regrowth interface outside the region of high current density [6], [9]. This complementary structure increases the versatility of the self-aligned structure, allowing any laser active region to be utilized. The complementary self-aligned laser structure is fabricated using a two step, selective MOCVD growth process which has been described previously [6]. Both growth steps are performed at 800°C in an atmospheric pressure MOCVD system.

Theoretical analyses of the lateral mode charactertistics in complex index guided structures indicate that the introduction of a built-in loss region outside the stripe width increases the threshold gain of higher order lateral modes sufficiently such that only the fundamental mode reaches threshold, even though the lateral optical waveguide can support higher order modes [24]. In the self-aligned laser, the built-in loss profile, due to the radiation and absorption loss of the transverse optical mode in the GaAs:n, provides strong higher order lateral mode discrimination.

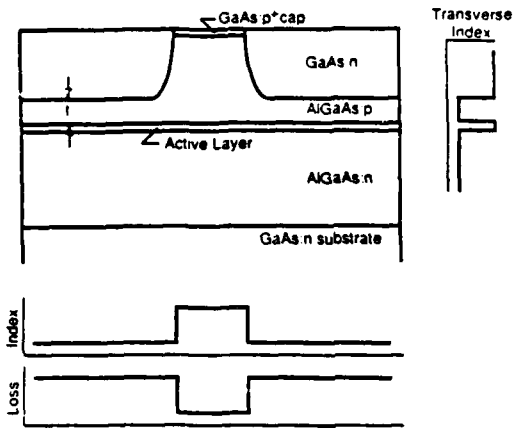

Fig. 5. Schematic diagram of self-aligned laser structure illustrating important design parameters including distance between GaAs : n layer and active layer (t), stripe width, and confining layer aluminum composition. Transverse and lateral refractive index variations are also illustrated.

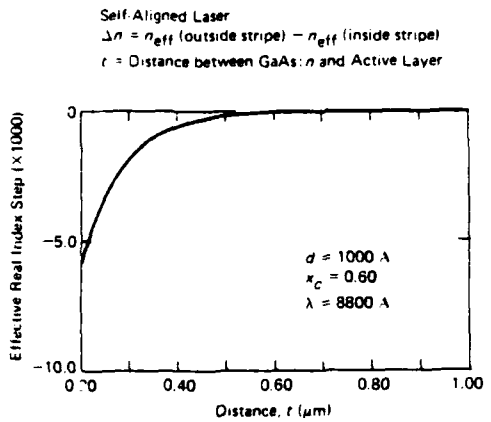

Fig. 6. Calculated real effective index step along the plane of the active layer as a function of distance (t) between GaAs : n layer and active layer. Strong real index guiding is obtained for values of t less than about 0.30 μm.

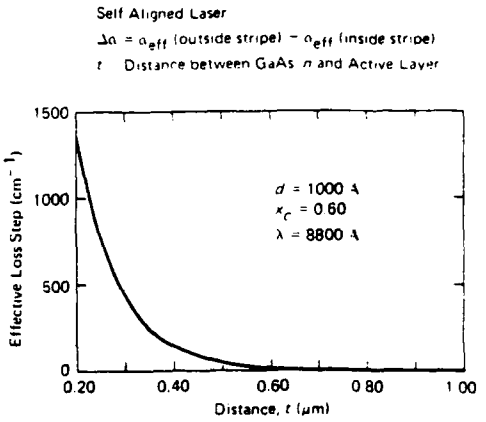

Fig. 7. Calculated effective loss step along the plane of the active layer as a function of distance between GaAs . n layer and active layer. Large values of loss are obtained for values of t less than 0.30 μm, providing strong higher order lateral mode discrimination.

This allows the self-aligned laser to operate in a stable fundamental lateral mode even in relatively large stripe width devices (which support higher order lateral modes). In addition, a large optical spot size at the facet improves the operating lifetime at higher output power levels [25]. The magnitude of the lateral effective complex index step is an important parameter from the standpoint of determining optimum values for layer thicknesses and aluminum compositions in the self-aligned laser structure. The waveguiding properties of the self-aligned laser structure can be analyzed using a technique previously applied to the InGaAsP / InP self-aligned laser structure [26]. Assuming a fundamental transverse mode both within and outside the stripe region, an analytical perturbation technique is used to obtain an estimate of the effective real index and loss variations along the plane of the junction. The effect on the lateral complex index step of varying the distance between the GaAs : n layer and the active layer is illustrated in Fig. 6 and 7. The effective real index step (Fig. 6) and the effective loss step (Fig. 7) have been calculated for a device with $x = 0.60$ confining layers and a 1000 Å GaAs active layer. These calculations indicate that strong real index guiding is obtained ($\Delta n \geq 10^{-3}$) for values of t (distance between GaAs : n active layer and active layer) less than about 0.35–0.30 μm. Also, a strong built-in loss variation is established for values of $t \leq 0.3$ μm. This loss variation will provide the higher order lateral mode discrimination which is characteristic of self aligned laser structures. Similar calculations can be performed utilizing a graded barrier quantum well active layer with the same qualitative behavior expected.

In order to clearly demonstrate higher order mode discrimination capabilities in self-aligned laser structures, comparison studies were performed with another real index-guided device, the shallow mesa laser. In contrast with the self-aligned laser structure, the shallow mesa laser structure is predominately real index-guided due to the structural variation of the transverse optical waveguide [27]. Light–current (L–I) characteristics and near-field measurements along the plane of the junction for both the shallow mesa and compiementary self-aligned laser structure are shown for comparsion in Figs. 8 and 9. Both structures have the same device dimensions (stripe width ≈ 10 μm, cladding thickness = 0.30 μm, length = 330–355 μm) and are fabricated from a conventional double heterostructure with a 500 Å GaAs active layer and x = 0.35 confining layers. Even with this large stripe width, the self-aligned laser maintains a stable fundamental lateral mode well above threshold, up to about 8 mW per uncoated facet. Above the kink point, spatial hole burning occurs and shifts the optical field toward the edge of the stripe. Due to the strong real index guiding, without any higher order mode discrimination capability, the shallow mesa laser operates in a higher order lateral mode beginning at laser threshold. A similar behavior has been observed in multiple stripe array structures [7]. By optimizing the stripe width as well as the distance between the GaAs : n layer and the active layer, the self-aligned

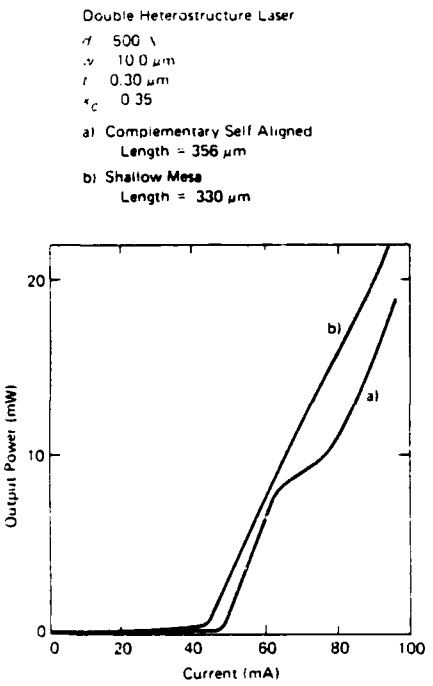

Fig. 8. Comparison of pulsed *L–I* characteristics for wide stripe complementary self-aligned laser and shallow mesa laser structures. The self-aligned laser structure shows linear characteristics up to a kink point, where higher order lateral modes reach threshold.

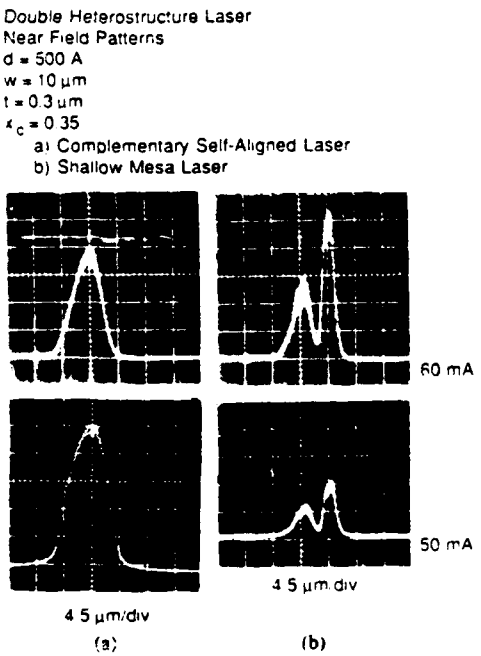

Fig. 9. Comparison of near-field patterns along the plane of the active layer for wide stripe complementary self-aligned laser and shallow mesa laser structures. Higher order lateral modes appear at laser threshold in the shallow mesa structure due to the strong index guiding and large stripe width utilized.

laser structure can operate in a stable fundamental mode with a large lateral spot size.

Very low threshold complementary self-aligned lasers have been fabricated using a 50 Å graded barrier quantum well active region (no AlAs barriers) with $x = 0.85$ confining layers. Threshold currents range from 11 to 13 mA for devices with 300–350 μm cavity lengths. These devices have 5.5 μm wide stripes with 0.2 μm spacings between the GaAs : n layer and the edge of the graded region. The pulsed *L–I* characteristics for a 300 μm long device are shown in Fig. 10. The near-field patterns for these devices, shown in Fig. 11, indicate stable fundamental lateral mode operation is observed up to 16 mW per uncoated laser facet. CW single longitudinal mode operation is observed up to 10 mW. The temperature dependence of the theshold current can be characterized by $T_o = 125°C$ in the temperature range 25–50°C. Devices with larger spacing between the GaAs : n layer and active layer ($T = 0.30$ μm) show stable fundamental lateral mode operation up to about 25 mW per uncoated facet with a 17 mA threshold current for a 4.5 μm wide stripe.

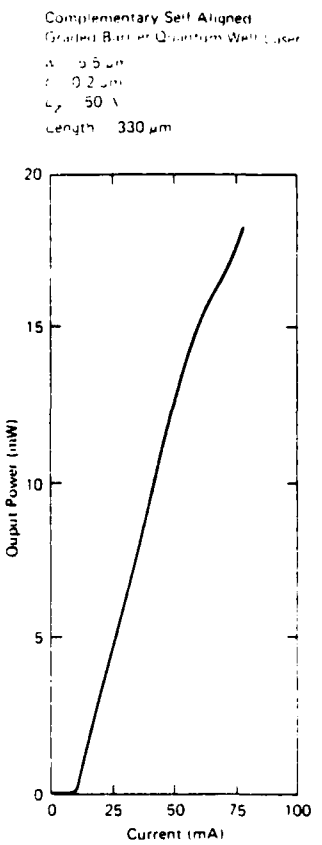

Fig. 10. Pulsed *L–I* characteristics of a complementary self-aligned laser utilizing a graded barrier quantum well active layer with a 50 Å quantum well. Very low thresholds currents (11 mA) are obtained at $\lambda = 8200$ Å.

Visible ($\lambda = 6950$–7150 Å) index-guided laser structures have been fabricated using the graded barrier structure containing two 24 or 27 Å GaAs quantum wells with 10 Å AlAs barriers and $x = 0.85$ confining layers. Structures with 27 Å quantum wells ($\lambda = 7150$ Å) have been fabricated into complementary self-aligned lasers with 6.5 μm wide stripes and 0.20 μm spacing between the GaAs : n layer and edges of the graded region. A scanning electron

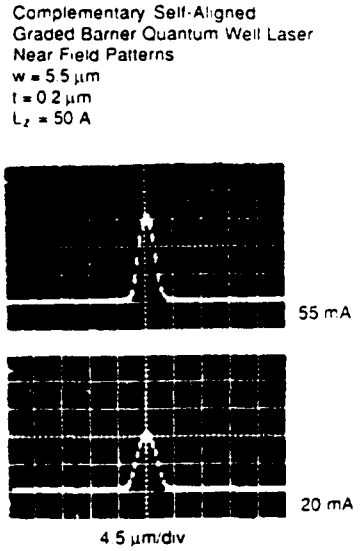

Fig. 11. Near-field radiation patterns along the plane of the junction for a complementary self-aligned laser structure. Stable fundamental lateral mode operation is obtained up to greater than 5X threshold current (11 mA).

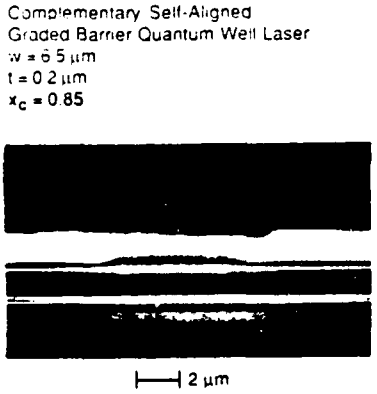

Fig. 12. Scanning electron micrograph of complementary self-aligned laser structure utilizing a graded barrier quantum well active layer and high aluminum composition (x = 0.85) confining layers.

micrograph of the structure is shown in Fig. 12. Pulsed L–I characteristics, shown in Fig. 13, indicated threshold currents of 55 mA for a 432 μm long cavity. Near-field patterns along the plane of the junction show (Fig. 14) stable fundamental lateral mode operation up to 15 mW per uncoated laser facet. Devices with larger stripe widths (w = 8 μm) show fundamental mode operation up to about 7 mW, above which higher order modes reach threshold. Laser structures with 24 Å quantum wells (λ = 6950 Å) have also been fabricated into complementary self-aligned lasers with 7.0 μm wide stripes and 0.20 μm spacing between the GaAs:n layer and the edges of the graded region. Threshold currents of 100 mA are obtained for a 356 μm long devices with fundamental mode operation up to about 11 mW. By optimizing both the stripe width and spacing between the GaAs:n layer and the active layer, higher output power levels can be expected.

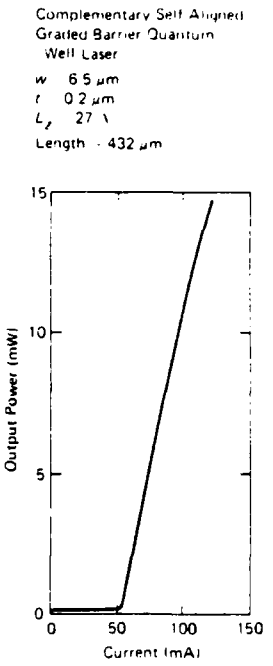

Fig. 13. Pulsed L–I characteristics of a complementary self-aligned laser utilizing a graded barrier quantum well active layer containing two 27 Å quantum wells surrounded by 10 Å AlAs barrier layers. Linear light output is obtained up to about 15mW with an emission wavelength of 7150 Å.

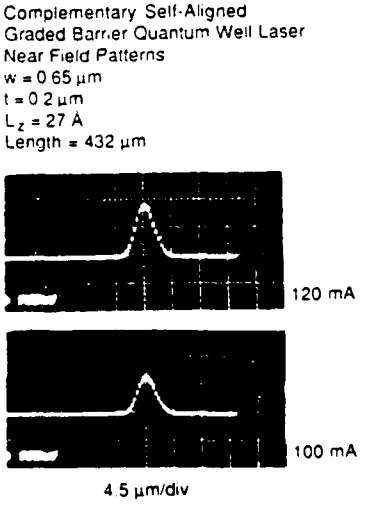

Fig. 14. Near-field radiation patterns along the plane of the active layer for a visible (λ = 7150 Å) complementary self-aligned laser. Stable fundamental lateral mode operation is obtained up to about 15 mW.

IV. Visible Array Structures

In order to obtain higher output power levels at visible wavelengths, multiple stripe shallow mesa array structures have been fabricated utilizing the graded barrier quantum well structure containing two 27 Å quantum wells with 10 Å AlAs barriers (λ = 7150 Å) and x = 0.85 confining layers. No attempt was made to optimize array dimensions for phase-locked operation. Six-element array structures were fabricated with 3 μm wide stripes on

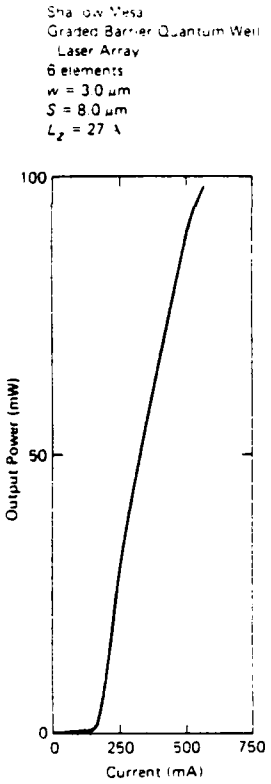

Fig. 15. Pulsed L-I characteristics of visible (λ = 7150 Å) 6-element shallow mesa graded barrier quantum well laser array. A maximum power output of 100 mW per uncoated laser facet is obtained.

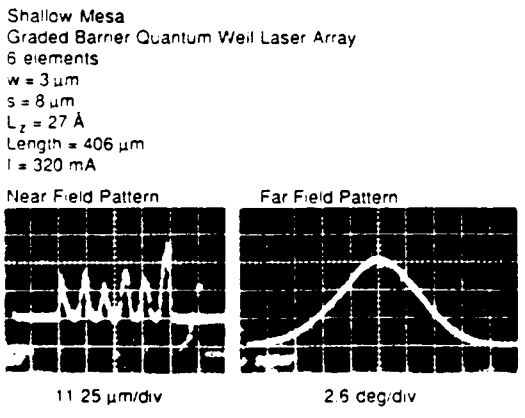

Fig. 16. Near- and far-field radiation patterns along the plane of the junction for 6-element shallow mesa laser array. The single-lobed far-field pattern indicates the elements of the array are not phase locked due to the strong optical confinement within the mesa regions.

8 μm centers. A 0.10 μm cladding layer thickness was utilized between mesa regions in order to obtain strong index guiding. Phase-locked operation is not obtained due to the strong index guiding and large center-center stripe spacing. The L-I characterisitics for a 6-element array is shown in Fig. 15. Pulsed output power levels of 100 mW are obtained with threshold currents of 25-30 mA per stripe. Near-field images, shown in Fig. 16, indicate all six array elements are lasing and, due to the small stripe width, higher order lateral modes are not observed within the individual array elements. Far-field images along the plane of the junction also shown in Fig. 16, indicate a single lobed pattern with a FWHM of 9.5°. Phase-locked operation can be expected for devices with greater optical field overlap between array elements. This can be accomplished by utilizing a smaller center-center spacing as well as a larger cladding layer thickness between mesa regions.

V. Conclusions

The graded barrier quantum well structure has been modified to include thin AlAs quantum well barrier layers, allowing low threshold visible emission lasers to be realized. Stable, fundamental mode, index-guided devices have been fabricated which incorporate the graded barrier quantum well structure. Index guiding is accomplished through the use of a complementary self-aligned two-step MOCVD growth process, which is compatible with low threshold, high aluminum composition confining layer structures. The optical waveguiding properties of the self-aligned laser structure have been discussed, illustrating higher order lateral mode discrimination capability. Complementary self-aligned lasers with threshold currents of 11 mA (λ = 8200 Å), 55 mA (λ = 7150 Å), and 100 mA (λ = 6950 Å) have been fabricated and characterized. High output power visible (λ = 7150 Å) shallow mesa laser arrays which utilize the graded barrier quantum well active layer have been demonstrated.

Acknowledgment

The authors gratefully acknowledge Y. S. Moroz, B. K. Moroz, and M. Artaki for helpful discussions and technical support.

References

[1] W. T. Tsang, "Extremely low threshold (AlGa)As graded-index waveguide separate-confinement heterostructure lasers grown by molecular beam epitaxy," *Appl. Phys. Lett.*, vol. 40, pp. 217-219, Feb. 1982.

[2] S. D. Hersee, M. Baldy, P. Assenat, B. De Cremoux, and J. P. Duchemin, "Very low threshold GRIN-SCH GaAs/GaAlAs laser structure grown by OM-VPE," *Electron. Lett.* vol. 18, pp. 870-871, Sept. 1982.

[3] D. Kasemset, C. S. Hong, N. B. Patel, and P. D. Dapkus, "Very narrow graded-barrier single quantum well lasers grown by metalorganic chemical vapor deposition," *Appl. Phys. Lett.*, vol. 41, pp. 912-914, Nov. 1982.

[4] M. E. Givens, L. J. Mawst, C. A. Zmudzinski, M. A. Emanuel, and J. J. Coleman, "Effect of compositionally graded and superlattice buffer layers on the device performance of graded barrier quantum well heterostructure laser diodes," *Appl. Phys. Lett.*, vol. 50, Feb. 1987.

[5] W. T. Tsang, R. A. Logan, and J. A. Ditzenberger, "Ultra-low threshold, graded-index waveguide, separate confinement, CW buried-heterostructure lasers," *Electron. Lett.* vol. 18, pp. 845-847, Sept. 1982.

[6] L. J. Mawst, G. Costrini, C. A. Zmudzinski, M. E. Givens, M. A. Emanuel, and J. J. Coleman, "Complementary self-aligned laser by metalorganic chemical vapour deposition," *Electron. Lett.*, vol. 21, pp. 903-905, Sept. 1985.

[7] L. J. Mawst, M. E. Givens, C. A. Zmudzinski, M. A. Emanuel, and J. J. Coleman, "Complementary self-aligned laser arrays by metalorganic chemical vapor deposition," *J. Appl. Phys.*, vol. 60, pp. 2633-2635, Oct. 1986.

[8] ——Near-and far-field observations of transient behavior in pulsed graded barrier quantum well lasers," *J. Appl. Phys.*, vol. 60, pp. 2613-2615, Oct. 1986.

[9] J. J. J. Yang, C. S. Hong, J. Niesen, and L. Figueroa, "High power operation of index-guided inverted channel substrate planar (ICSP) lasers," *Electron. Lett.*, vol. 21, pp. 751-752, Aug. 1985.
[10] W. T. Tsang, "Infared-visible (0.89-0.72 μm) $Al_xGa_{1-x}As$/$Al_yGa_{1-y}As$ double heterostructure lasers grown by molecular beam epitaxy," *J. Appl. Phys.*, vol. 51, pp. 917-919, Feb. 1980.
[11] K. Woodbridge, P. Blood, E. D. Fletcher, and P. J. Hulyer, "Short wavelength (visible) GaAs quantum well lasers grown by molecular beam epitaxy," *Appl. Phys. Lett.*, vol. 45, pp. 16-18, July 1984.
[12] T. Hayakawa, T. Suyama, K. Takahashi, M. Kondo, S. Yamamoto, and T. Hijikata, "Low current threshold AlGaAs visible laser diodes with an $(AlGaAs)_m(GaAs)_n$ superlattice quantum well," *Appl. Phys. Lett.*, vol. 49, pp. 636-638, Sept. 1986.
[13] H. Iwamura, T. Saku, Y. Hirayama, Y. Suzuki, and H. Okamoto, "Near room temperature CW operation of 660 nm visible AlGaAs multi-quantum-well laser diodes grown by molecular beam epitaxy," *Japan. J. Appl. Phys.*, vol. 24, pp. L911-913, Dec. 1985.
[14] B. A. Vojak, W. D. Laidig, N. Holonyak, Jr., M. D. Camras, J. J. Coleman, and P. D. Dapkus, "High-energy (visible-red) stimulated emission in GaAs," *J. Appl. Phys.*, vol. 52, pp. 621-626, Feb. 1981.
[15] L. J. Mawst, M. E. Givens, M. A. Emanuel, C. A. Zmudzinski, and J. J. Coleman, "Phase locked shallow mesa graded barrier quantum well laser arrays," *Appl. Phys. Lett.*, vol. 48, pp. 1337-1339, May 1986.
[16] W. Streifer, R. D. Burnham, and D. R. Scifres, "Modal analysis of separate-confinement heterojunction lasers with inhomogeneous cladding layers," *Opt. Lett.*, vol. 8, pp. 283-285, May 1983.
[17] R. D. Burnham, W. Streifer, D. R. Scifres, N. Holonyak, Jr., K. Hess, and M. D. Camras, "Low threshold photopumped $Al_xGa_{1-x}As$ quantum-well heterostructure lasers," *J. Appl. Phys.*, vol. 54, pp. 2618-2622, May 1983.
[18] J. Nagle, S. Hersee, M. Krakowski, T. Weil, and C. Weisbuch, "Threshold current of single quantum well lasers: The role of the confining layers," *Appl. Phys. Lett.*, vol. 49, pp. 1325-1327, Nov. 1986.
[19] H. Kroemer and H. Okamoto, "Some design considerations for multi-quantum-well lasers," *Japan. J. Appl. Phys.*, vol. 23, pp. 970-974, Aug. 1984.
[20] P. C. Chow, "Computer solutions to the Schrödinger equation," *Amer. J. Phys.*, vol. 40, pp. 730-734, May 1972.
[21] J. J. Coleman and P. D. Dapkus, "Single-longitudinal-mode metal-organic chemical-vapor-deposition self-aligned GaAlAs-GaAs double-heterostructure lasers," *Appl. Phys. Lett.* vol. 37, pp. 262-263, Aug. 1980.
[22] A. Watanabe, T. Yamada, K. Imanaka, H. Horikawa, Y. Kawai, and M. Sakuta, "AlGaAs/GaAs melt-etched inner stripe laser diode with self-aligned structure," *Appl. Phys. Lett.*, vol. 46, pp. 1023-1025, June 1985.
[23] H. Tanaka, M. Mushiage, Y. Ishida, and H. Fukuda, "Single-longitudinal-mode self-aligned (AlGa)As double-heterostructure lasers fabricated by molecular beam epitaxy," *Japan. J. Appl. Phys.*, vol. 24, pp. L89-L90, Feb. 1985.
[24] R. Lang, "Lateral transverse mode instability and its stabiliztion in stripe geometry injection lasers," *IEEE J. Quantum Electron.*, vol. QE-15, pp. 718-726, Aug. 1979.
[25] D. Botez, D. J. Channin, and M. Ettenberg, "High-power single-mode AlGaAs laser diodes," *Opt. Eng.*, vol. 21, pp. 1066-1073, Dec. 1982.
[26] M. Yano, H. Nishi, and M. Takusagawa, "Oscillation characteristics in InGaAsP/InP DH lasers with self-aligned structure," *IEEE J. Quantum Electon.*, vol. QE-15, pp. 1388-1395, Dec. 1979.
[27] G. P. Agrawal, "Lateral analysis of quasi-index-guided injection lasers: Transition from gain to index guiding," *J. Lightwave Technol.*, vol. LT-2, pp. 537-543, Aug. 1984.

Luke J. Mawst [redacted]. He received the B.S. degree in engineering physics, and the M.S. and Ph.D. degrees in electrical engineering from the University of Illinois at Urbana-Champaign, in 1982, 1984, and 1987, respectively. His dissertation research involved the development of index-guided semiconductor lasers and laser arrays grown by MOCVD.

He joined the TRW Electro-Optics Research Center, Redondo Beach, CA, in 1987, where he is currently enguged in research on semiconductor lasers.

Michael E. Givens [redacted]. He received the B.S. degree in electrical engineering from the University of Illinois at Urbana-Champaign in 1985.

Currently, he is working towards the Ph.D. in electrical engineering under an IBM Doctoral Fellowship at the NSF Engineering Research Center for Compound Semiconductor Microelectronics at the University of Illinois. His research interests include compound semiconductor epitaxial crystal growth by MOCVD and the development of semiconductor laser structures.

Charles A. Zmudzinski [redacted]. He received the B.S. degree in electrical engineering from the University of Notre Dame, South Bend, in 1984, and the M.S. degree in electrical engineering from the University of Illinois at Urbana-Champaign, in 1986.

Currently, he is working towards the Ph.D. degree in electrical engineering at the University of Illinois. His research has concentrated on the fabrication and characteristics of infrared and visible AlGaAs lasers and laser arrays.

Mark A. Emanuel [redacted]. He received the B.E.E. degree in 1979 from the University of Dayton, Dayton, OH, and the M.S.E.E. degree in 1984 from the University of Illinois at Urbana-Champaign.

He is presently working towards the Ph.D. degree in electrical engineering at the University of Illinois. His research is concentrated on the growth of III-V heterostructure devices by MOCVD.

James J. Coleman (S'73-M'76-SM'80) received the B.S., M.S. and Ph.D. degress in electrical engineering from the University of Illinois at Urbana-Champaign, in 1972, 1973, and 1975, respectively.

At Bell Laboratories, Murray Hill, NJ (1976-1978), he studied the materials properties of InGaAsP grown by liquid phase epitaxy (LPE) for CW lasers operating at wavelengths near 1.3 μm. At Rockwell International, Anaheim, CA (1978-1982) he contributed to the development of the MOCVD growth method and various CW room temperature, low threshold AlGaAs-GaAs laser devices such as the self-aligned laser and the narrow diffused stripe laser. By extension of the MOCVD growth process to large numbers of ultrathin (10-200 Å) layers and to all binary AlAs-GaAs structures, he was able to make unique quantum well heterostructures and superlattices which show two-dimensonal optical and electronic transport effects. He is currently a Professor of Electrical Engineering at the University of Illinois at Urbana-Champaign (1982-present). He and his students are involved in the study of optical processes and electronic transport in quantum well heterostructures, real-space transferred electron devices, and laser arrays. He has authored or co-authored more than 100 technical papers and holds two patents.

Prof. Coleman is the Guest Editor of the IEEE JOURNAL OF QUANTUM ELECTRONICS Special Issue on Quantum Well Heterostructures and Superlattices, scheduled for publication in mid-1988. He was the recipient of a Beckman Research Award in 1982. He is a member of the American Physical Society, the American Society for Metals, and Sigma Xi.